JUL 0 3
DEC 2 0
FEB 0 3 1984

AFWAL-TR-83-2002
Volume I

ROTATING STALL INVESTIGATIONS
VOLUME I – THEORETICAL INVESTIGATIONS

Aerodynamic Research Department
Arvin/Calspan Advanced Technology Center
P.O. Box 400
Buffalo, New York 14225

Property of U. S. Air Force
AEDC LIBRARY
F40600-81-C-0004

January 1983

TECHNICAL REPORTS
FILE COPY

Final Report for Period 15 August 1979 – 15 October 1982

Approved for public release; distribution unlimited

Aero Propulsion Laboratory
AIR FORCE WRIGHT AERONAUTICAL LABORATORIES
AIR FORCE SYSTEMS COMMAND
WRIGHT-PATTERSON AIR FORCE BASE, OHIO 45433

NOTICE

When Government drawings, specifications, or other data are used for any purpose other than in connection with a definitely related Government procurement operation, the United States Government thereby incurs no responsibility nor any obligation whatsoever; and the fact that the government may have formulated, furnished, or in any way supplied the said drawings, specifications, or other data, is not to be regarded by implication or otherwise as in any manner licensing the holder or any other person or corporation, or conveying any rights or permission to manufacture use, or sell any patented invention that may in any way be related thereto.

This report has been reviewed by the Office of Public Affairs (ASD/PA) and is releasable to the National Technical Information Service (NTIS). At NTIS, it will be available to the general public, including foreign nations.

This technical report has been reviewed and is approved for publication.

MARVIN A. STIBICH, TAM
Compressor Technology Group
Technology Branch

WALKER H. MITCHELL
Chief, Technology Branch
Turbine Engine Division

FOR THE COMMANDER

H. I. BUSH
Director
Turbine Engine Division
Aero Propulsion Laboratory

"If your address has changed, if you wish to be removed from our mailing list, or if the addressee is no longer employed by your organization please notify AFWAL/POTX *, W-PAFB, OH 45433 to help us maintain a current mailing list".*

Copies of this report should not be returned unless return is required by security considerations, contractual obligations, or notice on a specific document.

UNCLASSIFIED

SECURITY CLASSIFICATION OF THIS PAGE (When Data Entered)

REPORT DOCUMENTATION PAGE

READ INSTRUCTIONS BEFORE COMPLETING FORM

1. REPORT NUMBER
AFWAL-TR-83-2002, Vol. I

2. GOVT ACCESSION NO.

3. RECIPIENT'S CATALOG NUMBER

4. TITLE (and Subtitle)
Rotating Stall Investigations
Volume I - Theoretical Investigations

5. TYPE OF REPORT & PERIOD COVERED
Final Report for Period
15 Aug 1979 - 15 Oct 1982

6. PERFORMING ORG. REPORT NUMBER
6568-A-6

7. AUTHOR(s)
J. P. Nenni, G. F. Homicz and G. R. Ludwig

8. CONTRACT OR GRANT NUMBER(s)
F33615-79-C-2023

9. PERFORMING ORGANIZATION NAME AND ADDRESS
Aerodynamic Research Department
Arvin/Calspan Advanced Technology Center
P. O. Box 400, Buffalo, New York 14225

10. PROGRAM ELEMENT, PROJECT, TASK AREA & WORK UNIT NUMBERS
Project 3066 /04/55

11. CONTROLLING OFFICE NAME AND ADDRESS
Aero Propulsion Laboratory (AFWAL/POTX)
Air Force Wright Aeronautical Laboratories (AFSC)
Wright-Patterson Air Force Base, Ohio 45433

12. REPORT DATE
January 1983

13. NUMBER OF PAGES
108

14. MONITORING AGENCY NAME & ADDRESS (if different from Controlling Office)

15. SECURITY CLASS. (of this report)
Unclassified

15a. DECLASSIFICATION/DOWNGRADING SCHEDULE

16. DISTRIBUTION STATEMENT (of this Report)

Approved for public release; distribution unlimited.

17. DISTRIBUTION STATEMENT (of the abstract entered in Block 20, if different from Report)

18. SUPPLEMENTARY NOTES

19. KEY WORDS (Continue on reverse side if necessary and identify by block number)
Rotating Stall
Compressors
Unsteady Aerodynamics

20. ABSTRACT (Continue on reverse side if necessary and identify by block number)

This report presents the results of a research program on rotating stall in axial flow compressors and jet engines. The program had three major objectives which were: (1) develop and analysis for a three-dimensional, time-variant rotating stall and separation theory, (2) develop analysis for post-stall operation/recovery and aerodynamically induced exotic metal combustion and (3) consider the effects of distortion, water ingestion, and nuclear blasts on axial flow compressors. The work done towards accomplishing objective (1)

DD FORM 1 JAN 73 1473 EDITION OF 1 NOV 65 IS OBSOLETE

UNCLASSIFIED

SECURITY CLASSIFICATION OF THIS PAGE (When Data Entered)

is reported in Volume I. The work done towards the accomplishment of the remaining two objectives is reported in Volume II. Volume I contains the description of an implicit time marching Euler code, a small disturbance stability theory for the compressible flow through a compressor stage, and a three-dimensional unsteady lifting surface theory for annular blade rows.

FOREWORD

This is the final technical report prepared by Calspan Corporation on a portion of a multi-phase program sponsored by the Air Force Aeropropulsion Laboratory, Air Force Systems Command, Wright-Patterson Air Force Base, Ohio, under Contract F33615-79-C-2023. The work reported herein was performed as part of Project 3066, "Rotating Stall Investigations", with Mr. Marvin A. Stibich, AFWAL/POTX, as Project Engineer. Dr. Gary R. Ludwig of the Aerodynamic Research Department of Arvin/Calspan Advanced Technology Center, had overall technical responsibility for the program, and carried out the experimental measurements. The theoretical studies of rotating stall were performed by Dr. Jospeh P. Nenni and Dr. Gregory F. Homicz.

The authors are indebted to Drs. John A. Lordi and William J. Rae for numerous technical discussions regarding this work and to Mr. John R. Moselle for his invaluable assistance in programming the equations.

TABLE OF CONTENTS

Section		Page
I	INTRODUCTION	1
II	EULER CODE DEVELOPMENT	5
	1. INTRODUCTION	5
	2. BASIC FORMULATION	7
	3. TRANSFORMATION AND METRICS	13
	4. BOUNDARY AND INITIAL CONDITIONS	16
	5. NUMERICAL EXPERIENCE WITH CODES	19
	6. KUTTA CONDITION	21
	7. CONCLUDING REMARKS	22
III	TWO-DIMENSIONAL STABILITY THEORY	24
	1. INTRODUCTION	24
	2. TWO BLADE ROW ANALYSIS	24
	3. RESULTS	34
	4. CONCLUDING REMARKS	38
IV	THREE-DIMENSIONAL UNSTEADY LIFTING SURFACE THEORY FOR A ROTOR	39
	1. FLOW MODEL	39
	2. LOADING EXPANSION	40
	3. RADIAL INTEGRALS	41
	4. AXIAL INTEGRALS	43
	5. GOVERNING EQUATION	45
	6. ACOUSTIC FARFIELD	50
	7. CODE DEVELOPMENT	55
	8. NUMERICAL RESULTS	56
V	SUMMARY AND CONCLUSIONS	59
	REFERENCES	61
	APPENDIX A: EVALUATION OF AXIAL INTEGRALS	65
	APPENDIX B: GOVERNING INTEGRAL EQUATION	77

LIST OF ILLUSTRATIONS

Figure		Page
1	Computational Domain	79
2	Computational Grid in Physical Plane for TW-1 Cascade Solidity, σ = 1.16	80
3	Computational Grid in Physical Plane NACA 65(12) 10 Cascade Solidity, σ = 1.0	81
4	Surface Pressure Distribution for TW-1 Cascade	82
5	Surface Pressure Coefficient for TW-1 Cascade	83
6	Surface Pressure Distribution for NACA 65(12) 10 Cascade	84
7	Surface Pressure Coefficient for NACA 65(12) 10 Cascade	85
8	Surface Pressure Distribution for NACA 65(12) 10 Cascade	86
9	Surface Pressure Distribution NACA 65(12) 10 Cascade With Exit Conditions Specified	87
10	Surface Pressure Distribution of NACA 65(12) 10 Cascade	88
11	Surface Pressure Distribution NACA 65(12) 10 Cascade	89
12	Surface Pressure Distribution NACA 65(12) 10 Cascade With and Without Kutta Condition	90
13	Surface Pressure Distribution NACA 65(12) 10 Cascade With and Without Kutta Condition	91
14	Finite Thickness Model for Two Blade Row Theory	92
15	Theoretical Stability Characteristics of Stator Set No. 4, Single Blade Row Theory	93
16	Theoretical Propagation Velocities for Stator Set No. 4, Single Blade Row Theory	94
17	Theoretical Stability Characteristics of Rotor No. 1, Single Blade Row Theory	95
18	Theoretical Propagation Velocities of Rotor No. 1, Single Blade Row Theory	96
19	Theoretical Stability Characteristics of Rotor-Stator Stage, Stator Stagger Angle, δ_{SM}=37.2 deg	97
20	Influence of Axial Mach No. on Stage Stability Characteristics, of Rotor-Stator Stage; δ_{SM}=28.2°, n=1	98
21	Influence of Axial Mach No. on Stage Stability Characteristics of Rotor-Stator Stage; δ_{SM}=37.2°, n=1	99
22	Effects of Blade Row Spacing at M_1=0.4, δ_{SM}=28.2°, n=1	100
23	Rotor Geometry and Coordinate System	101
24	Comparison of Present Theory Versus 2-D Strip Theory For a High Hub/Tip Ratio, Low Solidity, Low Speed Blade Row	102
25	Comparison of Present Theory Versus 2-D Strip Theory For Case With Nearly Constant Circulation	103

SECTION I
INTRODUCTION

The optimum performance of a turbo-propulsion system is usually achieved when the compressor is operating near its maximum pressure ratio. However, this optimum is generally not attainable because it occurs close to compressor stall and unstable flow conditions. In actual operation, a stall margin must be provided to prevent the compressor from penetrating the stall boundary and developing destructive unsteady flow phenomena such as rotating stall and surge. This is usually done by prescheduling the engine controls. When an aircraft has a varied flight envelope, the prescheduling approach can lead to the requirement for a large stall margin to keep the engine out of stall under all possible transient and steady flight conditions. This stall margin represents a significant performance penalty. Also, in many instances of engine failure, rotating stall has been identified as a precursor to destructive unsteady flows in an engine. Furthermore, blade fatigue considerations will not allow a compressor to operate for prolonged periods in a large amplitude rotating stall mode. Clearly then, it is desirable to develop methods of estimating the stall boundaries of a compressor and if possible to develop an engine control system that can sense incipient destructive unsteady flows in a compressor and take corrective action to prevent compressor stall. Recognition of these goals has been the motivation for a continuing program of research that the Aeropropulsion Laboratory has sponsored at Calspan since 1962. The last program at Calspan was carried out under Contract No. F33615-76-C-2092 and the results are reported in Refs. 1 through 3.

The work at Calspan has been both theoretical and experimental in nature and has been aimed at obtaining a sufficient understanding of the rotating stall phenomenon such that its onset and its properties can be predicted and controlled. Demonstrated progress has been made toward these goals in that a theory has been developed which is capable of predicting inception of rotating stall on a high hub-to-tip ratio compressor stage (rotor plus stator) in low speed flows (provided that the appropriate steady state blade row performance

data are available). In addition, a prototype rotating stall control system has been designed and demonstrated successfully by tests conducted by Calspan on a J85-5 turbojet engine and by the Air Force Aero Propulsion Laboratory on a J85-13 turbojet engine.

The latest three-year program has the objectives of (1) develop an analysis for a three-dimensional time-variant rotating stall and separation theory, (2) develop analyses for post-stall operation/recovery and aerodynamically induced exotic metal combustion and (3) consider the effects of distortion, water ingestion, and nuclear blasts on axial flow compressors. The work done towards accomplishing objective (1) is reported on herein. The work done towards the accomplishments of the remaining objectives are reported in Volume 2 of this report.

The theoretical work performed under the present program was aimed at developing methods of analysis to predict the unsteady, viscous, three-dimensional flow through a blade row. The effects of viscosity and unsteadiness were considered separately. Thus the attempt was to develop a three-dimensional, steady-flow theory to predict the turning and loss performance of a blade row and a method to estimate the lossless unsteady, three-dimensional flow through a blade row due to inlet distortion.

Past correlations made with the small disturbance stability theory in incompressible flows have shown that if the steady-state loss and turning performance of a blade row or stage are known, the rotating stall inception boundary could be predicted quite accurately. Moreover, the two-dimensional stability theory worked well for distinctly three-dimensional flows if radially averaged blade row performance was used. Consequently, the theoretical work under this program concentrated on extending the stability theory to compressible flow and initiating the development of methods to predict the loss and turning performance of viscous flow through blade rows. A version of the stability theory applicable to a single blade row in two-dimensional compressible flow had been previously formulated[3], but no results were presented. This analysis was extended to consider two blade rows and was implemented into a computer code.

The basic philosophy that was chosen to analyze the viscous flow through a blade row was to split the flow into an inviscid region and a viscous boundary layer. The two flows were to be calculated simultaneously. It was thought that this was a more feasible task than trying to solve the Reynolds averaged Navier-Stokes equations directly. Because of the important rotational effects introduced by the blade row when large turning is involved, the Euler equations were used to describe the inviscid parts of the flowfield. Unfortunately, it was found at the beginning of the present program that the state of the art for calculating numerical solutions to the Euler equations for the flow through blade rows was not sufficient to support the overall goals of the program. In fact, two-dimensional and three-dimensional Euler code solutions for cascades are only recently emerging in the open literature. Furthermore, the majority of these schemes are explicit time marching schemes that are extremely long running codes that make it impractical to incorporate an interacting boundary layer.

The approach that was followed in the present program to calculate the inviscid flow was to complete the development of an implicit time marching Euler code that was initiated under AFOSR sponsorship.[4,5] The two-dimensional version of this code has now been developed for cases of subsonic relative inflow where either a Kutta condition is specified at the blade trailing edges or the conditions at downstream infinity are specified. The inclusion of a Kutta condition proved to be particularly troublesome and consumed so much effort that inclusion of an interacting boundary layer was not feasible under the present program. However, now that this problem is solved, the extension of the code to three dimensions is straightforward although a viable algorithm for incorporating an interactive boundary layer is yet to be developed.

The work on analysis of the unsteady flow through a blade row was initially approached from two viewpoints. The specific problem of interest was the response of a blade row to inlet distortion. The first approach was the completion of the linearized, unsteady, lifting-surface theory that was initiated under a previous program.[2] Also considered was the development of a nonlinear transonic theory that would account for finite blade thickness and loading effects. However, after some study it was realized that the time marching Euler code being

developed for the prediction of steady state performance could also handle the unsteady distortion problem if the boundary conditions at infinity and the spatially periodic boundary conditions are modified to show the appropriate time varying behavior. Hence this work was expended on the Euler code development and every effort was made to keep the resulting code time accurate (i.e., to make the calculations follow the actual flow development with time).

The Euler code development is described in Section II. The two-dimensional stability theory work is described in Section III and the unsteady lifting surface theory is described in Section IV.

SECTION II
EULER CODE DEVELOPMENT

1. INTRODUCTION

The present algorithm that has been developed to calculate the inviscid flow through a blade row consists of two computer codes. The first code generates a boundary-fitting coordinate system that maps the physical blade row and flow under consideration into a box-like computational domain. This greatly facilitates the application of blade surface boundary conditions and the specification (or calculation) of flow conditions at infinity upstream and downstream of the blade row. The basic mapping method used is a modification of one due to Ives and Liutermoza.[6] The modifications concern the final destination of the blade surface and the points at infinity which were assigned similarly to Dulikravich.[7,8] The mapping code writes the metrics on a tape which is input into the second code. The second code integrates the transformed Euler equations in the computational domain and applies the appropriate boundary conditions. The basic integration method is an implicit time marching scheme that uses approximate factorization. The steady state solution is obtained as the long time limit of an unsteady problem with steady boundary conditions. This integration scheme was developed for external aerodynamic problems and is most clearly described in a series of papers by Beam and Warming.[9,10] This integration scheme was selected, originally, because it was judged to be the most promising in terms of computational efficiency and running time of any of the methods then available and it is still thought to be a leading candidate from this viewpoint. The explicit time marching codes require much longer running times because of the CFL stability requirements on time step size.

The development of both codes used in the present program was initiated under an AFOSR sponsored program and the status of the codes at the end of that program is reported in Refs. 4 and 5. At that time, the integration code was not converging and the reason suspected was the singular behavior of the metrics of the transformation at the blade trailing edge. This problem was solved and made little difference in the results. The critical points turned out to be the analytical method that was being used to calculate the metrics in general, the time differencing scheme being used, and the method of evaluating

quantities on the blade surfaces. In addition, after the code was revised to include these points and produced converged results, it was found that a revised treatment of the numerical viscosity term eliminated undesirable spatial oscillations that appeared in the initial calculation. All of these points have been cleared up satisfactorily and the integration code works over a range of subsonic relative inlet conditions with either a Kutta condition specified or the conditions at downstream infinity specified. Global conservation of mass flow is not a problem with the present code in contrast to other published results of Euler codes.[11]

The overall algorithm developed here is time accurate except for the treatment of the inlet and outlet conditions. This feature was deliberately maintained so that the code would only require slight modification in order to consider the response of the blade row to unsteady inlet distortion. Thus, several techniques that have been used on time marching schemes to speed the approach to the steady state limit have been avoided in order to maintain the time accuracy.

The basic analysis upon which the present codes are based is given in Refs. 4 and 5. In order to fully explain the critical points mentioned above and to give a coherent description of the existing codes, it will be necessary to duplicate some of the material contained in the earlier references. Also, because the coordinate mapping used influences the manner in which the boundary conditions are applied, it is not possible to separate totally the discussion of the mapping from the discussion of the integration scheme. Thus the basic part of the discussion will be dealing with the Euler equations written in a general curvilinear coordiate system with a subsection on the particular coordinate transformation that was used. In addition, the basic analysis was originally performed for three-dimensional flow and this point of view is continued here even though only the two dimensional analysis has been fully implemented into the code.

2. BASIC FORMULATION

The geometry of concern and an axially symmetric coordinate system in physical space are shown in the following sketch.

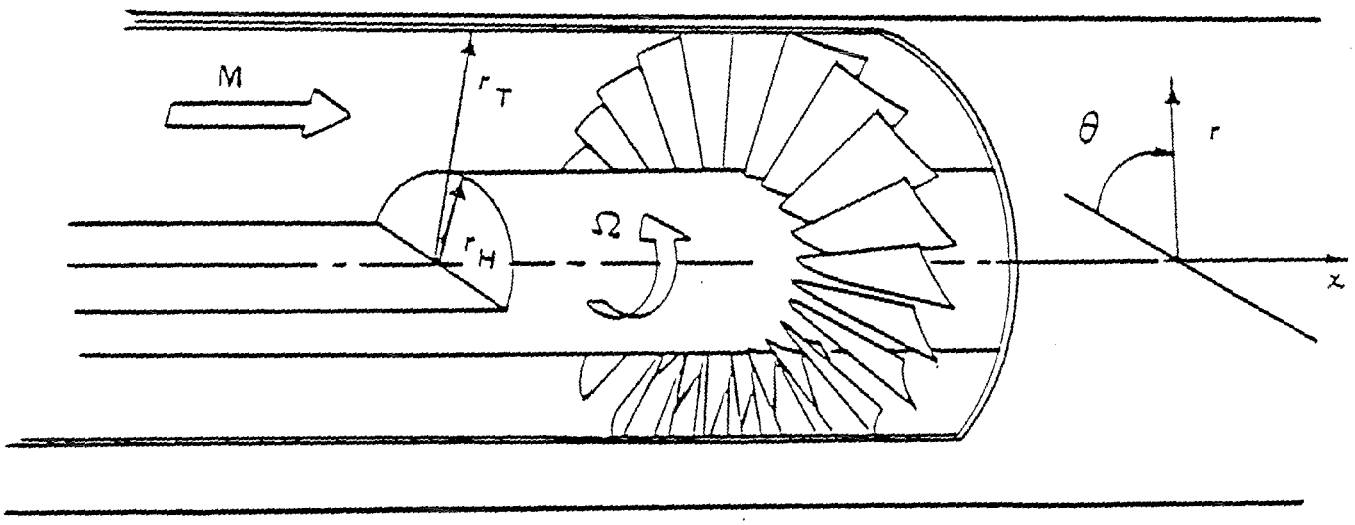

SKETCH OF COORDINATE SYSTEM IN PHYSICAL SPACE

As shown in Ref. 4, the Euler equations for the inviscid flow through a blade row may be written in a cylindrical coordinate system fixed to the blades as

$$\frac{\partial U}{\partial t} + \frac{\partial E}{\partial x} + \frac{\partial F}{\partial r} + \frac{1}{r}\frac{\partial G}{\partial \theta} = \frac{H-E}{r}$$

where

$$U = \begin{bmatrix} \rho \\ \rho W_x \\ \rho W_r \\ \rho W_\theta \\ K \end{bmatrix} ; \quad E = \begin{bmatrix} \rho W_x \\ p + \rho W_x^2 \\ \rho W_x W_r \\ \rho W_x W_\theta \\ W_x (K+p) \end{bmatrix} ; \quad F = \begin{bmatrix} \rho W_r \\ \rho W_x W_r \\ p + \rho W_r^2 \\ \rho W_r W_\theta \\ W_r (K+p) \end{bmatrix} \qquad (1)$$

$$G = \begin{bmatrix} \rho W_\theta \\ \rho W_x W_\theta \\ \rho W_r W_\theta \\ p + \rho W_\theta^2 \\ W_\theta (K + p) \end{bmatrix} \quad ; \quad H = \begin{bmatrix} 0 \\ 0 \\ p + \rho (W_\theta + r\omega)^2 \\ -\rho W_r (2\omega r + W_\theta) \\ 0 \end{bmatrix}$$

and where

ρ	is the density
p	is static pressure
W_x, W_r, W_θ	are respectively the axial, radial and circumferential velocities in the system fixed to the blades
ω	is the rotation rate of the blade row
γ	is the specific heat ratio

$$K = \frac{p}{\gamma - 1} + \frac{\rho}{2} \left[W_x^2 + W_r^2 + W_\theta^2 - r^2 \omega^2 \right]$$

A general transformation of geometric coordinates is introduced

$$\xi = \xi(x, r, \theta) \quad , \quad \eta = \eta(x, r, \theta) \quad , \quad \zeta = \zeta(x, r, \theta)$$

where the surface $\zeta = 0$ will eventually be the blade surfaces and η will be the radial variable. The Jacobian of the transformation is defined as

$$\mathcal{D} \equiv \frac{\partial(\xi, \eta, \zeta)}{\partial(x, r, \theta)} = \begin{vmatrix} \xi_x & \xi_r & \xi_\theta \\ \eta_x & \eta_r & \eta_\theta \\ \zeta_x & \zeta_r & \zeta_\theta \end{vmatrix}$$

where the subscripts stand for partial differentiation.

Following Viviand,[12] it is possible to redefine the dependent variables in such a fashion that the transformed Euler equations retain the same semi-conservation form as Eq. (1). This is accomplished by defining the following quantities:

$$\hat{U} = \frac{U}{\mathcal{D}} \quad , \quad \hat{E} = \frac{1}{\mathcal{D}}\left[\xi_x E + \xi_r F + \frac{\xi_\theta G}{r} \right]$$

$$\hat{F} = \frac{1}{\mathcal{D}}\left[\eta_x E + \eta_r F + \frac{\eta_\theta G}{r} \right]$$

$$\hat{G} = \frac{1}{\mathcal{D}}\left[\zeta_x E + \zeta_r F + \frac{\zeta_\theta G}{r} \right]$$

$$\hat{H} = \frac{H - F}{r\mathcal{D}}$$

Then Eq. (1) becomes

$$\frac{\partial \hat{U}}{\partial t} + \frac{\partial \hat{E}}{\partial \xi} + \frac{\partial \hat{F}}{\partial \eta} + \frac{\partial \hat{G}}{\partial \zeta} = \hat{H} \tag{2}$$

Next, following Beam and Warming[9], the time differencing scheme is considered. Let the superscript "n" denote the time step; then Taylor series expansion may be used to show

$$\hat{U}^{n+1} = \hat{U}^{n} + \Delta t\left[\alpha \left(\frac{\partial \hat{U}}{\partial t}\right)^{n} + (1-\alpha)\left(\frac{\partial \hat{U}}{\partial t}\right)^{n+1} \right]$$

$$+ \; O\left(\left(\alpha - \tfrac{1}{2}\right)\Delta t^2 \right) \tag{3}$$

When $\alpha = \frac{1}{2}$, this is known as trapezoidal differencing, when $\alpha = 0$ it is known as Euler implicit, when $\alpha = 1$ it is known as Euler explicit. Clearly when $\alpha = 1/2$ the greatest time accuracy is achieved as seen from the error term. Eq. (2) will eventually be used to replace the time derivatives which appear in the right-hand side of Eq. (3); but, some preliminary work is required in order to end up with a scheme that minimizes the computations. First, use is made of the homogeneity property of the matrices appearing in Eq. (2), that is, they may be expressed as

$$\begin{aligned} \hat{E} &= \hat{A}\,\hat{U} \\ \hat{F} &= \hat{B}\,\hat{U} \\ \hat{G} &= \hat{C}\,\hat{U} \\ \hat{H} &= \hat{D}\,\hat{U} \end{aligned}$$

where

$$\hat{A} = \frac{\partial \hat{E}}{\partial \hat{U}} \; ; \; \hat{B} = \frac{\partial \hat{F}}{\partial \hat{U}} \; ; \; \hat{C} = \frac{\partial \hat{G}}{\partial \hat{U}}$$

and

$$\hat{D} = \frac{\partial \hat{H}}{\partial \hat{U}}$$

This property allows a time linearization, at least to the order of Eq. (3), for then by Taylor series expansion one obtains

$$\hat{E}^{n+1} = \hat{E}^{n} + \hat{A}^{n}(\hat{U}^{n+1} - \hat{U}^{n}) + O(\Delta t^{2}) \tag{4a}$$

$$\hat{F}^{n+1} = \hat{F}^{n} + \hat{B}^{n}(\hat{U}^{n+1} - \hat{U}^{n}) + O(\Delta t^{2}) \tag{4b}$$

$$\hat{G}^{n+1} = \hat{G}^{n} + \hat{C}^{n}(\hat{U}^{n+1} - \hat{U}^{n}) + O(\Delta t^{2}) \tag{4c}$$

$$\hat{H}^{n+1} = \hat{H}^{n} + \hat{D}(\hat{U}^{n+1} - \hat{U}^{n}) + O(\Delta t^{2}) \tag{4d}$$

Introducing the new independent variable $\Delta \hat{U}^n = \hat{U}^{n+1} - \hat{U}^n$ the combination of Eqs. (1), (3) and (4) can be put in the so-called "delta form"

$$\left\{ I + \Delta t (1-\alpha)\left(\frac{\partial \hat{A}^n}{\partial \xi} + \frac{\partial \hat{B}^n}{\partial \eta} - \hat{D}^n + \frac{\partial \hat{C}^n}{\partial \zeta} \right) \right\} \Delta \hat{U}^n =$$

$$- \Delta t \left(\frac{\partial \hat{E}^n}{\partial \xi} + \frac{\partial \hat{F}^n}{\partial \eta} + \frac{\partial \hat{G}^n}{\partial \zeta} - \hat{H}^n \right) + O\left((\alpha - \tfrac{1}{2})\Delta t^2\right) \tag{5}$$

where I is the identity matrix and differentials operate on all products formed to their right. That is, the first differential expression appearing on the left hand side of Eq. (5) should be interpreted as $\frac{\partial}{\partial \xi}(\hat{A}^n \Delta \hat{U}^n)$. Adding terms of order Δt^3 to the left hand side of Eq. (5), the following approximate factorization is achieved:

$$\left(I + (1-\alpha)\Delta t \frac{\partial}{\partial \xi} \hat{A}^n \right) \Delta \hat{U}^{**n} = -\Delta t \left(\frac{\partial \hat{E}^n}{\partial \xi} + \frac{\partial \hat{F}^n}{\partial \eta} + \frac{\partial \hat{G}^n}{\partial \zeta} - \hat{H}^n \right) \tag{6a}$$

$$\left(I + (1-\alpha)\Delta t \left(\frac{\partial \hat{B}^n}{\partial \eta} - \hat{D}^n \right) \right) \Delta \hat{U}^{*n} = \Delta \hat{U}^{**n} \tag{6b}$$

$$\left(I + (1-\alpha)\Delta t \frac{\partial}{\partial \zeta} \hat{C}^n \right) \Delta \hat{U}^n = \Delta \hat{U}^{*n} \tag{6c}$$

This system has the same time accuracy as Eq. (5).

This factorization effectively decouples the original three-dimensional equation (Eq. (5)) into a sequence of three one-dimensional equations (Eq. (6)) which allows a great reduction and simplification of the following computations. When central differencing is used for the spatial derivatives, second order accuracy in the spatial variables is obtained. However, it has generally been found necessary to add numerical viscosity terms to this system of equations in order to prevent the occurence of spatial oscillations which can destroy the validity of the solution. The actual system of equations solved is then

$$\left(I + (1-\alpha)\Delta t \frac{\partial}{\partial \xi}\hat{A}^n - \epsilon_A \frac{(\Delta \xi)^2}{\mathcal{D}} \frac{\partial^2}{\partial \xi^2}\mathcal{D}\right)\Delta \hat{U}^{**n} = -\Delta t\left(\frac{\partial \hat{E}^n}{\partial \xi} + \frac{\partial \hat{F}^n}{\partial \eta} + \frac{\partial \hat{G}^n}{\partial \zeta} - \hat{H}^n\right) - \frac{\epsilon_B}{\mathcal{D}}(\Delta \xi)^4 \frac{\partial^4}{\partial \xi^4}(\mathcal{D}\hat{U}^n) \tag{7a}$$

$$\left(I + (1-\alpha)\Delta t\left(\frac{\partial \hat{B}^n}{\partial \eta} - \hat{D}^n\right) - \frac{\epsilon_A (\Delta \eta)^2}{\mathcal{D}} \frac{\partial^2}{\partial \eta^2}\mathcal{D}\right)\Delta \hat{U}^{*n} = \Delta \hat{U}^{**n} - \frac{\epsilon_B}{\mathcal{D}}(\Delta \eta)^4 \frac{\partial^4}{\partial \eta^4}(\mathcal{D}\hat{U}^n) \tag{7b}$$

$$\left(I + (1-\alpha)\Delta t \frac{\partial}{\partial \zeta}\hat{C}^n - \epsilon_A \frac{(\Delta \zeta)^2}{\mathcal{D}} \frac{\partial^2}{\partial \zeta^2}\mathcal{D}\right)\Delta \hat{U}^n = \Delta \hat{U}^{*n} - \frac{\epsilon_B}{\mathcal{D}}(\Delta \zeta)^4 \frac{\partial^4}{\partial \zeta^4}(\mathcal{D}\hat{U}^n) \tag{7c}$$

Where ϵ_A is the implicit numerical viscosity coefficient and ϵ_B is the explicit numerical viscosity coefficient. In the application of this method to external aerodynamic problems,[13,14] all of the explicit damping terms were appended to the first factorization. However, better results were obtained in the present investigation by associating the explicit damping term in a given direction with the approximate factorization in that direction.

Generally the numerical viscosity coefficients are chosen to be of order Δt with ϵ_A chosen to be twice ϵ_B after the stability analysis performed by Desideri.[15] When central difference expressions are used for the spatial derivatives, Eqs. (7a), (7b) and (7c) each represent a block tri-diagonal system of equations which is solved using the Thomas algorithm.[16] The order of each system and the number of times it must be solved depend upon the size of the computational grid used. The subcase of two dimensional flow is obtained by ignoring the η factorization in the preceeding analysis.

3. TRANSFORMATION AND METRICS

As previously mentioned, the purpose of transforming coordinate systems is to map the actual complex, three-dimensional geometry of the blade row and flow field into a box-like computational domain where blade surface boundary conditions are easily applied.

With reference to the previous sketch, mapping starts from a cylindrical coordinate system in the physical space, (r, θ, x) where r is along the blade span and x is in the downstream axial flow direction. First, the geometry of the axisymmetric flow passage is used to define a fractional distance between hub and tip. Let

$$\eta = \frac{r - r_H(x)}{r_T(x) - r_H(x)}$$

where $r_H(x)$ is the hub (inner) radius of the passage and $r_T(x)$ is the tip (outer) radius of the passage. The intersection of the blade surfaces with

surfaces of constant η defines a two-dimensional cascade with x and θ as coordinates. This cascade is ultimately mapped to a rectangle in ξ-ζ space as shown in Fig. 1 In this figure, K is the index in the ξ direction and L is the index in the ζ direction. The figure depicts the case for a 10 by 40 grid which was used throughout code development. The mapping is patterned after the work of Ives and Liutermoza[6] with the exception of the last step. The mapping consists of a sequence of six conformal transformations followed by a shearing of coordinates such that the blades end up along the bottom of the computational domain and the points at infinity end up along the top of the computational domain. (This is a feature of the mappings used by Dulikravich.[7,8]) All steps except the last one are performed as reported in Ref. 7.

The important features of the transformation used here are that the cascade blade trailing edges and the points at downstream infinity (far downstream of the blade row) map to the corners of the computational domain. The metrics are singular at these points. However, since these points are located at the corners one avoids the need to evaluate the difference equations containing the metrics. Any information required in the scheme at these points is found by extrapolation or averaging from the neighboring points.

Two different cascade geometries have been used in the program development. The first cascade blade is that given in Ref. 17. It is a relatively fat, blunt blade shape with high solidity, σ , and is here denoted as TW-1. The blade shape and the boundary conforming coordinate mesh are shown in the physical plane in Fig. 2. Only one blade is shown and the width of the mesh corresponds to the blade spacing in the cascade. This type of boundary conforming coordinate system is generally referred to as an "O" coordinate system because the ζ equal to constant lines close on themselves downstream of the blade. This blade shape is not a practical aerodynamic shape but was merely chosen in Ref. 17 as a demonstration case whose ordinates were easily defined. It does, however, represent a severe test for any numerical method because of its extreme thickness and high solidity. Hence it was retained here for initial development purposes. In addition, a more conventional cascade, the NACA 65(12)10

with solidity of 1 was chosen for preliminary investigation. The ordinates for this blade shape are given in Ref. 18. Transonic calculations for this cascade are aslo given in Ref. 16. The blade shape and boundary conforming coordinate mesh for this cascade in the physical plane are shown in Fig. 3.

In Ref. 5, the metrics were calculated analytically by application of the chain rule to the intermediate transformations. As such, the metrics will not satisfy the finite difference form of Eq. (7) exactly when the flow is uniform. Although the error is theoretically second order or higher in the spatial differences, it produces a distributed source-like effect which evidently accumulates errors to result in divergence of the calculations after only a few time steps. This problem was solved by calculating the metrics numerically by use of the same spatial difference scheme that is used to discretize the Euler equations. Then the metrics satisfy the equation exactly and the source-like effects are avoided. The metrics are calculated directly from the coordinates themselves by using either central differences or the appropriate one-sided differences along the boundary of the computational domain. The appropriate expressions used are:

$$\xi_x = (r_\eta \theta_\zeta - r_\zeta \theta_\eta) / \mathcal{D}^{-1}$$

$$\eta_x = (r_\zeta \theta_\xi - r_\xi \theta_\zeta) / \mathcal{D}^{-1}$$

$$\zeta_x = (r_\xi \theta_\eta - r_\eta \theta_\xi) / \mathcal{D}^{-1}$$

$$\xi_r = (\theta_\eta x_\zeta - \theta_\zeta x_\eta) / \mathcal{D}^{-1}$$

$$\eta_r = (\theta_\zeta x_\xi - \theta_\xi x_\zeta) / \mathcal{D}^{-1}$$

$$\zeta_r = (\theta_\xi x_\eta - \theta_\eta x_\xi) / \mathcal{D}^{-1}$$

$$\xi_\theta = (x_\eta r_\zeta - x_\zeta r_\eta) / \mathcal{D}^{-1}$$

$$\eta_\theta = (x_\zeta r_\xi - x_\xi r_\zeta) / \mathcal{D}^{-1}$$

$$\zeta_\theta = (x_\xi r_\eta - x_\eta r_\xi) / \mathcal{D}^{-1}$$

where

$$\mathcal{D}^{-1} \equiv \frac{\partial(x, r, \theta)}{\partial(\xi, \eta, \zeta)} = \frac{1}{\mathcal{D}}$$

is the Jacobian of the transformation.

The problem with the metrics is essentially the same problem as maintaining the proper free stream conditions in external flow calculations. This problem is discussed by Pulliam and Steger,[13] but they indicate that the problem is not critical for external aerodynamic calculations. Evidently, the boundary conditions on the external aerodynamics problem make it a more forgiving algorithm.

4. BOUNDARY AND INITIAL CONDITIONS

With the exception of the corner grid points in the transformed computational domain, initial conditions at $t = 0$ are needed at all grid points and boundary conditions are needed at each time step for grid points along the boundary of the computational domain. First of all, the boundary conditions will be discussed starting with conditions on the blade surfaces.

The general treatment of the boundary conditions follows Refs. 10 and 11. While evaluating field points $\Delta\hat{U}$ is held at zero on the boundaries, then $\hat{U}$ is explicitly updated before proceeding on to the next time step calculation of $\Delta\hat{U}$. Along the blade, surface flow tangency is imposed by considering the components of the velocity vector in the computational domain. They are defined as

$$W_1 = \xi_x W_x + \xi_r W_r + \frac{\xi_\theta}{r} W_\theta \tag{8a}$$

$$W_2 = \eta_x W_x + \eta_r W_r + \frac{\eta_\theta}{r} W_\theta \tag{8b}$$

$$W_3 = \zeta_x W_x + \zeta_r W_r + \frac{\zeta_\theta}{r} W_\theta \tag{8c}$$

These definitions become a system of equations suitable for determining w_x, w_r, and w_θ on the surface when $w_3 = 0$ is imposed and extrapolated values of w_1 and w_2 are used. The value of surface pressure is found from the following expression derived in Ref. 4.

$$\frac{\partial p}{\partial \xi}\left(\zeta_x \xi_x + \zeta_r \xi_r + \frac{\zeta_\theta \xi_\theta}{r^2}\right) + \frac{\partial p}{\partial \eta}\left(\zeta_x \eta_x + \zeta_r \eta_r + \frac{\zeta_\theta \eta_\theta}{r^2}\right)$$

$$\frac{\partial p}{\partial \zeta}\left(\zeta_x^2 + \zeta_r^2 + \frac{\zeta_\theta^2}{r^2}\right) = \frac{\rho \zeta_r}{r}\left(w_\theta + r\omega\right)^2 - \frac{\zeta_\theta}{r^2}\rho w_r\left(w_\theta + 2\omega r\right)$$

$$- \rho w_1\left(\zeta_x \frac{\partial w_x}{\partial \xi} + \zeta_r \frac{\partial w_r}{\partial \xi} + \frac{\zeta_\theta}{r}\frac{\partial w_\theta}{\partial \xi}\right) - \rho w_2\left(\zeta_x \frac{\partial w_x}{\partial \eta} + \frac{\partial w_r}{\partial \eta} + \frac{\zeta_\theta}{r}\frac{\partial w_\theta}{\partial \eta}\right) \tag{9}$$

As explained in Ref. 4, this equation is derived from the momentum equations and the continuity equation without benefit of the energy equation. The equation has the desirable quality that it does not contain any time derivatives. After all of the quantities on the right-hand side of the equation are determined either by the solution of Eqs. (8) or extrapolation, Eq. (9) may be integrated implicitly to determine surface pressures. (In Ref. 4, this equation was integrated explicitly. However, it was determined that this was introducing an instability into the algorithm.) Then sufficient information is known to calculate $\hat{U}$ on the blade surfaces. For the subcase of two dimensional flow, we have $w_2 = 0$ and η derivatives are neglected. This drastically simplifies the solution of Eqs. (8) and (9). For three-dimensional flows, an equation analogous to Eq. (9) is given in Ref. 4, and $w_2 = 0$ is used in Eq. (8) along with extrapolated values for w_1 and w_3 to provide sufficient relations to determine $\hat{U}$ at the hub and shroud boundaries.

The remainder of this discussion deals with the two-dimensional case. The lines K = 1 and K = 40 are the same line in the physical plane (see Figs. 2 and 3) and $\hat{U}$ is determined on these lines by averaging quantities at fixed L values from the lines K = 2 and K = 39 (with the exception of the values at L = 1, 2, 9 and 10 whose treatment depends upon whether the Kutta condition is applied or not). The line L = 10 corresponds to the periodic boundary in the physical plane so that these values must be symmetric about the $\xi = 0$ point (or the midpoint). The proper symmetry is obtained by averaging from the proper points on the line L = 9. For instance, the values at K = 3, L = 10 are obtained by averaging from the values at K = 3, L = 9 and K = 37, L = 9 and assigning the averaged values to the point K = 37, L = 10 also. These averagings along the boundary are performed once for each time step after the interior field points have been calculated.

The treatment of the inlet and outlet conditions that are used in the present investigation would appear to constitute an overspecification of the problem if the point of view appearing in Refs. 19 and 20 is adopted. These references present an argument for specifying three out of the four dependent variables at the inlet and one out of the four dependent variables at the outlet. These arguments are based upon consideration of the origin of the characteristic lines that pass through a given point on the upstream or downstream calculation boundary. The unknown quantities at each boundary are then to be solved for by using the compatibility relation along the characteristics that pass through each grid point on the boundary. It would appear that the definitive analysis of the proper boundary conditions to apply would involve applying a radiation condition at each boundary. Although preliminary analysis along these lines have appeared,[21,22] this approach has not been fully implemented. Moreover, several methods of specifying inlet and outlet conditions appear to produce converged results. With this situation prevailing, it was decided to investigate the simplest conditions first and to choose the easiest, most computationally economical boundary conditions to apply. In this vein, the conditions that apply in the steady state limit have proved satisfactory and are described in the following.

In all cases, the inlet conditions at $-\infty$ are completely assigned. This corresponds to assigning all the components of $\hat{U}$ at L = 10, K =20 and 21 (a common value for all time steps). In cases where the outlet conditions are fixed, the outlet conditions are calculated from an assigned static pressure ratio and use of the isentropic relationship, the steady state continuity equation, and the specified inlet conditions. These calculated outlet values are applied at the points K = 1, L = 9 and K = 2, L = 10 and also at the corresponding points K = 40, L = 9 and K = 39, L = 10. In cases when the outlet condition is fixed, no flow quantities are calculated at the trailing edges of the blades, i.e., at L = 1, K = 1 and 40.

In cases when a Kutta condition is applied, the conditions at the trailing edge are calculated by averaging the values at neighboring points on the blade surface and one step above (i.e., L = 2 neighbors). This value is also assigned at the points L = 2, K = 1 and 40. The outlet condtions at K = 2, L = 10 are found by requiring no gradient in the streamwise direction to exist at this point. These values are also assigned at K = 1, L = 9 and the corresponding points K = 39, L =10 and K = 40, L = 9. In addition, the outlet mass flow is preserved at each time step by assigning ρw_x the value it has at upstream infinity.

The initial conditions used correspond to those of uniform flow at the inlet conditions. The boundary conditions imposed on the blade surface also correspond initially to the same uniform flow and are gradually switched over to the correct boundary condition using an exponential function to smoothly transfer conditions. Generally about 50 to 100 time steps are required before the blade surface boundary conditions are fully applied.

5. NUMERICAL EXPERIENCE WITH CODES

The initial modifications made on the codes described in Refs. 4 and 5 were concerned with the metrics, the transformation of the points at infinity and the implicit calculation of blade surface boundary conditions. These modifications had the effect of greatly increasing the number of time steps before divergence occurred, but divergence still occurred!

Then the effect of the time differencing scheme used was investigated. In the original integration code, the trapezoidal differencing was used ($\alpha = 1/2$) because of its greater time accuracy. However, it was found that converged results could be obtained at the lower inlet Mach numbers with Euler implicit differencing ($\alpha = 0$). The results from these first converged calculations are shown in Figs. 4 through 7. In Fig. 4, the normalized surface pressure is plotted for the TW-1 cascade for several elapsed times after initiation of the calculations. The surface pressures are plotted as a function of K, the ξ index, in the computational plane. Inspection of Fig. 2 shows that $\Delta\xi$ is nearly constant in arc length along the blade surface so that Fig. 4 is nearly equivalent to unwrapping the blade surface shape and plotting surface pressure against arc length beginning at the trailing edge on the upper surface. The surface pressure is normalized by the product of free stream density and square of the free stream axial velocity. The calculation starts with blade boundary conditions that correspond to uniform flow in the physical plane (as if the blade were absent). The correct flow tangency boundary conditions are then gradually approached in an exponential fashion being fully applied after the first 100 time steps. The time steps are counted by the index IT with a nondimensional time increment between steps of $\Delta t = .005$. The real time is normalized by U/c where U is the undisturbed velocity in the axial direction far upstream of the blade row and c is the blade chord. A disturbance is then convected along one chord length at free stream conditions during a nondimensional time of unity. For the TW-1 cascade, there is still a very small time dependence for the surface pressure at the end points after 1800 steps, but all of the other points have settled out.

It can be seen that the basic character of the solution has been established after 300 time steps. The vast majority of calculation time is spend merely in refining the solution. For the case shown, where the relative inlet Mach number $M_i = 0.5$, there is evidently a shock on the upper surface, being smeared over a couple of mesh widths.

The surface pressure results for the NACA 65(12)10 cascade are shown in Figs. 6 and 7. The relative inlet Mach number is 0.5 and the relative inlet angle is 45°. Under these conditions, the flow is subcritical everywhere and

there are no shocks. This probably results in the quicker convergence to a steady state solution compared to the TW-1 cascade. Attempts to obtain converged results (with this early version of the integration code) for this blade row at an inlet Mach of .76 were unsuccessful. This problem was initially thought to be due to possible overspecification of the inlet and outlet conditions.

Further analysis of the numerical results reveals a slight loss in rothalpy,

$$I = \frac{\gamma}{\gamma-1}\frac{p}{\rho} + \frac{1}{2}\left(W_x^2 + W_\theta^2 - r^2\omega^2\right)$$

at the surface points near the leading edge. This is worse for the TW-1 blade row. However, the biggest failings of the calculation are spatial oscillations that occur near the trailing edge on the upper surface. These oscillations were removed by revising the numerical viscosity treatment as previously explained.

Results for the NACA 65(12)10 cascade using the revised numerical viscosity formulation are shown in Fig. 8 and the results are compared to those obtained with the original numerical viscosity formulation. It can be seen that the oscillations at the trailing edge were affecting the whole solution. In addition to smoothing the results near the trailing edge, it was found that converged solutions could be obtained at higher inlet Mach numbers over a range of pressure ratio. Examples of these calculations are shown in Figs. 9 through 11. These cases were run to compare with the results presented in Ref. 19. However, an exact comparison cannot be made because the calculation of Reference 19 contains the effects of a boundary layer. However, the present calculations show similar trends to those of Ref. 19. Moreover, it may be seen from Figs. 9, 10 and 11 that the surface pressure distribution is extremely sensitive to the prescribed pressure ratio, especially at the lower pressure ratio where there may be a shock on the lower surface.

6. KUTTA CONDITION

A number of schemes were investigated in order to incorporate the Kutta condition in the present algorithm. These included attempts to integrate

the Euler equations along the blade surface boundaries and/or along the K = 1, 40 boundaries in place of the previously described averaging and extrapolation techniques. Various end conditions at downstream infinity were also investigated. Generally the integration schemes seemed to go awry because there turn out to be conflicting requirements on the metrics in order to avoid producing source-like effects at the points adjacent to the corners of the computational domain. This dilemma arises because different one-sided differencing techniques than those used on the field points must be used on the boundaries in order to avoid the use of data at the corner points where the metrics are theoretically infinite.

It was found, however, that averaging along the K = 1 and 40 boundaries produced satisfactory results when the outlet mass flow was prescribed. In conjunction with these procedures, the conditions at K = 2, L = 10 could either be found by extrapolation or requiring no gradients in the streamwise direction. This later condition was the one selected for the final code configuration. Calculations resulting from this version of the Kutta condition are shown in Figs. 12 and 13 for inlet Mach numbers of .5 and .76 respectively. Also, as a consistency check on the code, the outlet conditions obtained from the case when the Kutta condition was applied were used as inputs for the case when downstream conditions are specified. These results are also shown in Figs. 12 and 13. For an inlet Mach number of .5, the correlation of the two calculations is good. The only significant differences appear in the vicinity of the trailing edge and as would be expected the application of a Kutta condition smooths the results in this region. The correlation of the two calculations at an inlet Mach number of .76 is also good. In this case, there is a shock on the upper surfaces of the blades. This shock is evidently very sensitive to any differences in the flow at the trailing edge as the correlation of the two calculations is slightly off in the shock vicinity.

7. CONCLUDING REMARKS

In summary, the two-dimensional version of the Euler code developed works well over a range of subsonic inlet conditions including cases where shock waves form in the blade passages. The code works with either a Kutta condition or conditions at downstream infinity specified. The integration code

requires approximately 2.5×10^{-3} seconds per grid point per time step on a Cyber 750 computing machine and requires 160,000 octal words of central memory. For the grid used which was 10 by 40 approximately, 800 to 1200 time steps were required to reach the steady state. The cases with shock waves required the longer times. The size of the time steps used correspond to Courant numbers of 5 to 10. The upper limit for convergence was not established; however, the results for an inlet Mach number of .76 appeared to suffer excessive rothalpy loss near the leading edge with the larger time step sizes. The results for an inlet Mach number of .5 did not show such effects so that computing times for these cases can probably be reduced substantially.

Although the basic integration methods used for the Euler euqations have been well publicized in the external aerodynamics literature, several modifications were found to be crucial in order to apply the method to internal flows. The calculation of the metrics of the transformation proves to be extremely important and a revision of the numerical viscosity treatment enlarges and enchances the domain where converged solutions can be obtained. In particular, it was found that the metrics must be discretized in the same spatial fashion as the governing partial differential equation in order to avoid introducing source-like terms which would quickly destroy the solution.

SECTION III
TWO DIMENSIONAL STABILITY THEORY

1. INTRODUCTION

A two dimensional stability theory to predict the rotating stall inception boundary for incompressible flow through an isolated blade row and stage (two blade rows) was presented in Ref. 24 and 25. Correlations of the theory with experiment on a number of blade rows and stages show that if the steady state loss and turning performance for each blade row of interest is known, the inception boundary for rotating stall can be predicted quite accurately. Basically the theory shows that geometric parameters such as solidity, blade chord, stagger angle, etc. influence the inception boundary and propogation speed via the fashion that these parameters influence the steady state performance of the blade row or stage. In the case of a stage, the blade row spacing determines the number of stall cells. Although the blade row performance data required as input by the theory is often not available, especially for compressible flow conditions, the extension of the theory to subsonic compressible flow has been accomplished so that qualitative trends may be obtained by using the incompressible blade row performance.

The extension of the theory to a single blade row in compressible flow was given in Ref. 26 and revised in Ref. 3. The revised theory was extended to two blade rows and numerical results were obtained under the present program. The results of these analyses will be given in the following sections.

2. TWO BLADE ROW ANALYSIS

The same general type of analysis as used in the single blade row case[3] has been applied to the two blade row problem. The blade rows are modeled by finite-thickness actuator sheets as shown in Fig. 14. There are now three flow regions designated by i = 1, 2 and 3, and the flow quantities are broken into mean time-independent and time-dependent parts as follows:

Axial velocity: $\tilde{U}_i(x,y,t) = U_i + u_i(x,y,t)$

Tangential velocity: $\tilde{W}_i(x,y,t) = W_i + w_i(x,y,t)$

Pressure: $\tilde{P}_i(x,y,t) = P_i + p_i(x,y,t)$

Density: $\tilde{\rho}_i(x,y,t) = R_i + \rho_i(x,y,t)$

The mean quantities are assumed constant in each flow region. The absolute swirl is denoted by S_i and is equal to W_i/U_i . The swirl relative to the first blade row is denoted by $\mathcal{S}_i$ and is equal to $(W_i - W_b)/U_i$. The swirl relative to the second blade row is denoted by $\mathcal{S}_i^+$ and is equal to $(W_i - W_s)/U_i$. The disturbance quantities are assumed to have a time and dependency of the form $\exp j(ct + ny/r)$. These are " n " celled waves propagating around the annulus. Here $c = c_R + jc_I$ and the flow is neutrally stable when $c_I = 0$, unstable if $c_I < 0$ and stable if $c_I > 0$. The time-dependent quantities are assumed to be much smaller than their corresponding steady parts. Under these assumptions, the equations of motion may be linearized and the disturbance quantities have the following forms:

$$u_i = \left\{ D_i e^{\alpha_{3i} x} - \frac{A_i \alpha_{1i} e^{\alpha_{1i} x}}{R_i U_i (\alpha_{1i} - \alpha_{3i})} - \frac{B_i \alpha_{2i} e^{\alpha_{2i} x}}{R_i U_i (\alpha_{2i} - \alpha_{3i})} \right\} F \tag{10a}$$

$$w_i = \left\{ D_i j \frac{n}{r} \alpha_{3i} e^{\alpha_{3i} x} - \frac{A_i j \frac{n}{r} e^{\alpha_{1i} x}}{R_i U_i (\alpha_{1i} - \alpha_{3i})} - \frac{B_i j \frac{n}{r} e^{\alpha_{2i} x}}{R_i U_i (\alpha_{2i} - \alpha_{3i})} \right\} F \tag{10b}$$

$$p_i = \left\{ A_i e^{\alpha_{1i} x} + B_i e^{\alpha_{2i} x} \right\} F \tag{10c}$$

$$\rho_i = \left\{ \frac{A_i}{a_i^2} e^{\alpha_{1i} x} + \frac{B_i}{a_i^2} e^{\alpha_{2i} x} + E_i e^{\alpha_{3i} x} \right\} F \tag{10d}$$

where a_i = speed of sound in flow region i

$$\alpha_{1i} = \frac{j M_i^2 m_i - \frac{n}{r}\left\{1 - M_i^2\left(1 + \frac{r^2}{n^2} m_i^2\right)\right\}^{1/2}}{1 - M_i^2}$$

$$\alpha_{2i} = \frac{j M_i^2 m_i + \frac{n}{r}\left\{1 - M_i^2\left(1 + \frac{r^2}{n^2} m_i^2\right)\right\}^{1/2}}{1 - M_i^2}$$

$$\alpha_{3i} = -j m_i$$

$$F = \exp j\left(ct + \frac{ny}{r}\right)$$

$$m_i = \frac{1}{U_i}\left(c + W_i \frac{n}{r}\right)$$

$$M_i = \frac{U_i}{a_i}$$

Here A_i, B_i, D_i and E_i are constants to be determined by the matching conditions. The terms associated with D_i represent vorticity waves, the term associated with E_i represents an entropy wave and the remaining terms represent potential (irrotational) disturbances. Requiring irrotational, isentropic flow upstream gives $D_1 = E_1 = 0$. Requiring bounded flow conditions upstream and downstream, results in $A_1 = B_3 = 0$. These considerations reduce the number of unknown constants to eight. These remaining unknowns are determined by applying four matching conditions across each actuator. These matching conditions are:

Conservation of Mass Flow

$$R_{i+1} u_{i+1} + \rho_{i+1} U_{i+1} - R_i u_i - \rho_i U_i + \frac{l_i}{2} \cos\delta_1 (\dot{\rho}_{i+1} + \dot{\rho}_i) = 0 \qquad (11)$$

Blade Row Turning Relation

$$\omega_{i+1} - \mathcal{S}_{i+1} u_{i+1} = \frac{U_{i+1}}{U_i} G_i'(\omega_i - \mathcal{S}_i u_i) \tag{12}$$

Vorticity Compatibility (derived from the momentum equation)

$$\dot{\omega}_{i+1} - \dot{\omega}_i - \sec\delta_i \frac{\ell_i}{2}\left(\frac{\partial \dot{u}_{i+1}}{\partial y_0} + \frac{\partial \dot{u}_i}{\partial y_0}\right) + U_{i+1}\eta_{i+1} - U_i \eta_i$$

$$= U_i \frac{\partial u_i}{\partial y_0}\left(\chi_i - \frac{\mathcal{S}_i \chi_i'}{2}(1+\mathcal{S}_i^2)\right) + U_i \frac{\partial \omega_i}{\partial y_0}\left\{\mathcal{S}_i \chi_i + \frac{\chi_i'}{2}(1+\mathcal{S}_i^2)\right\} \tag{13}$$

Conservation of Energy

$$p_i U_i + \frac{U_i}{\gamma-1}(p_i - a_i^2 \rho_i) + u_i R_i U_i^2 + \omega_i \mathcal{S}_i R_i U_i^2$$

$$- p_{i+1} U_{i+1} - \frac{U_{i+1}}{\gamma-1}(p_{i+1} - a_{i+1}^2 \rho_{i+1}) - u_{i+1} R_{i+1} U_{i+1}^2 - \omega_{i+1} \mathcal{S}_{i+1} R_{i+1} U_{i+1}^2$$

$$- \frac{\ell_i}{2}\frac{\cos\delta_i}{\gamma-1}(\dot{p}_{i+1} - a_{i+1}^2 \dot{\rho}_{i+1} + \dot{p}_i - a_i^2 \dot{\rho}_i) - \frac{\ell_i}{2}\cos\delta_i (R_i U_i \dot{u}_i$$

$$+ R_i U_i \mathcal{S}_i \dot{\omega}_i + R_{i+1} U_{i+1} \dot{u}_{i+1} + R_{i+1} U_{i+1} \mathcal{S}_{i+1} \dot{\omega}_{i+1}) = 0 \tag{14}$$

In these relations, $\chi_i(\mathcal{S}_i)$ is the loss coefficient for blade row i and $G_i(\mathcal{S}_i)$ is the turning relation for blade row i. A prime on a quantity indicates its derivative with respect to its argument. These relations are all applied in a blade fixed coordinate system. A dot over a quantity stands for its time derivative and η_i is the vorticity in region i. In order to apply these relations, i is set equal to the actuator number and Equations 1a-1d are used to calculate the required quantities. At actuator 1, flow quantities with a subscript 1 are evaluated at $x = 0, y = \bar{y}$ and quantities with a subscript 2 are evaluated at $x = \ell_1 \cos\delta_1$, $y = \bar{y} + \ell_1 \sin\delta_1$. At actuator 2, flow quantities with

a subscript 2 are evaluated at $x = T, y = \bar{y}$ and quantities with a subscript 3 are evaluated at $x = T + l_2 \cos \delta_2$, $y = \bar{y} + l_2 \sin \delta_2$. The result of performing all these operations is a matrix equation:

$$\left[A_{ij}\right] \begin{bmatrix} B_1 \\ D_2 \\ A_2 \\ E_2 \\ B_2 \\ A_3 \\ D_3 \\ E_3 \end{bmatrix} = 0$$

where the A matrix is 8 x 8. This equation has non-trivial solution only when

$$\det \left[A_{ij} \right] = 0 \tag{15}$$

This is the characteristic equation which determines the value of C for a given flow configuration and blade row. After factoring out common exponential factors, the expression for the A_{ij} are as follows:

$$A_{11} = \frac{\alpha_{21}}{U_1 d_{21}} - \frac{U_1}{a_1^2} K_1$$

$$A_{12} = R_2 e^{Q_1}$$

$$A_{13} = \left\{ \frac{-\alpha_{12}}{U_2 d_{12}} + \frac{U_2}{a_2^2} K_2 \right\} e^{Q_2}$$

$$A_{14} = U_2 K_2 e^{Q_1}$$

$$A_{15} = \left\{ \frac{-\alpha_{22}}{U_2 d_{22}} + \frac{U_2}{a_2^2} K_2 \right\} e^{Q_3}$$

$$A_{16} = A_{17} = A_{18} = 0$$

$$A_{21} = \frac{G_1' U_2}{R_1 U_1^2 d_{21}} \left(j \frac{n}{r} - \delta_1 \alpha_{21} \right)$$

$$A_{22} = \left(j \frac{r}{n} \alpha_{32} - \delta_2 \right) \cdot e^{Q_1}$$

$$A_{23} = \frac{1}{R_2 U_2 d_{12}} \left(- j \frac{n}{r} + \delta_2 \alpha_{12} \right) e^{Q_2}$$

$$A_{24} = 0$$

$$A_{25} = \frac{1}{R_2 U_2 d_{22}} \left(- j \frac{n}{r} + \delta_2 \alpha_{22} \right) e^{Q_3}$$

$$A_{26} = A_{27} = A_{28} = 0$$

$$A_{31} = - \bar{c} \frac{n}{r} \frac{1}{R_1 U_1 d_{21}} \left[1 + \frac{l_1}{2} \sec \delta_1 \alpha_{21} \right] + \frac{n/r}{R_1 d_{21}} \left[j \alpha_{21} L_{11} - \frac{n}{r} L_{21} \right]$$

$$A_{32} = \left\{ \frac{l_1}{2} \sec \delta_1 \bar{c} \frac{n}{r} - \bar{c} \frac{n}{r} \alpha_{32} + U_2 j \frac{r}{n} \left(\alpha_{32}^2 - \left(\frac{n}{r} \right)^2 \right) \right\} e^{Q_1}$$

$$A_{33} = \bar{c} \frac{n}{r} \frac{1}{R_2 U_2 d_{12}} \left(1 - \frac{l_1}{2} \sec \delta_1 \alpha_{12} \right) e^{Q_2}$$

$$A_{34} = 0$$

$$A_{35} = \frac{\bar{c} \frac{n}{r}}{R_2 U_2 d_{22}} \left(1 - \frac{l_1}{2} \sec \delta_1 \alpha_{22} \right) e^{Q_3}$$

$$A_{36} = A_{37} = A_{38} = 0$$

$$A_{41} = U_1 - U_1(\alpha_{21} + \delta j \frac{n}{r}) \frac{K_1}{d_{21}}$$

$$A_{42} = -(1 + j \frac{r}{n} \delta_2 \alpha_{32}) R_2 U_2^2 K_2 e^{Q_1}$$

$$A_{43} = \left\{ -U_2 + U_2(\alpha_{12} + \delta_2 j \frac{n}{r}) \frac{K_2}{d_{12}} \right\} e^{Q_2}$$

$$A_{44} = \frac{a_2^2 U_2}{\gamma - 1} K_2 e^{Q_1}$$

$$A_{45} = \left\{ -U_2 + \frac{U_2}{d_{22}} (\alpha_{22} + \delta_2 j \frac{n}{r}) K_2 \right\} e^{Q_3}$$

$$A_{46} = A_{47} = A_{48} = 0$$

$$A_{51} = 0$$

$$A_{52} = -R_2 e^{\alpha_{32} T}$$

$$A_{53} = \left\{ \frac{\alpha_{12}}{U_2 d_{12}} - \frac{U_2}{a_2^2} K_3 \right\} e^{\alpha_{12} T}$$

$$A_{54} = -U_2 K_3 e^{\alpha_{32} T}$$

$$A_{55} = \left\{ \frac{\alpha_{22}}{U_2 d_{22}} - \frac{U_2}{a_2^2} K_3 \right\} e^{\alpha_{22} T}$$

$$A_{56} = \left\{ \frac{-\alpha_{13}}{U_3 d_{13}} + \frac{U_3}{a_3^2} K_4 \right\}$$

$$A_{57} = R_3$$

$$A_{58} = U_3 K_4$$

$$A_{61} = 0$$

$$A_{62} = \frac{U_3}{U_2} G_2' \left[\mathcal{S}_2^+ - j \frac{r}{n} \alpha_{32} \right] e^{\alpha_{32} T}$$

$$A_{63} = \frac{U_3}{R_2 U_2^2} \frac{G_2'}{d_{12}} \left[j \frac{n}{r} - \mathcal{S}_2^+ \alpha_{12} \right] e^{\alpha_{12} T}$$

$$A_{64} = 0$$

$$A_{65} = \frac{U_3}{R_2 U_2^2} \frac{G_2'}{d_{22}} \left[j \frac{n}{r} - \mathcal{S}_2^+ \alpha_{22} \right] e^{\alpha_{22} T}$$

$$A_{66} = \left(\mathcal{S}_3^+ \alpha_{13} - j \frac{n}{r} \right) \frac{1}{R_3 U_3 d_{13}}$$

$$A_{67} = j \frac{r}{n} \alpha_{33} - \mathcal{S}_3^+$$

$$A_{68} = 0$$

$$A_{71} = 0$$

$$A_{72} = \left\{ \frac{r}{n} \alpha_{32} \left(\bar{\bar{c}} + \frac{n}{r} U_2 L_{22} \right) - U_2 j \frac{r}{n} \left(\alpha_{32}^2 - \left(\frac{n}{r} \right)^2 \right) \right.$$

$$\left. + \left(\bar{\bar{c}} \frac{n}{r} \sec \delta_2 \frac{l_2}{2} - j \frac{n}{r} U_2 L_{12} \right) \right\} e^{\alpha_{32} T}$$

$$A_{73} = \frac{-e^{\alpha_{12} T} \frac{n}{r}}{R_2 U_2 d_{12}} \left\{ \bar{\bar{c}} + \frac{n}{r} U_2 L_{22} + \alpha_{12} \left(\bar{\bar{c}} \sec \delta_2 \frac{l_2}{2} - j U_2 L_{22} \right) \right\}$$

$$A_{74} = 0$$

$$A_{75} = \frac{-e^{\alpha_{22}T}\frac{n}{r}}{R_2 U_2 d_{22}} \left\{ \bar{\bar{c}} + \frac{n}{r} U_2 L_{22} + \alpha_{22}\left(\bar{\bar{c}} \sec\delta_2 \frac{l_2}{2} - j U_2 L_{12}\right) \right\}$$

$$A_{76} = \frac{\bar{\bar{c}}\,\frac{n}{r}}{R_3 U_3 d_{13}} \left(1 - \alpha_{13}\frac{l_2}{2}\sec\delta_2\right)$$

$$A_{77} = \frac{n}{r}\bar{\bar{c}}\frac{l_2}{2}\sec\delta_2 - \bar{\bar{c}}\frac{r}{n}\alpha_{33} + U_3 j \frac{r}{n}\left(\alpha_{33}^2 - \left(\frac{n}{r}\right)^2\right)$$

$$A_{78} = 0$$

$$A_{81} = 0$$

$$A_{82} = R_2 U_2^2 \left(1 + \mathcal{S}_2^+ j \frac{r}{n}\alpha_{32}\right) K_3 e^{\alpha_{32}T}$$

$$A_{83} = \left\{ U_2 - \frac{U_2}{d_{12}}\left(\alpha_{12} + \mathcal{S}_2^+ j \frac{n}{r}\right) K_3 \right\} e^{\alpha_{12}T}$$

$$A_{84} = \frac{-U_2}{\gamma - 1} a_2^2 K_3 e^{\alpha_{32}T}$$

$$A_{85} = \left\{ U_2 - \frac{U_2}{d_{22}}\left(\alpha_{22} + \mathcal{S}_2^+ j \frac{n}{r}\right) K_3 \right\} e^{\alpha_{22}T}$$

$$A_{86} = -U_3 + \frac{U_3}{d_{13}}\left(\alpha_{13} + \mathcal{S}_3^+ j \frac{n}{r}\right) K_4$$

$$A_{87} = -R_3 U_3^2 \left(1 + \mathcal{S}_3^+ j \frac{n}{r}\alpha_{33}\right) K_4$$

$$A_{88} = \frac{U_3}{\gamma - 1} a_3^2 K_4$$

where $$K_1 = 1 - j \frac{\bar{c}}{U_1} \frac{\ell_1}{2} \cos \delta_1$$

$$K_2 = 1 + j \frac{\bar{c}}{U_2} \frac{\ell_1}{2} \cos \delta_1$$

$$K_3 = 1 - j \frac{\bar{\bar{c}}}{U_3} \frac{\ell_2}{2} \cos \delta_2$$

$$K_4 = 1 + j \frac{\bar{\bar{c}}}{U_3} \frac{\ell_2}{2} \cos \delta_2$$

$$\bar{c} = c + W_b \frac{n}{r}$$

$$\bar{\bar{c}} = c + W_s \frac{n}{r}$$

$$\alpha_{1i} = \alpha_{1i} - \alpha_{3i}$$

$$\alpha_{2i} = \alpha_{2i} - \alpha_{3i}$$

$$L_{11} = \chi_1 - \frac{\mathcal{S}_1 \chi_1'}{2} (1 + \mathcal{S}_1^2)$$

$$L_{12} = \mathcal{S}_1 \chi_1 + \frac{\chi_1'}{2} (1 + \mathcal{S}_1^2)$$

$$L_{21} = \chi_2 - \frac{\mathcal{S}_2^+ \chi_2'}{2} (1 + \mathcal{S}_2^{+2})$$

$$L_{22} = \mathcal{S}_2 \chi_2 + \frac{\chi_2'}{2} (1 + \mathcal{S}_2^{+2})$$

$$Q_1 = \alpha_{32} \ell_1 \cos \delta_1 + j \frac{n}{r} \ell_1 \sin \delta_1$$

$$Q_2 = \alpha_{12} \ell_1 \cos \delta_1 + j \frac{n}{r} \ell_1 \sin \delta_1$$

$$Q_3 = \alpha_{22} \ell_1 \cos \delta_1 + j \frac{n}{r} \ell_1 \sin \delta_1$$

Inspection of the eighth column of the matrix shows that one root of Equation (15) is $K_4 = 0$ or

$$c = -W_s \frac{n}{r} + j \frac{2U_3}{\ell_2 \cos \delta_2} \tag{16}$$

This is a stable wave fixed to the second blade row. This root is subsequently factored out of A_{48} and A_{88}. Inspection of the A_{ij} terms shows that Eq. (15) is transcendental in c and therefore must be solved numerically.

The analysis for a single blade row may be considered as a subcase of the above analysis. For the single blade row the characteristic determinant, $|A|$, is four by four and its elements may be obtained from those presented by ignoring the A_{ij} for $i,j > 4$ and then factoring out common exponential terms. Also, for the single blade row case one root can be determined analytically as

$$\frac{c}{U_z} = -\Omega_z \frac{r}{n} + 2j \sec \delta_1$$

This root represents a wave fixed to the blade row and is always stable. The remaining stability determinant is also transcendental in c and must be solved numerically.

3. RESULTS

Computer codes were written to solve both the single blade row and two blade row characteristic equations. Both programs are quite similar; the characteristic equation is solved iteratively using a Newton-Raphson scheme. The initial guess required at the first set of inlet conditions is obtained from the incompressible result for the first (or only) blade row. After the solution has been obtained at this inlet condition, the inlet angle is then increased by a small increment and the first solution is used as the initial guess. The inlet angle is then incremented until the solution is obtained over the range required. The single blade row program has been applied to two blade sets, Rotor No. 1 and Stator Set No. 4 of Ref. 25. Both blade rows were run with inlet conditions corresponding to sea level standard conditions and an inlet axial velocity of

60 ft/sec. These conditions approximate closely the actual tested conditions. The upstream axial Mach number is 0.057, which is essentially incompressible flow. The resulting stability curves and propagation velocities agree well with the predictions for incompressible flow. Stator Set No. 4 has also been analyzed with upstream axial flow Mach numbers of 0.2 and 0.4 using the turning and loss performance from incompressible flow. These calculations are shown in Figs. 15 and 16 where they are compared with the results of our previous compressible flow stability theory from Ref. 26 (Figs. 37 and 38). The solid lines in both figures are the new calculations and the symbols are the calculations from Ref. 26. The difference between the analysis presented in Ref. 26 and the present analysis lies in the energy matching condition used. The present analysis eliminates consideration of the viscous dissipation function within the blade row. This function was evidently numerically very small because it scales with the viscosity and the condition under consideration corresponds to relatively high Reynolds number. The smallness of the dissipation function evidently is responsible for the close numerical agreement in stability boundaries for the two forms of the energy matching condition.

The calculations from the present single blade row program for Rotor No. 1 are shown in Figs. 17 and 18. The incompressible loss and turning performance were used for all the Mach numbers shown. These calculations then give the influence of compressibility in the flow outside the blade row on the rotating stall boundary; the effect of compressibility on blade row turning and loss performance is not included. For both the rotor and the stator these compressibility effects are seen to reduce the stability of the flow with only a small change in the neutral stability boundary. Likewise, the propagation velocities for the stator set are uniformly reduced. The propagation velocities for the rotor show a mixed effect.

The two-blade-row program was run to correlate with the high hub-to-tip ratio rotor-stator tests reported in Ref. 3. The rotor had a stagger angle of -40.0 degrees and the cases for stator stagger angles of 28.2 degrees and 37.2 degrees were considered. The rotor had a chord of 0.12057 feet and the stator chord was 0.10833 feet. The axial velocity for the tests was 59.46 feet per second (M_1 = .053).

As a check out of this program, the input data were adjusted such that one of the two blade rows did not influence the flow. That is, one of the blade rows did not turn the flow or introduce any losses; this blade row will be referred to as the inactive blade row. Although this blade row did not influence the flow, the flow is still divided into three regions and matching conditions are still applied at both blade row locations so that the full program is exercised in calculating the stability of this case. The turning and loss performance of the rotor (in the presence of the stator) was used for the blade row which influenced the flow. The results of these calculations for a stator stagger angle of 37.2 degrees are shown in Fig. 19. The solid curve in this figure is the stability curve for the stage as presented in Fig. 23, Ref. 26. The dashed curve is the stability curve for the rotor alone but with rotor turning and loss performance as measured in the presence of the stator. Both these curves are calculated using the incompressible flow stability theory from Ref. 25. The symbols represent values calculated from the present compressible stability program with one or the other of the blade rows inactive as noted and with an axial velocity of 59.46 feet per second. The agreement with the rotor-alone calculations for incompressible flow is quite good and validates the code.

The two-blade row program was then used to investigate the effects of inlet axial Mach number and blade row spacing assuming that these parameters do not inlfuence the blade row turning and loss performance of either rotor or stator (in the absence of the appropriate blade row data under compressible flow conditions).

The influence of axial Mach number on the stability characteristics of the rotor-stator stage with stator stagger angle of 28.2 degrees is shown in Fig. 20. There the results are for one stall cell ($n = 1$) which has the lowest stability. The neutral stability point, where the damping factor goes to zero, is slightly decreased in magnitude by increasing axial Mach number. However, the stability in the stable range of inlet swirls is drastically affected. The influence of compressibility seems to drive the stage stability curve closer to the rotor alone curve near the neutral stability point. Similar calculations

are shown in Fig. 21 for the rotor-stator with stator stagger angle of 37.2 degrees. For this particular geometry, increasing axial Mach number has a more pronounced effect over the entire range of inlet swirl. The magnitude of the inlet swirl for the neutral stability point decreases markedly with axial Mach number, falling approximately 18 percent between $M_1 = 0$ and $M_1 = 0.3$. Again, the shape of the neutral stability curve for the stage tends toward that of the stability curve for the rotor alone as axial Mach number is increased. The greater influence of compressibility on this case evidently occurs because the rotor alone becomes unstable at a greatly reduced inlet swirl magnitude compared to the stage.

The effects of blade row spacing for the rotor-stator stage with stator stagger angle of 28.2 degrees has been investigated at an axial Mach number of 0.4. (Again, the blade row turning and loss performance is assumed not to vary with Mach number and also blade spacing in this case.) The results are shown in Fig. 22. In this figure, T is the distance, in feet, between the leading edge of the rotor and leading edge of the stator. The value of T for the configuration tested was T = .12196 resulting in a gap of .02952 feet between trailing edge of the rotor and leading edge of the stator. This corresponds to a ratio of gap to rotor chord of .244. Calculations were made with values of T (in feet) of .1823, .2426 and 1.823 corresponding to ratios of gap to rotor chord of .744, 1.244 and 14.34. The calculation for T = .1823 are not shown as they were only slightly less than those for T = .2426. It is seen that increasing the gap initially is slightly stabilizing; however, as the gap is made very large, the results approach the rotor alone case.

The axial wavelength of the rotating stall wave has been calculated for purposes of comparing the blade spacing to the axial wavelength of the rotating stall wave at neutral stability conditions. For this case, there are two axial wavelengths; one associated with the rotational part of the disturbance, and one associated with the irrotational part. At neutral stability conditions, the irrotational portion has a wavelength of approximately 17.4 feet and the rotational part has a wavelength of approximately 3.2 feet. It is seen then that the spacings investigated in Fig. 22 are generally much smaller than either of the axial wavelengths associated with the stall wave.

4. CONCLUDING REMARKS

A small disturbance stability analysis has been presented for the two-dimensional, compressible flow through a rotor-stator combination. The theory has been implemented into a computer code which predicts the stability boundary and propagation speed of allowable disturbance for given blade row performance data. The theory and numerical results reduce to the incompressible flow case as inlet Mach number approaches zero. The calculations show that even for fixed blade row performance, compressibility has a significant effect on the stability boundary. It is generally found that this effect is destabilizing compared to the incompressible flow results.

SECTION IV

THREE-DIMENSIONAL UNSTEADY LIFTING SURFACE THEORY FOR A ROTOR

This portion of the work is concerned with predicting the unsteady aerodynamic response of an annular blade row to inlet flow distortion. A linearized, but fully three-dimensional, lifting-surface analysis was chosen for this purpose. With small modifications, the analysis could be applied to the study of blade flutter as well.

1. FLOW MODEL

The same geometry is assumed for the present case as had been used in our earlier study of the steady load problem.[2] That is, the blade row is assumed to be housed in an infinitely long, hard-walled annular duct of constant hub/tip ratio, h , as shown in Fig. 23. The flow is assumed to be inviscid and to contain a uniform subsonic axial component at Mach number M = U/a_o , where a_o is the undisturbed sound speed. Any inflow distortions are viewed as small perturbations about this undisturbed state. The blades rotate with a constant angular velocity, which in this analysis is denoted Ω , rather than ω as used previously. In keeping with the usual convention, the latter symbol will be used for the harmonic time dependence below. Since the blade boundary conditions are more easily expressed in blade-fixed coordinates, we again express the governing equations in these terms. In this frame, the time-averaged undisturbed inflow has a velocity $U_R = \left[U^2 + (\Omega R)^2\right]^{1/2}$, and follows the helical stream surfaces defined by $\zeta = \theta - \frac{\Omega}{U} z$ = constant. The unsteady flow is assumed to be a small perturbation about this flow, so the disturbance field will be irrotational and isentropic. The linearization again allows us to apply the blade boundary conditions along the undisturbed stream surfaces, so that to first order in the perturbation scheme, blade thickness and camber do not affect the unsteady loads. We also assume that the undisturbed relative Mach number is subsonic all along the span.

Under the above assumptions, one can derive a linear integral equation relating the prescribed normal velocity distribution on the blade surfaces to the unknown loading, which appears under the integral. The steps involved have already been described in some detail in Ref. 2, and the final result is quoted there as Eq. (63); because of its length, it is reproduced here in Appendix B. This equation then is the starting point for the work reported

2. LOADING EXPANSION

As anticipated in Ref. 2, we have applied the same techniques to inverting this integral equation as we had used in the steady problem. The first step is to assume that the unsteady pressure difference across the blades can be expanded in the following form:*

$$\Delta\hat{p}\,(\sigma_o, x_o) \equiv \frac{p(\zeta = 0^-) - p(\zeta = 0^+)}{\frac{1}{2}\rho_o U^2}$$

$$= \sqrt{\frac{1 - x_o}{1 + x_o}} \sum_{j=1}^{NJ} p_{ij}\,\sigma_o^{j-1} + \sum_{i=2}^{NI}\sum_{j=1}^{NJ} p_{ij}\,\sigma_o^{j-1} \sin(i-1)\,\phi_o \qquad (17)$$

Here σ and x are dimensionless radial and axial coordinates defined by:

$$\sigma = \frac{r}{r_T} \qquad h \leq \sigma \leq 1 \qquad (18a)$$

$$x = \frac{z - C_a/2}{C_a/2} \qquad -1 \leq x \leq 1 \qquad (18b)$$

where r_T is the tip radius, and C_a is the axial projection of the blade chord, which for simplicity is assumed constant. We will use (σ , x) to refer to an arbitrary field point, and (σ_o , x_o) to refer to a source location on the reference blade surface, $\zeta = 0$. The variable ϕ_o is related to x_o through the relation

$$\phi_o = \cos^{-1} x_o \qquad (19)$$

Finally, ρ_o refers to the undisturbed density.

---

*It should be remembered that all of the dependent variables carry an implied harmonic time factor, $e^{i\omega t}$ which is suppressed for the sake of brevity.

The above expansion is completely analogous to that used in the steady flow problem. It contains the appropriate square root singularity at the leading edge, $x_o = -1$, in the $i = 1$ term. Moreover, each term vanishes identically at the trailing edge, $x_o = +1$, thus automatically satisfying the Kutta condition. Generally speaking, at each point there will be a phase shift between the unsteady loading and the normal velocity which will depend on position, the reduced frequency $\bar{\omega} = \frac{\omega c_a}{2U}$, and Mach number. This was not true in the steady flow problem, where by definition everything is "in phase". To account for this, $\Delta\hat{p}$ must now be allowed to be a complex quantity, having both real and imaginary parts. This is reflected in the unknown coefficients, p_{ij}, which are now complex:

$$p_{ij} = a_{ij} + i b_{ij} \tag{20}$$

(The symbol i will be used as both a subscript and as $\sqrt{-1}$; the appropriate meaning should always be clear from the context in which it appears.) From Eqs. (17) and (20) we see that we now have a total of 2 x NI x NJ unknowns.

A significant advantage of using the expansion in Eq. (17) is that when it is substituted into Eq. (B-1), analytical expressions can be derived for both the radial and axial integrations which result.

3. RADIAL INTEGRALS

Most of the radial integrations which result from the above substitution have the form:

$$I^{j}_{nk} = \int_{h}^{1} \sigma^{j} R_{nk}(K_{nk}\sigma)\, d\sigma \tag{21}$$

where j is an integer that can take on positive or negative values. Here K_{nk} and R_{nk} denote the radial eigenvalues and eigenfunctions which are an

outgrowth of the requirement that the radial velocity vanish at the hub and tip walls.[2] The integers n and k are the azimuthal and radial mode numbers, respectively. This class of integrals is identical to those which arose in the steady flow problem; as shown in Appendix B of Ref. 2, they can be evaluated in terms of Lommel functions, for which computer subroutines were already available.

There are, however, a few radial integrations which appear in the wake terms of the governing equation which deviate from the form quoted above. These have integrands which differ from that in Eq. (21) by factors of:

$$D_\alpha(\sigma) = [1 + (\phi_T \sigma)^2]^{-\alpha} \qquad \alpha = 1, 2, 3 \tag{22}$$

where $\phi_T = \Omega r_T / U$. Such factors prevent using the analytical evaluation directly because now the dependence on σ outside the R_{nk} is not as simple as just being raised to an integral power. However, $D_\alpha(\sigma)$ is a simple function which decreases monotonically from hub to tip; this suggests that it could be accurately replaced with a polynomial fit. In experimenting with such fits, it was found that an expansion in inverse powers of σ gave a better representation than one in positive powers of σ. Hence, we set

$$D_\alpha(\sigma) \simeq \sum_{\nu=1}^{N_\nu} \Delta_{\alpha\nu} \, \sigma^{1-\nu} \tag{23}$$

For $\alpha = 3$, $\phi_T = 2$, and $N_\nu = 4$ this was found to represent $D_3(\sigma)$ with a maximum error of approximately 1.7% over the range $0.4 \leq \sigma \leq 1.0$. The original function was matched at the points $\sigma = 0.4$, 0.6, 0.8 and 1.0. This is probably an extreme case; for $\alpha = 1$ or 2 and lower values of ϕ_T, the fit would be even better. Using such a procedure, the radial integrals involving $D_\alpha(\sigma)$ can be represented as a sum of integrals of the form given in Eq. (21), and thence evaluated analytically.

4. AXIAL INTEGRALS

A greater variety of axial integrals occurs than was the case in the steady flow problem. As a convenience, define the following shorthand for the axial loading functions in Eq. (17):

$$W_1(x_0) = \sqrt{\frac{1-x_0}{1+x_0}} = \frac{1-\cos\phi_0}{\sin\phi_0} \tag{24a}$$

$$W_i(x_0) = \sin(i-1)\phi_0 \qquad i \geq 2 \tag{24b}$$

The integrals which arise from the wake terms in the integral equation then have the form:

$$\begin{Bmatrix} C^i(x) \\ S^i(x) \end{Bmatrix} = \begin{Bmatrix} \mathcal{R}e \\ \mathcal{I}m \end{Bmatrix} \int_{-1}^{x} W_i(x_0)\, e^{i\bar{\omega}(x-x_0)}\, dx_0 \tag{25}$$

where $\mathcal{R}e$ and $\mathcal{I}m$ indicate real and imaginary parts, respectively.

Before quoting the form of the integrals in the exponential terms, a few words are in order regarding the notation. As above, a capital C or S will be used to refer to integrals involving the cosine or sine function, respectively. This is followed by a lower case s if in addition the function sgn ($x - x_0$) appears in the integrand. The subscripts n and k again refer to a specific combination of azimuthal and radial mode numbers. The superscript i refers to one of the axial loading functions defined by Eq. (24). Finally, a second superscript, A or B, is used to indicate whether the integral is appropriate to a mode above or below the cut-off condition.

The form of the integrals above cut-off is then

$$\begin{Bmatrix} C^{iA}_{nk}(x) \\ S^{iA}_{nk}(x) \end{Bmatrix} = \begin{Bmatrix} \mathcal{R}e \\ \mathcal{I}m \end{Bmatrix} \int_{-1}^{+1} W_i(x_0)\, e^{i[a(x-x_0) - b|x-x_0|]}\, dx_0 \tag{26a}$$

and

$$\begin{Bmatrix} C_{s_{nk}}^{iA}(x) \\ S_{s_{nk}}^{iA}(x) \end{Bmatrix} = \begin{Bmatrix} \mathcal{R}e \\ \mathcal{I}m \end{Bmatrix} \int_{-1}^{+1} W_i(x_o)\, sgn(x - x_o)\, e^{i[a(x-x_o) - b|x-x_o|]}\, dx_o \tag{26b}$$

where

$$\left.\begin{aligned} a &= \left(\frac{M}{\beta}\right)^2 \bar{\omega} \\ b &= \frac{\eta_T}{\beta}\beta_{ok} \end{aligned}\right\} n = 0$$

$$\left.\begin{aligned} a &= \frac{n\,\eta_T\,\alpha_n}{\beta^2} - \bar{\omega} \\ b &= \frac{|n|\,\eta_T}{\beta}\beta_{nk} \end{aligned}\right\} n \neq 0 \tag{26c}$$

Also,

$$\beta = (1 - M^2)^{1/2}$$

$$\eta_T = \frac{c_a}{2 r_T}$$

$$\alpha_n = \phi_T + \frac{\bar{\omega}}{n\,\eta_T} \qquad n \neq 0$$

$$\beta_{nk} = \begin{cases} \left[\left(\frac{M}{\beta}\right)^2 \left(\frac{\bar{\omega}}{\eta_T}\right)^2 - K_{ok}^2\right]^{1/2} & n = 0 \\ sgn(\alpha_n)\left[\left(\frac{M}{\beta}\right)^2 \alpha_n^2 - \left(\frac{K_{nk}}{n}\right)^2\right]^{1/2} & n \neq 0 \end{cases} \tag{26d}$$

Below cut-off, the integrals take on the form:

$$\begin{Bmatrix} C_{nk}^{iB}(x) \\ S_{nk}^{iB}(x) \end{Bmatrix} = \begin{Bmatrix} \mathcal{R}e \\ \mathcal{I}m \end{Bmatrix} \int_{-1}^{+1} W_i(x_o)\, e^{-c|x-x_o| + id(x-x_o)}\, dx_o \tag{27a}$$

and

$$\begin{Bmatrix} C\, s^{iB}_{nk}(x) \\ S\, s^{iB}_{nk}(x) \end{Bmatrix} = \begin{Bmatrix} \mathcal{R}e \\ \mathcal{I}m \end{Bmatrix} \int_{-1}^{+1} W_i(x_o)\, sgn(x-x_o)\, e^{-c|x-x_o| + i\alpha(x-x_o)}\, dx_o \tag{27b}$$

where

$$\left.\begin{aligned} c &= \frac{\eta_T}{\beta} B_{ok} \\ \alpha &= \left(\frac{M}{\beta}\right)^2 \bar{\omega} \end{aligned}\right\} \quad n = 0$$

$$\left.\begin{aligned} c &= \frac{|n|\,\eta_T}{\beta} B_{nk} \\ \alpha &= \frac{n\,\eta_T\,\alpha_n}{\beta^2} - \bar{\omega} \end{aligned}\right\} \quad n \neq 0 \tag{27c}$$

Also,

$$B_{nk} = \begin{cases} \left[K_{ok}^2 - \left(\frac{M}{\beta}\right)^2 \left(\frac{\bar{\omega}}{\eta_T}\right)^2\right]^{1/2} & n = 0 \\ \left[\left(\frac{K_{nk}}{n}\right)^2 - \left(\frac{M}{\beta}\right)^2 \alpha_n^2\right]^{1/2} & n \neq 0 \end{cases} \tag{27d}$$

The analytical evaluation of these axial integrals can be carried out using exactly the same method outlined in Appendix C of Ref. 2. Although straightforward, the algebraic manipulations are tedious; the final results are given in Appendix A. It should be noted that the number of wake term integrals is limited by the fact that they do not depend on the mode numbers. Also, for a given (n, k) mode, one need evaluate only one or the other of the sets of integrals defined in Eqs. (26) and (27), since a given mode is either above or below cut-off.

5. GOVERNING EQUATION

We can now quote the new form of the governing equation, with the above definitions and substitutions for $\Delta\hat{p}$. Due to its length, we will

separate it into its component parts, viz., the wake terms, the axisymmetric (n = 0) exponential terms, and the asymmetric ($n \neq 0$) exponential terms. The wake terms are given by

$$\begin{Bmatrix} \mathcal{R}e \dfrac{v_n}{U_R}(\sigma, x) \\ \mathcal{I}m \dfrac{v_n}{U_R}(\sigma, x) \end{Bmatrix} = \sum_{i=1}^{NI} \sum_{j=1}^{NJ} \left[\frac{-\beta \eta_T \delta_{po} \sigma^{j-1}}{4\pi\sigma[1+(\phi_T\sigma)^2]} \begin{Bmatrix} C^i(x) a_{ij} + S^i(x) b_{ij} \\ C^i(x) b_{ij} - S^i(x) a_{ij} \end{Bmatrix} \right.$$

$$+ \frac{B\eta_T(\phi_T\sigma)^2 \delta_{po}}{4\pi\sigma[1+(\phi_T\sigma)^2]} \begin{Bmatrix} C^i(x) a_{ij} + S^i(x) b_{ij} \\ C^i(x) b_{ij} - S^i(x) a_{ij} \end{Bmatrix} (j-1)^2 \sum_{k=1}^{NK} \frac{I_{ok}^{j-2} R_{ok}(\sigma)}{A_{ok}}$$

$$+ \frac{B\eta_T}{4\pi\sigma[1+(\phi_T\sigma)^2]} \begin{Bmatrix} C^i(x) a_{ij} + S^i(x) b_{ij} \\ C^i(x) b_{ij} - S^i(x) a_{ij} \end{Bmatrix} \sum_{\substack{m=-NM \\ n\neq 0}}^{NM} \sum_{k=1}^{NK} \frac{R_{nk}(\sigma)}{n^2 A_{nk}}$$

$$\cdot \left[(1+\phi_T \alpha_n \sigma^2)(j-1)^2 I_{nk}^{j-2} - \left(\frac{\bar{\omega}}{\eta_T}\right)^2 (1+(\phi_T\sigma)^2 + \phi_T \alpha_n \sigma^2) I_{nk}^{j} \right]$$

$$+ \frac{B\phi_T\bar{\omega}}{4\pi\sigma} \begin{Bmatrix} C^i(x) a_{ij} + S^i(x) b_{ij} \\ C^i(x) b_{ij} - S^i(x) a_{ij} \end{Bmatrix} \sum_{\substack{m=-NM \\ n\neq 0}}^{NM} \sum_{k=1}^{NK} \frac{R_{nk}(\sigma)}{n^2 A_{nk}}$$

$$\cdot \left[\frac{2\sigma_o^{j+1} R_{nk}(\sigma_o)}{n[1+(\phi_T\sigma_o)^2]^2} \Bigg|_h^1 - \frac{1}{n} \sum_{\nu=1}^{N_\nu} \left(\Delta_{1\nu}(j-1)^2 I_{nk}^{j-\nu+1} + 4\Delta_{2\nu}(j-1) I_{nk}^{j-\nu+1} \right.\right.$$

$$\left.\left. + 4\Delta_{3\nu}\left(I_{nk}^{j-\nu+1} - \phi_T^2 I_{nk}^{j-\nu+3}\right)\right) + \frac{\bar{\omega}(\phi_T+\alpha_n)}{\eta_T} \sum_{\nu=1}^{N_\nu} \Delta_{1\nu} I_{nk}^{j-\nu+3} \right] \Bigg\} \quad (28)$$

where the upper and lower lines in the curly brackets represent the contribution to the real or imaginary part of v_n/U_R. On the right side, B is the blade number, and the factors A_{nk} are defined by

$$A_{nk} = \begin{cases} K_{ok}^2 + \left(\frac{\bar{\omega}}{\eta_T}\right)^2 & n = 0 \\ \left(\frac{K_{nk}}{n}\right)^2 + \alpha_n^2 & n \neq 0 \end{cases} \tag{29}$$

Recall that the azimuthal mode number, n, is related to the summation index, m, by (Ref. 2, p. 38):

$$n = mB + p \tag{30}$$

where p is the shift in azimuthal mode number produced by the interblade phase shift, μ_B ; viz.,

$$p = \frac{B\mu_B}{2\pi} \tag{31}$$

The asymmetry in the values of n allowed by Eq. (30) prevents us from combining the contributions from the $-m$ terms with those from the $+m$ terms, as we were able to do in the steady problem.

The first two lines in Eq. (28) are the axisymmetric contribution, i.e., the $n = 0$ modes. We see that such modes can arise only in the special case $m = p = 0$. For this reason, these terms have been written with the Kronecker delta symbol, δ_{po}, which is unity when $p = 0$, but zero otherwise.

Note that the terms proportional to $(j - 1)^2$ in the second line and the first portion of the fourth line vanish when $j = 1$. Since this is the only term in Eq. (17) representing uniform radial loading, it can be inferred that these terms arise from trailing vorticity. This component of the wake vorticity, also present in the steady problem, has its axis aligned with the helical undisturbed stream, and is produced by spanwise gradients in the loading. There are other terms in Eq. (28) which remain for $j = 1$,

but vanish when $\bar{\omega} = 0$. These terms can be inferred to arise from the shed vorticity, whose axis is along the blade span, and which results from temporal fluctuations in the loading.

The contribution from the axisymmetric exponential terms is given by:

$$\sum_{i=1}^{NI}\sum_{j=1}^{NJ}\left\{-\frac{B\eta_T\phi_T^2\sigma\delta_{po}}{8\pi[1+(\phi_T\sigma)^2]}\right.$$

$$\cdot\left[\sum_{k=0}^{k^*}\frac{R_{ok}(\sigma)}{\beta_{ok}A_{ok}}I_{ok}^{j}\left\{\begin{matrix}\beta_{ok}F_1(Cs_{ok}^{iA}a_{ij}-Ss_{ok}^{iA}b_{ij})+F_2(C_{ok}^{iA}a_{ij}-S_{ok}^{iA}b_{ij})\\ \beta_{ok}F_1(Ss_{ok}^{iA}a_{ij}+Cs_{ok}^{iA}b_{ij})+F_2(S_{ok}^{iA}a_{ij}+C_{ok}^{iA}b_{ij})\end{matrix}\right\}\right.$$

$$\left.\left.+\sum_{k=k^*+1}^{NK}\frac{R_{ok}(\sigma)}{B_{ok}A_{ok}}I_{ok}^{j}\left\{\begin{matrix}B_{ok}F_1(Cs_{ok}^{iB}a_{ij}-Ss_{ok}^{iB}b_{ij})-F_2(S_{ok}^{iB}a_{ij}+C_{ok}^{iB}b_{ij})\\ B_{ok}F_1(Ss_{ok}^{iB}a_{ij}+Cs_{ok}^{iB}b_{ij})+F_2(C_{ok}^{iB}a_{ij}-S_{ok}^{iB}b_{ij})\end{matrix}\right\}\right]\right\} \tag{32}$$

which is also proportional to δ_{po} for the reason cited above. F_1 and F_2 are defined by:

$$F_1 = \left(\frac{\bar{\omega}}{\eta_T}\right)^2 - \frac{A_{ok}}{\beta^2}$$

$$F_2 = \frac{\bar{\omega}}{\beta\eta_T}\left[\left(\frac{M}{\beta}\right)^4\left(\frac{\bar{\omega}}{\eta_T}\right)^2 + \left(\frac{M^2}{\beta^2}-1\right)B_{ok}^2\right] \tag{33}$$

The first sum is over those modes which are above cut-off, the last of which is denoted by k^*; the higher order modes in the second sum are all below cut-off. In general, k^* will be a function of the reduced frequency, $\bar{\omega}$, and the operating parameters of the rotor. It will also be different for different values of the azimuthal index, n (see pp. 35-36 of Ref. 2).

The contribution from the asymmetric exponential terms is given by:

$$\sum_{i=1}^{NI}\sum_{j=1}^{NJ}\left\{\frac{-B\eta_T}{8\pi[1+(\phi_T\sigma)^2]}\sum_{\substack{m=-NM\\ n\neq 0}}^{NM}\left[\sum_{k=1}^{k^*}\frac{R_{nk}(\sigma)}{\beta_{nk}A_{nk}}\right.\right.$$

$$\cdot\left\{\begin{array}{l}\beta_{nk}(G^+I_{nk}^{j}+G^-I_{nk}^{j-2})(Cs_{nk}^{iA}a_{ij}-Ss_{nk}^{iA}b_{ij})+\frac{sgn(n)}{\beta}(Q^+I_{nk}^{j}+Q^-I_{nk}^{j-2})(C_{nk}^{iA}a_{ij}-S_{nk}^{iA}b_{ij})\\ \beta_{nk}(G^+I_{nk}^{j}+G^-I_{nk}^{j-2})(Ss_{nk}^{iA}a_{ij}+Cs_{nk}^{iA}b_{ij})+\frac{sgn(n)}{\beta}(Q^+I_{nk}^{j}+Q^-I_{nk}^{j-2})(S_{nk}^{iA}a_{ij}+C_{nk}^{iA}b_{ij})\end{array}\right\}$$

$$+\sum_{k=k^*+1}^{NK}\frac{R_{nk}(\sigma)}{B_{nk}A_{nk}}$$

$$\left.\left.\cdot\left\{\begin{array}{l}B_{nk}(G^+I_{nk}^{j}+G^-I_{nk}^{j-2})(Cs_{nk}^{iB}a_{ij}-Ss_{nk}^{iB}b_{ij})-\frac{sgn(n)}{\beta}(Q^+I_{nk}^{j}+Q^-I_{nk}^{j-2})(S_{nk}^{iB}a_{ij}+C_{nk}^{iB}b_{ij})\\ B_{nk}(G^+I_{nk}^{j}+G^-I_{nk}^{j-2})(Ss_{nk}^{iB}a_{ij}+Cs_{nk}^{iB}b_{ij})+\frac{sgn(n)}{\beta}(Q^+I_{nk}^{j}+Q^-I_{nk}^{j-2})(C_{nk}^{iB}a_{ij}-S_{nk}^{iB}b_{ij})\end{array}\right\}\right]\right\} \tag{34}$$

where

$$G^+ = \left[\phi_T\alpha_n\left(\frac{1}{\sigma}+\phi_T\alpha_n\sigma\right)-\left(\frac{\phi_T}{\beta}\right)^2 A_{nk}\sigma\right]$$

$$G^- = \frac{1}{\sigma}+\phi_T\alpha_n\sigma$$

$$Q^+ = -\phi_T\left[\left(\frac{1}{\sigma}-\frac{M^2}{\beta^2}\phi_T\alpha_n\sigma\right)\left(\frac{M^2}{\beta^2}\alpha_n^2+B_{nk}^2\right)+\phi_T\alpha_n\sigma B_{nk}^2\right]$$

$$Q^- = \left[\alpha_n\left(\frac{1}{\sigma}-\frac{M^2}{\beta^2}\phi_T\alpha_n\sigma\right)-\phi_T B_{nk}^2\sigma\right] \tag{35}$$

The significance of the two sums and the index k^* is the same as described for the axisymmetric terms, except here of course $k^* = k^*(n)$. Note that the algebraic forms of F_1, F_2, $G^{\pm}$ and $Q^{\pm}$ remain the same whether a mode is above or below cut-off; all that changes is the sign of B_{nk}^2.

Another step that has been taken in writing the above results is the truncation of the azimuthal and radial mode series. The original limits

on m and k have been reduced from $\pm\infty$ and ∞ to $\pm$ NM and NK, respectively. The magnitude of these truncation limits directly affects the dimensioning of the computer program. By estimating the magnitude of the radial eigenvalues, K_{nk} , and the resultant $k^*(n)$ for various extreme cases, it was felt that roughly the same dimensioning used in the steady flow code should be sufficient; viz. NM = 5, corresponding to 11 azimuthal modes, and NK = 30 radial modes.

The full equation for the normal velocity field is given by the sum of Eqs. (28), (32) and (35). The next step is the specification of v_n , in terms of the prescribed inflow distortion pattern, at a discrete set of collocation points on the reference blade surface denoted by:

$$\begin{aligned} \sigma &= \sigma_{\bar{n}} \qquad & \bar{n} &= 1, 2 \ldots NN \\ x &= x_{\ell} \qquad & \ell &= 1, 2 \ldots NL \end{aligned} \tag{36}$$

At each point two equations will result, one each for the real and imaginary parts of v_n . Thus, if NN x NL is chosen equal to NI x NJ, a determinate set of 2 x NI x NJ simultaneous, linear algebraic equations will result. This system can then be viewed as a single matrix equation to be solved for the column vector of unknows consisting of a_{ij} and b_{ij} . The rank of the matrix may be reduced by recognizing that the hard-wall boundary conditions require that $\partial \Delta\hat{p}/\partial\sigma$ vanish at both the hub and tip. This can be used directly in Eq. (17) to reduce the number of unknowns (and hence collocation points) to 2 x NI x (NJ-2), as was done in Ref. 2. The reduced system is then solved using Gaussian elimination with pivoting. The local loading then follows directly from Eq. (17). The real and imaginary parts of the sectional lift and moment coefficients, $C_L(\sigma)$ and $C_M(\sigma)$, are obtained from Eqs. (19) and (20) of Ref. 2, with a_{ij} replaced by $(a_{ij} + i\, b_{ij})$.

6. ACOUSTIC FARFIELD

In addition to the unsteady aerodynamic loading, this model is also capable of predicting the acousting farfield within the duct. This field is composed

of the modes above cut-off, which propagate undamped away from the rotor. We will now show how this sound field may be directly related to the loading coefficients, a_{ij} and b_{ij}, which result from solving the integral equation.

The starting point is Eq. (51) of Ref. 2 which expresses the pressure perturbation in blade-fixed coordinates. This is transformed to duct-fixed coordinates by changing θ to $\theta + \Omega t$, and only those modes above cut-off, i.e. $k \leq k^*$, are retained. The result is

$$p^{u,d}(\sigma, x, \theta, t) = \sum_{m=-\infty}^{\infty} \sum_{k=0}^{\infty} p_{nk}^{u,d} R_{nk}(K_{nk}\sigma) e^{i(\omega + n\Omega t)} \cdot e^{in[\theta - \phi_T \eta_T (x+1)] + i a_{nk}^{u,d} x} \tag{37a}$$

where $a_{nk}^{u,d}$ is a constant defined by

$$a_{nk}^{u,d} = [n\phi_T \eta_T + M^2 \bar{\omega} \pm \beta(|n| + \delta_{no})\eta_T \beta_{nk}] / \beta^2 \tag{37b}$$

Note that the $n = 0$ mode, if present, has been included in the sum, as has the $k = 0$ radial mode. It should be recalled, however, that the latter is trivially zero ($K_{no} = 0$) unless $n = 0$. The superscripts u, d are used to indicate up- or downstream radiation, and correspond to using the upper/lower signs on the right-hand side of the equation. Eq. (37) is just a superposition of propagating duct acoustic modes. All of the information on the spatial variations and propagation characteristics of the waves is contained in the radial eigenfunctions R_{nk} and in the complex exponential.

On the other hand, all of the information on how the noise was generated is contained in the mode amplitudes, $p_{nk}^{u,d}$, which are independent of both space and time. The latter are complex, and are expressible as an integral of the loading over the rotor blade surfaces. The form of the loading expansion series again allows the radial and chordwise integrations to be done analytically. Without giving the intermediate details, one obtains the following relationship between the acoustic mode amplitudes, $p_{nk}^{u,d}$, and the loading expansion coefficients, a_{ij} and b_{ij}:

$$\begin{Bmatrix} \mathcal{R}e\, p_{ok}^{u,d} \\ \mathcal{I}m\, p_{ok}^{u,d} \end{Bmatrix} = \frac{-B\,\phi_T\,\eta_T\,\rho_o\,U^2}{8\pi\beta^2}\left[\frac{\bar{\omega}\,M^2}{\eta_T\,\beta\,\beta_{ok}} \pm 1\right]$$

$$\bullet \sum_{i=1}^{NI}\sum_{j=1}^{NJ} I_{ok}^{j} \begin{Bmatrix} a_{ij}\,C_{ok}^{i} + b_{ij}\,S_{ok}^{i} \\ b_{ij}\,C_{ok}^{i} - a_{ij}\,S_{ok}^{i} \end{Bmatrix}^{u,d} \quad n = 0 \tag{38a}$$

$$\begin{Bmatrix} \mathcal{R}e\, p_{nk}^{u,d} \\ \mathcal{I}m\, p_{nk}^{u,d} \end{Bmatrix} = \frac{-B\,\eta_T\,\rho_o\,U^2}{8\pi\beta^2}\sum_{i=1}^{NI}\sum_{j=1}^{NJ}\left[\phi_T\left(\frac{M^2\alpha_n}{\beta^2} \pm 1\right) I_{nk}^{j}\right.$$

$$\left. - \frac{\beta}{\beta_{nk}}\,\mathrm{sgn}(n)\, I_{nk}^{j-2}\right] \begin{Bmatrix} a_{ij}\,C_{nk}^{i} + b_{ij}\,S_{nk}^{i} \\ b_{ij}\,C_{nk}^{i} - a_{ij}\,S_{nk}^{i} \end{Bmatrix}^{u,d} \quad n \neq 0 \tag{38b}$$

Here the I_{nk}^{j} are the same radial integrals encountered in the integral equation, and so will have already been evaluated in the determination of the blade loading. The axial integrals, on the other hand, are even simpler than those in the integral equation, because in the farfield all of the dependence on x can be factored out (cf. Eq. (37)). They are defined by

$$\begin{Bmatrix} C_{nk}^{i} \\ S_{nk}^{i} \end{Bmatrix}^{u,d} = \begin{Bmatrix} \mathcal{R}e \\ \mathcal{I}m \end{Bmatrix} \int_{-1}^{+1} W_i(x_o)\, e^{i\,a_{nk}^{u,d}\,x_o}\, dx_o \tag{39}$$

where the $W_i(x_0)$ are defined in Eq. (24). These integrals may be done analytically following the same procedures as before, and the results are quoted at the end of Appendix A.

Eqs. (37)-(39) allow the evaluation of the unsteady pressure at any point in the farfield. In practice, however, the quantities of most interest are the mean square pressure at any point, and the total power radiated away from the rotor. The former is defined as

$$\langle p^2 \rangle^{u,d} \equiv \frac{1}{T} \int_0^T \left[\mathcal{R}e\, p^{u,d} \right]^2 dt \tag{40}$$

For the case of present interest, i.e., the response to a steady inlet distortion, only harmonics of the blade passage frequency will occur, and hence, $T = (B\Omega)^{-1}$. Substituting from Eq. (37), one obtains

$$\langle p^2 \rangle^{u,d} = \frac{1}{2} \left| \sum_{m=-\infty}^{\infty} \sum_{k=0}^{k^*} p_{nk}^{u,d} R_{nk}(K_{nk}\sigma)\, e^{in[\theta - \phi_T \eta_T (x+1)] + i a_{nk}^{u,d} x} \right|^2 \tag{41}$$

Note that the right-hand side of Eq. (41) still depends on σ, x, and θ, as it should.

From Ref. 27, the total power radiated upstream or downstream of the rotor, $P^{u,d}$, may be expressed as

$$P^{u,d} = r_T^2 \int_h^1 \int_0^{2\pi} \Big[(1+M^2) \langle p\, v_z \rangle^{u,d} + \rho_0 a_0 M \langle v_z^2 \rangle^{u,d} + \frac{M}{\rho_0 a_0} \langle p^2 \rangle^{u,d} \Big] \sigma\, d\sigma\, d\theta \tag{42}$$

The last term is seen to be proportional to the integral of Eq. (41) over the duct cross-section. This is easily performed by taking advantage of the orthogonality properties of the duct modes in the azimuthal and radial coordinates, and the contribution to Eq. (42) is found to be

$$\frac{\pi r_T^2 M}{\rho_0 a_0} \sum_{m=-\infty}^{\infty} \sum_{k=0}^{k^*} \left| p_{nk}^{u,d} \right|^2$$

The other terms in Eq. (42) involve the perturbation field of the axial velocity component, v_z . Since v_z satisfies the same differential equation as p , it too can be expressed as a superposition of duct modes of the same form used in Eq. (37). The mode amplitudes for v_z waves, say $v_{nk}^{u,d}$, can be related to the pressure mode amplitudes through the axial momentum equation (Ref. 28, pp. 30-31), viz.,

$$v_{nk}^{u,d} = A_{nk}^{u,d} \frac{p_{nk}^{u,d}}{\rho_0 a_0} \tag{43}$$

where $A_{nk}^{u,d}$ is the dimensionless acoustic admittance for the (n, k) mode,

$$A_{nk}^{u,d} = -\frac{1}{M} \left[\frac{M^2(\bar{\omega} + n\phi_T \eta_T) \pm (|n| + \delta_{n0})\beta \eta_T \beta_{nk}}{(\bar{\omega} + n\phi_T \eta_T) \pm (|n| + \delta_{n0})\beta \eta_T \beta_{nk}} \right] \tag{44}$$

With Eqs. (43) and (44) one can immediately write down an expression for v_z analogous to Eq. (37) for the pressure. Expressions for $p v_z$ and v_z^2 required in the first two terms of Eq. (42) are then formed. The integrations over time and the duct cross-section go through just as before, since the only additional factors are the $A_{nk}^{u,d}$, which are independent of space and time. Finally then, the full result for $P^{u,d}$ may be written as

$$P^{u,d} = \frac{\pi r_T^2}{\rho_0 a_0} \sum_{m=-\infty}^{\infty} \sum_{k=0}^{k^*} \left[(1 + M^2) A_{nk}^{u,d} + (1 + A_{nk}^{u,d\,2}) M \right] \left| p_{nk}^{u,d} \right|^2 \tag{45}$$

We note here that Eqs. (41) and (45) agree with our previous results in the rotor-stator interaction problem (Ref. 28, Eqs. (22) and (28)), if there one sets the mode amplitudes generated by one of the two rows equal to zero.

7. CODE DEVELOPMENT

In developing the associated computer program on the AFWAL/ASD computers, a storage limitation was encountered. As a result, the maximum allowable values for each of NL and NN (the number of chordwise and spanwise collocation points), and NI and NJ (the number of chordwise and spanwise terms in the loading expansion), were reduced from 10 down to 5. This lowered the total program storage requirements down to about 76K words. Even at that, and despite the fact that CPU time on the ASD CYBER 74 was typically less than a minute, turnaround time was limited to about one run a day. This could prove to be a problem in applying the code to high reduced frequencies, where more collocation points and loading expansion terms would likely be required.

Another issue which had to be addressed concerned the axial integrals, of which there are several thousand, due to the various combinations of i, l, n, and k which can occur. One of the principal advantages of our approach is that we have been able to derive exact analytical expressions for these integrals (Appendix A) which results in an enormous decrease in the amount of time needed for their evaluation. Unfortunately, comparisons with numerical evaluations of the same integrals showed that a portion of them was being calculated inaccurately due to round-off error in the arithmetic. The problem is that the integrals naturally express themselves as a sum of modified Bessel functions. As n and k increase in magnitude, the magnitude of the integrals should monotonically decrease. But the size of the individual terms in the sum grows exponentially, and when the disparity between the two approaches 14 significant digits (CDC single precision) all accuracy is lost. Essentially, we find ourselves trying to take very small differences of very large numbers. A similar difficulty was encountered in the earlier steady flow code (see Ref. 2, Appendix C).

Accordingly, an effort was made to develop an asymptotic evaluation of these integrals which would be valid in the limit where the appropriate parameter becomes large. For those integrals with $i \geq 2$, an asymptotic expansion was found which yielded acceptable accuracy, i.e., about 1% or better. For $i = 1$, the leading edge singularity was first subtracted out and integrated analytically, with the asymptotic analysis applied to the remaining integral. Unfortunately, the resulting combined expression did not provide the desired 1% accuracy. Further, it does not help to carry out the asymptotic expansion to more terms, since, as is often the case with such series, it does not converge.

Because of this lack of an overlap region for i = 1, where both the analytical and asymptotic methods could be expected to agree, and the need to expedite program development, it was decided to use a numerical quadrature scheme for all those integrals where round-off error would compromise the analytical results. An efficient scheme, which minimizes the number of integrand evaluations required to achieve a specified accuracy, was chosen for this purpose.[29] This increased the program running time somewhat, but not as much as had been expected. In any case, run times were still well below what one would expect a finite-difference solution to the 3-D equations to take,

8. NUMERICAL RESULTS

Our choice for an inlet distortion pattern was one which is steady in duct coordinates, independent of x and σ, and consists solely of a sinusoidal variation in θ of the axial perturbation velocity, v_z. The number of cycles in the variation is denoted by n_D, and its amplitude by $(v_z/U)_o = \epsilon \ll 1$. Such a variation can be viewed as a single Fourier component of a more complex distortion pattern. If such a pattern is expressed in blade-fixed coordinates, the distortion component felt by the blade normal to the undisturbed stream direction, v_n, can be shown to be:

$$v_n = \epsilon U_R \left[\frac{\phi_T \sigma}{1 + (\phi_T \sigma)^2} \right] e^{-i\bar{\omega}} \, e^{i(\omega t - \bar{\omega} \hat{s})} \tag{46}$$

where $\hat{s} = (s - c/2)/(c/2) = x$ is the non-dimensional chordwise coordinate. The reduced frequency is related to n_D by $\bar{\omega} = n_D \phi_T \eta_T$. The radially

dependent factor in brackets simply reflects the fact that the orientation of v_n and U_R relative to v_z and U varies with radius.

No exact solutions are available for the response of a full 3-D blade row to such a pattern. However, at high hub/tip ratio, the results should approach those available for 2-D flows. The simplest such flow, attained in the limit of low solidity and low Mach number, is the response of an isolated airfoil in incompressible flow to a convected gust of the form given by Eq. (46). The dynamic response in this case has been expressed in closed form by Sears.[30] For the gust amplitude of Eq. (46), a stripwise application of Sears analysis yields for the lift coefficient,

$$\begin{aligned} C_L &\equiv L(\sigma) \Big/ \left(\tfrac{1}{2}\rho_0 U^2 c_a\right) \\ &= 2\pi \phi_T \sigma \epsilon \sqrt{1+(\phi_T \sigma)^2}\; e^{-i\bar{\omega}}\, S(\bar{\omega}) \end{aligned} \tag{47}$$

where $S(\bar{\omega})$ is the so-called Sears function, which has been tabulated by Kemp.[31]

In order to compare the present program's predictions against Eq. (47), it was run with the following inputs: M = 0.01, h = 0.8, B = 30, ϕ_T = 1.0, η_T = 0.05 n_D = 10 and ϵ = 0.01. The conditions correspond to a reduced frequency $\bar{\omega}$ = 0.5. In Eq. (17), NI and NJ were each 5, and NL = 5, NN = 3 collocation points were used. The azimuthal and radial mode series were truncated at NM = 5 and NK = 20, respectively. The two calculations are compared in Fig. 24a, which shows the magnitude of the complex lift coefficient as a function of span. Very good agreement is exhibited right at the hub, but the two predictions diverge significantly as the tip region is approached.

The chordwise load distribution in such a flow is just the same flat-plate loading exhibited in steady flow - i.e., the entire chord responds in-phase. This distribution is compared with that predicted by the present code at the hub in Fig. 24b. The agreement is seen to be excellent. Unfortunately, the results for the phase of C_L showed poor agreement: the phase given by Eq. (47) is independent of radius and equal to -33.4°, while that predicted by the code varied monotonically from +129.9° at the hub to +134.4° at the tip.

In attempting to resolve the discrepancies in the C_L predictions, it was realized that, again based on strip theory, the radial variation of the gust amplitude in Eq. (46) would result in a nearly linear spanwise variation in the circulation, Γ . This would result in a trailing vortex pattern of uniform strength, which is not accounted for by strip theory, but whose influence is present in the 3-D code. In an attempt to eliminate this effect, the same case was re-run with the amplitude in Eq. (46) (and hence, also (47)) multiplied by $(\phi_T \sigma)^{-1}$. The resulting comparison of $|C_L|$ is shown in Fig. 25. As expected, both calculations display less spanwise variation than in Fig. 24; however, now the strip theory predictions are 8-15% higher than the present results over the entire span. The phase, which in the strip theory is unaffected by the change, is now predicted by the code to vary from 131.3° to 133.3°.

Efforts to improve the agreement by increasing the hub/tip ratio and/or lowering the reduced frequency were unsuccessful. It may be that a programming error remains in the code, or perhaps an insufficient number of azimuthal and radial modes were included in the calculation. At present, we believe the latter is more likely, but to correct it would require further increases in computer storage requirements. For the reasons outlined in Section IV. G., this was not practicable on the present system. Accordingly, the remaining effort was concentrated on the development of the finite difference code described in Section B.

SECTION V
SUMMARY AND CONCLUSIONS

This report presents the results of a research program on rotating stall in axial flow compressors. Three major tasks are described which were: (1) the development of an Euler code for rotor rows, (2) the development of a two-dimensional stability theory for the compressible flow through two blade rows, and (3) the development of an unsteady lifting surface theory for the flow through a three-dimensional blade row.

The two-dimensional version of the Euler code developed works well over a range of subsonic inlet conditions including cases where shock waves form in the blade passages. The code works with either a Kutta condition or conditions at downstream infinity specified. The integration code requires approximately 2.5×10^{-3} seconds per grid point per time step on a Cyber 750 computing machine and required 160,000 octal words of central memory. For the grid used which was 10 by 40 approximately, 800 to 1200 time steps were required to reach the steady state. The cases with shock waves required the longer times. The size of the time steps used correspond to Courant numbers of 5 to 10. The upper limit for convergence was not established; however, the results for an inlet Mach number of .76 appeared to suffer excessive rothalpy loss near the leading edge with the larger time step sizes. The results for an inlet Mach number of .5 did not show such effects so that computing times for these cases can probably be reduced substantially.

Although the basic integration methods used for the Euler equations have been well publicized in the external aerodynamics literature, several modifications were found to be crucial in order to apply the method to internal flows. The calculation of the metrics of the transformation proves to be extremely important and a revision of the numerical viscosity treatment enlarges and enhances the domain where converged solutions can be obtained. In particular, it was found that the metrics must be discretized in the same spatial fashion as the governing partial differential equation in order to avoid introducing source-like terms which would quickly destroy the solution.

A small disturbance stability analysis has been presented for the two-dimensional, compressible flow through a rotor-stator combination. The theory has been implemented into a computer code which predicts the stability boundary and propagation speed of disturbances for given steady state blade row performance data. The theory and numerical results reduce to the incompressible flow case as inlet Mach number approaches zero. The calculations show that even for fixed blade row performance, compressibility has a significant effect on the stability boundary. It is generally found that this effect is destabilizing compared to the incompressible flow results.

The unsteady lifting surface theory was developed for the purpose of predicting the aerodynamic response of an annular blade row to inlet flow distortion. A linearized but fully three-dimensional lifting surface analysis was used. The model is also capable of predicting the acoustic far field within the duct. Numerical calculations were performed to determine the unsteady spanwise and chordwise load distribution on a rotor row subjected to a circumferentially sinusoidal perturbation of the axial inlet velocity. In an attempt to validate the model, its results were compared in the limit of low Mach number, low solidity, and high hub/tip ratio against a stripwise application of Sears analysis for an isolated airfoil subjected to a sinusoidal gust. The predicted magnitudes of the unsteady lift coefficients agree reasonably well near the hub, and the chordwise load distributions there are in excellent agreement. However, the discrepancies between the two predictions grow as the tip region is approached. Also, there are major differences in the phase of the lift coefficient predicted by the two methods. The reason for these differences is unresolved at present.

REFERENCES

1. Ludwig, G.R. "Test of an Improved Rotating Stall Control System on a J-85 Turbojet Engine" AFAPL-TR-79-2060 August 1979

2. Homicz, G.F., Lordi, J.A. and Ludwig, G.R. "Aerodynamic and Acoustic Investigations of Axial Flow Fan and Compressor Blade Rows, Including Three-Dimensional Effects" AFAPL-TR-79-2061 August 1979

3. Ludwig, G.R. and Nenni, J.P. "Basic Studies of Rotating Stall in Axial Flow Compressors" AFAPL-TR-79-2083 September 1979

4. Rae, William J. "An Application of Implicit Time Marching to Three-Dimensional Flow Through a Compressor Blade Row" AFOSR-TN-81-0153 November 1980 (ADA096354)

5. Rae, William J. "A Computer Program for the Ives Transformation in Turbomachinery Cascades" AFOSR-TN-81-0154 November 1980 (ADA096416)

6. Ives, D.C. and Liutermoza, J.F. "Analysis of Transonic Cascade Flow Using Conformal Mapping and Relaxation Techniques" AIAA Journal 15 pp. 647-652 1977

7. Dulikravich, D.S. "Numerical Calculation of Inviscid, Potential Transonic Flows Through Rotors and Fans" Ph.D. Thesis Cornell University January 1979

8. Dulikravich, D.S. "CAS2D - FORTRAN Program for Nonrotating Blade-to-Blade, Steady, Potential Transonic Cascade Flows" NASA TP 1705 July 1980

9. Beam, Richard M. and Warming, R.F. "An Implicit Finite-Difference Algorithm for Hyperbolic Systems in Conservation-Law Form" Journal of Computational Physics 22 pp. 87-110 1976

10. Warming, R.F. and Beam, Richard M. "On the Construction and Application of Implicit Factored Schemes for Conservation Laws" Proceedings of the Symposium in Applied Mathematics of the American Mathematical Society and the Society for Industrial and Applied Mathematics pp. 85-129 April 1977

11. Sorathy, K.P. "Computation of Three-Dimensional Flow Fields Through Rotating Blade Rows and Comparison With Experiment" Transactions of the ASME, Journal of Engineering for Power Vol. 104 pp. 65-66 April 1982

12. Viviand, H. "Formes Conservatives des Equations de la Dynamique des Gas" La Recherche Aerospatiale (1974) No. 1 Janaury-February pp. 65-66

13. Pulliam T.H. and Steger, J.L. "On Implicit Finite-Difference Simulation of Three Dimensional Flow" AIAA Paper 78-10 January 1978

14. Steger, J.L. "Implicit Finite-Difference Simulation of Flow About Arbitrary Two-Dimensional Geometries" AIAA Journal Vol. 16 No. 7 July 1978

15. Desideri, J.A. , Steger, J.L. and Tannehill, J.C. "On Improving the Iterative Convergence Properties of an Implicit Approximate-Factorization Finite Difference Algorithm" NASA TM-78495 June 1978

16. Richtmeyer, R.D. and Morton, K.N. "Difference Methods for Initial-Value Problems" Second Edition, Interscience Publisher pp. 274-278 1967

17. Rae, W.J. and Homicz, G.F. "A Rectangular-Coordinate Method for Calculating Nonlinear Transonic Potential Flowfields in Compressor Cascades" AIAA Paper 78-248 January 1978

18. Bogdanoff, L.M. "Performance of Compressor Blade Cascades at High Mach Numbers" NACA RM No. L7D11a June 1947

19. Steger, J.L., Pulliam, T.H. and Chima, R.V. "An Implicit Finite-Difference Code for Inviscid and Viscous Cascade Flow" AIAA Paper 80-1427 June 1980

20. Gopalakrishnan, S. and Bozzola, R. "Numerical Representation of Inlet and Exit Boundary Conditions in Transient Flow" Journal of Engineering for Power Transactions of the ASME pp. 340-344 October 1973

21. Rae, W.J. and Lordi, J.A. "A Study of Inlet Conditions for Three-Dimensional Compressor Flows" Calspan Report No. XE-6129-A-4 June 1978

22. Thompkins, W.T., Jr. "A Fortran Program for Calculating Three-Dimensional, Inviscid, Rotational Flows with Shock Waves in Axial Compressor Blade Rows" MIT Gas Turbine and Plasma Dynamics Lab. GT + PDL Report No. 162 September 1981

23. Briggs, N.B. "Effect of Mach Number on the Flow and Application of Compressibility Corrections in a Two-Dimensional Subsonic-Transonic Compression Cascade Having Varied Porous-Wall Suction at the Blade Tips" NACA TN-2649 March 1952

24. Nenni, J.P. and Ludwig, G.R. "A Theory to Predict the Inception of Rotating Stall in Axial Flow Compressors" AIAA Paper 74-528 June 1974

25. Ludwig, G.R., Nenni, J.P. and Arendt, R.H. "Investigation of Rotating Stall in Axial Flow Compressor and the Development of a Prototype Rotating Stall Control System" AFAPL-TR-73-45 May 1973

26. Ludwig, G.R., Nenni, J.P. and Erickson, J.C., Jr. "Investigation of Rotating Stall Phenomena in Axial Flow Compressors, Vol. I - Basic Studies of Rotating Stall" AFAPL-TR-76-48 Vol. I June 1976

27. Morfey, C.L. "Sound Transmission and Generation in Ducts With Flow" J. Sound and Vibration Vol. 14 No. 1 37-55 January 1971

28. Lordi, J.A., Homicz, G.F. and Ludwig, G.R. "Investigation of Rotating Stall Phenomena in Axial Flow Compressors, Volume II - Investigation of Rotor-Stator Interaction Noise and Lifting Surface Theory for a Rotor" AFAPL-TR-76-48 June 1976

29. O'Hara, H. and Smith, F.J. "The Evaluation of Definite Integrals by Internal Subdivision" Computer Journal Vol. 12 1969

30. Sears, W.R. "Some Aspects of Non-Stationary Airfoil Theory and Its Practical Application" J. of the Aeronautical Sciences Vol. 8 No. 3 pp. 104-108 1941

31. Kemp, N.H. "On the Lift and Circulaion of Airfoils in Some Unsteady-Flow Problems" J. of the Aeronautical Sciences Vol. 19 No. 10 pp. 713-714 October 1952

32. Luke, Y.L. "On Generating Bessel Functions by Use of the Backward Recurrence Formula" Aerospace Research Laboratories, Wright-Patterson Air Force Base ARL 72-0030 1972

Appendix A

EVALUATION OF AXIAL INTEGRALS

This appendix summarizes the analytical expressions obtained for the axial integrals which arise in the three-dimensional unsteady lifting-surface theory. In what follows, $\phi = \cos^{-1} x$, and I_n denotes the modified Bessel function of order n (not to be confused with the azimuthal mode number). In general, I_n will be complex; its argument will vary according to the class of integrals being evaluated, as will be described below.

For the wake term integrals, Eq. (25), one obtains:

$$C'(x) = (\pi - \phi + \sin\phi)\cos\bar{\omega}x \, \mathcal{R}e\, I_0 - \pi \sin\bar{\omega}x \, \mathcal{I}m\, I_1$$
$$+ \sum_{n=1}^{\infty} (-1)^n \left[\frac{\sin(n-1)\phi}{n-1} - 2\frac{\sin n\phi}{n} + \frac{\sin(n+1)\phi}{n+1} \right]$$
$$\cdot \begin{Bmatrix} \cos\bar{\omega}x \, \mathcal{R}e\, I_n \\ \sin\bar{\omega}x \, \mathcal{I}m\, I_n \end{Bmatrix} \begin{Bmatrix} n \text{ EVEN} \\ n \text{ ODD} \end{Bmatrix} \tag{A-1}$$

$$S'(x) = (\pi - \phi + \sin\phi)\sin\bar{\omega}x \, \mathcal{R}e\, I_0 + \pi \cos\bar{\omega}x \, \mathcal{I}m\, I_1$$
$$+ \sum_{n=1}^{\infty} \left[\frac{\sin(n-1)\phi}{n-1} - 2\frac{\sin n\phi}{n} + \frac{\sin(n+1)\phi}{n+1} \right]$$
$$\begin{Bmatrix} \sin\bar{\omega}x \, \mathcal{R}e\, I_n \\ \cos\bar{\omega}x \, \mathcal{R}e\, I_n \end{Bmatrix} \begin{Bmatrix} n \text{ EVEN} \\ n \text{ ODD} \end{Bmatrix} \tag{A-2}$$

$$C^{i}(x) = \frac{\pi}{2}(-1)^{i} \begin{Bmatrix} \cos\bar{\omega}\, x\,(\mathcal{R}e\, I_{i-2} - \mathcal{R}e\, I_{i}) \\ \sin\bar{\omega}\, x\,(\mathcal{I}m\, I_{i-2} - \mathcal{I}m\, I_{i}) \end{Bmatrix} \begin{Bmatrix} i & \text{EVEN} \\ i & \text{ODD} \end{Bmatrix}$$

$$+ \left[\frac{\sin i\phi}{2i} - \frac{\sin(i-2)\phi}{2(i-2)}\right] \cos\bar{\omega}\, x\, \mathcal{R}e\, I_{0}$$

$$+ \sum_{n=1}^{\infty}(-1)^{n}\left[\frac{\sin(n-i)\phi}{2(n-i)} + \frac{\sin(n+i)\phi}{2(n+i)} - \frac{\sin(n-i+2)\phi}{2(n-i+2)} - \frac{\sin(n+i-2)\phi}{2(n+i-2)}\right]$$

$$\cdot \begin{Bmatrix} \sin\bar{\omega}\, x\, \mathcal{R}e\, I_{n} \\ \cos\bar{\omega}\, x\, \mathcal{I}m\, I_{n} \end{Bmatrix} \begin{Bmatrix} n & \text{EVEN} \\ n & \text{ODD} \end{Bmatrix} \qquad i \geq 2 \qquad \text{(A-3)}$$

$$S^{i}(x) = \frac{\pi}{2} \begin{Bmatrix} \sin\bar{\omega}\, x\,(\mathcal{R}e\, I_{i-2} - \mathcal{R}e\, I_{i}) \\ \cos\bar{\omega}\, x\,(\mathcal{I}m\, I_{i-2} - \mathcal{I}m\, I_{i}) \end{Bmatrix} \begin{Bmatrix} i & \text{EVEN} \\ i & \text{ODD} \end{Bmatrix}$$

$$+ \left[\frac{\sin i\phi}{2i} - \frac{\sin(i-2)\phi}{2(i-2)}\right] \sin\bar{\omega}\, x\, \mathcal{R}e\, I_{0}$$

$$+ \sum_{n=1}^{\infty}\left[\frac{\sin(n-i)\phi}{2(n-i)} + \frac{\sin(n+i)\phi}{2(n+i)} - \frac{\sin(n-i+2)\phi}{2(n-i+2)} - \frac{\sin(n+i-2)\phi}{2(n+i-2)}\right]$$

$$\cdot \begin{Bmatrix} \sin\bar{\omega}\, x\, \mathcal{R}e\, I_{n} \\ \cos\bar{\omega}\, x\, \mathcal{I}m\, I_{n} \end{Bmatrix} \begin{Bmatrix} n & \text{EVEN} \\ n & \text{ODD} \end{Bmatrix} \qquad i \geq 2 \qquad \text{(A-4)}$$

where all the I_n have the imaginary argument, $(-i\bar{\omega})$. It should be noted that with such an argument, I_n is purely real/imaginary for n even/odd.

The results for the exponential integrals above cut-off, Eq. (26), are:

$$C_{nk}^{1A}(x) = \pi\left[\cos(a-b)\times \mathcal{R}e\, I_0^- - \sin(a-b)\times \mathcal{I}m\, I_1^-\right]$$
$$+(\sin\phi-\phi)\left[\cos(a-b)\times \mathcal{R}e\, I_0^- - \cos(a+b)\times \mathcal{R}e\, I_0^+\right]$$
$$+\sum_{n=1}^{\infty}(-1)^n\left(\frac{\sin(n-1)\phi}{n-1}-\frac{2\sin n\phi}{n}+\frac{\sin(n+1)\phi}{n+1}\right)$$
$$\cdot\begin{Bmatrix}\cos(a-b)\times \mathcal{R}e\, I_n^- - \cos(a+b)\times \mathcal{R}e\, I_n^+\\ \sin(a-b)\times \mathcal{I}m\, I_n^- - \sin(a+b)\times \mathcal{I}m\, I_n^+\end{Bmatrix}\quad\begin{Bmatrix}n & \text{EVEN}\\ n & \text{ODD}\end{Bmatrix}\qquad\text{(A-5)}$$

$$S_{nk}^{1A}(x) = \pi\left[\sin(a-b)\times \mathcal{R}e\, I_0^- + \cos(a-b)\times \mathcal{I}m\, I_1^-\right]$$
$$+(\sin\phi-\phi)\left[\sin(a-b)\times \mathcal{R}e\, I_0^- - \sin(a+b)\times \mathcal{R}e\, I_0^+\right]$$
$$+\sum_{n=1}^{\infty}\left(\frac{\sin(n-1)\phi}{n-1}-\frac{2\sin n\phi}{n}+\frac{\sin(n+1)\phi}{n+1}\right)$$
$$\cdot\begin{Bmatrix}\sin(a-b)\times \mathcal{R}e\, I_n^- - \sin(a+b)\times \mathcal{R}e\, I_n^+\\ \cos(a-b)\times \mathcal{I}m\, I_n^- - \cos(a+b)\times \mathcal{I}m\, I_n^+\end{Bmatrix}\quad\begin{Bmatrix}n & \text{EVEN}\\ n & \text{ODD}\end{Bmatrix}\qquad\text{(A-6)}$$

$$C_{\underset{\sim}{s}nk}^{1A}(x) = \pi\left[\cos(a-b)\times \mathcal{R}e\, I_0^- - \sin(a-b)\times \mathcal{I}m\, I_1^-\right]$$
$$+(\sin\phi-\phi)\left[\cos(a-b)\times \mathcal{R}e\, I_0^- + \cos(a+b)\times \mathcal{R}e\, I_0^+\right]$$
$$+\sum_{n=1}^{\infty}(-1)^n\left(\frac{\sin(n-1)\phi}{n-1}-\frac{2\sin n\phi}{n}+\frac{\sin(n+1)\phi}{n+1}\right)$$
$$\cdot\begin{Bmatrix}\cos(a-b)\times \mathcal{R}e\, I_n^- + \cos(a+b)\times \mathcal{R}e\, I_n^+\\ \sin(a-b)\times \mathcal{I}m\, I_n^- + \sin(a+b)\times \mathcal{I}m\, I_n^+\end{Bmatrix}\quad\begin{Bmatrix}n & \text{EVEN}\\ n & \text{ODD}\end{Bmatrix}\qquad\text{(A-7)}$$

$$S_{S_{nk}}^{1A}(x) = \pi\left[\sin(a-b)\times Re\, I_0^- + \cos(a-b)\times Im\, I_1^-\right]$$
$$+ (\sin\phi - \phi)\left[\sin(a-b)\times Re\, I_0^- + \sin(a+b)\times Re\, I_0^+\right]$$
$$+ \sum_{n=1}^{\infty}\left(\frac{\sin(n-1)\phi}{n-1} - \frac{2\sin n\phi}{n} + \frac{\sin(n+1)\phi}{n+1}\right)$$
$$\cdot\begin{Bmatrix}\sin(a+b)\times Re\, I_n^- + \sin(a+b)\times Re\, I_n^+ \\ \cos(a-b)\times Im\, I_n^- + \cos(a+b)\times Im\, I_n^+\end{Bmatrix}\begin{Bmatrix} n \text{ EVEN} \\ n \text{ ODD}\end{Bmatrix} \qquad \text{(A-8)}$$

$$C_{nk}^{iA}(x) = \frac{\pi}{2}(-1)^i\begin{Bmatrix}\cos(a-b)\times(Re\, I_{i-2}^- - Re\, I_i^-) \\ \sin(a-b)\times(Im\, I_{i-2}^- - Im\, I_i)\end{Bmatrix}\begin{Bmatrix} i \text{ EVEN} \\ i \text{ ODD}\end{Bmatrix}$$
$$+ \frac{1}{2}\left(\frac{\sin i\phi}{i} - \frac{\sin(i-2)\phi}{i-2}\right)\left[\cos(a-b)\times Re\, I_0^- - \cos(a+b)\times Re\, I_0^+\right]$$
$$+ \sum_{n=1}^{\infty}(-1)^n\left(\frac{\sin(n-i)\phi}{2(n-i)} + \frac{\sin(n+i)\phi}{2(n+i)} - \frac{\sin(n-i+2)\phi}{2(n-i+2)} - \frac{\sin(n+i-2)\phi}{2(n+i-2)}\right)$$
$$\cdot\begin{Bmatrix}\cos(a-b)\times Re\, I_n^- - \cos(a+b)\times Re\, I_n^+ \\ \sin(a-b)\times Im\, I_n^- - \sin(a+b)\times Im\, I_n^+\end{Bmatrix}\begin{Bmatrix} n \text{ EVEN} \\ n \text{ ODD}\end{Bmatrix} \qquad \text{(A-9)} \quad i \geq 2$$

$$S_{nk}^{iA}(x) = \frac{\pi}{2}\begin{Bmatrix}\sin(a-b)\times(Re\, I_{i-2}^- - Re\, I_i^-) \\ \cos(a-b)\times(Im\, I_{i-2}^- \; Im\, I_i^-)\end{Bmatrix}\begin{Bmatrix} i \text{ EVEN} \\ i \text{ ODD}\end{Bmatrix}$$
$$+ \frac{1}{2}\left(\frac{\sin i\phi}{i} - \frac{\sin(i-2)\phi}{i-2}\right)\left(\sin(a-b)\times Re\, I_0^- - \sin(a+b)\times Re\, I_0^+\right)$$
$$+ \sum_{n=1}^{\infty}\left(\frac{\sin(n-i)\phi}{2(n-i)} + \frac{\sin(n+i)\phi}{2(n+i)} - \frac{\sin(n-i+2)\phi}{2(n-i+2)} - \frac{\sin(n+i-2)\phi}{2(n+i-2)}\right)$$
$$\cdot\begin{Bmatrix}\sin(a-b)\times Re\, I_n^- - \sin(a+b)\times Re\, I_n^+ \\ \cos(a-b)\times Im\, I_n^- - \cos(a+b)\times Im\, I_n^+\end{Bmatrix}\begin{Bmatrix} n \text{ EVEN} \\ n \text{ ODD}\end{Bmatrix} \qquad \text{(A-10)} \quad i \geq 2$$

$$
\begin{aligned}
C_{s_{nk}}^{iA}(x) = {} & \frac{\pi}{2}(-1)^i \begin{Bmatrix} \cos(a-b)\,x\,(\mathrm{Re}\,I_{i-2}^- - \mathrm{Re}\,I_i^-) \\ \sin(a-b)\,x\,(\mathrm{Im}\,I_{i-2}^- - \mathrm{Im}\,I_i^-) \end{Bmatrix} \begin{Bmatrix} i \ \text{EVEN} \\ i \ \text{ODD} \end{Bmatrix} \\
& + \frac{1}{2}\left(\frac{\sin i\phi}{i} - \frac{\sin(i-2)\phi}{i-2}\right)\left[\cos(a-b)\,x\,\mathrm{Re}\,I_0^- + \cos(a+b)\,x\,\mathrm{Re}\,I_0^+\right] \\
& + \sum_{n=1}^{\infty}(-1)^n\left(\frac{\sin(n-i)\phi}{2(n-i)} + \frac{\sin(n+i)\phi}{2(n+i)} - \frac{\sin(n-i+2)\phi}{2(n-i+2)} - \frac{\sin(n+i-2)\phi}{2(n+i-2)}\right) \\
& \cdot \begin{Bmatrix} \cos(a-b)\,x\,\mathrm{Re}\,I_n^- + \cos(a+b)\,x\,\mathrm{Re}\,I_n^+ \\ \sin(a-b)\,x\,\mathrm{Im}\,I_n^- + \sin(a+b)\,x\,\mathrm{Im}\,I_n^+ \end{Bmatrix} \begin{Bmatrix} n \ \text{EVEN} \\ n \ \text{ODD} \end{Bmatrix} \qquad i \geq 2
\end{aligned}
\tag{A-11}
$$

$$
\begin{aligned}
S_{s_{nk}}^{iA}(x) = {} & \frac{\pi}{2} \begin{Bmatrix} \sin(a-b)\,x\,(\mathrm{Re}\,I_{i-2}^- - \mathrm{Re}\,I_i^-) \\ \cos(a-b)\,x\,(\mathrm{Im}\,I_{i-2}^- - \mathrm{Im}\,I_i^-) \end{Bmatrix} \begin{Bmatrix} i \ \text{EVEN} \\ i \ \text{ODD} \end{Bmatrix} \\
& + \frac{1}{2}\left(\frac{\sin i\phi}{i} - \frac{\sin(i-2)\phi}{i-2}\right)\left(\sin(a-b)\,x\,\mathrm{Re}\,I_0^- + \sin(a+b)\,x\,\mathrm{Re}\,I_0^+\right) \\
& + \sum_{n=1}^{\infty}\left(\frac{\sin(n-i)\phi}{2(n-i)} + \frac{\sin(n+i)\phi}{2(n+i)} - \frac{\sin(n-i+2)\phi}{2(n-i+2)} - \frac{\sin(n+i-2)\phi}{2(n+i-2)}\right) \\
& \cdot \begin{Bmatrix} \sin(a-b)\,x\,\mathrm{Re}\,I_n^- + \sin(a+b)\,x\,\mathrm{Re}\,I_n^+ \\ \cos(a-b)\,x\,\mathrm{Im}\,I_n^- + \cos(a+b)\,x\,\mathrm{Im}\,I_n^+ \end{Bmatrix} \begin{Bmatrix} n \ \text{EVEN} \\ n \ \text{ODD} \end{Bmatrix} \qquad i \geq 2
\end{aligned}
\tag{A-12}
$$

where in the above expressions

$$I_n^{\pm} = I_n\,[-i(a \pm b)]$$

where a and b are defined in Eq. (26c).

The results for the exponential integrals below cut-off, Eq. (27), are:

$$
\begin{aligned}
C^{1B}_{nk}(x) &= \pi e^{-cx}\left[\cos dx\,(Re\,I_0 - Re\,I_1) - \sin dx\,(Im\,I_0 - Im\,I_1)\right] \\
&- 2(\sin\phi - \phi)\left[\sinh cx \cos dx\, Re\,I_0 + \cosh cx \sin dx\, Im\,I_0\right] \\
&+ 4\sum_{n=1}^{\infty}(-1)^{n+1}\left[\frac{\sin(n-1)\phi}{2(n-1)} - \frac{\sin n\phi}{n} + \frac{\sin(n+1)\phi}{2(n+1)}\right] \\
&\cdot\left[\begin{Bmatrix}\sinh cx \\ \cosh cx\end{Bmatrix}\cos dx\, Re\,I_n + \begin{Bmatrix}\cosh cx \\ \sinh cx\end{Bmatrix}\sin dx\, Im\,I_n\right]\begin{Bmatrix}n \text{ EVEN} \\ n \text{ ODD}\end{Bmatrix}
\end{aligned}
\tag{A-13}
$$

$$
\begin{aligned}
S^{1B}_{nk}(x) &= \pi e^{-cx}\left[\cos dx\,(Im\,I_0 - Im\,I_1) + \sin dx\,(Re\,I_0 - Re\,I_1)\right] \\
&+ 2(\sin\phi - \phi)\left[\cosh cx \cos dx\, Im\,I_0 - \sinh cx \sin dx\, Re\,I_0\right] \\
&+ 4\sum_{n=1}^{\infty}(-1)^{n}\left[\frac{\sin(n-1)\phi}{2(n-1)} - \frac{\sin n\phi}{n} + \frac{\sin(n+1)\phi}{2(n+1)}\right] \\
&\cdot\left[\begin{Bmatrix}\cosh cx \\ \sinh cx\end{Bmatrix}\cos dx\, Im\,I_n - \begin{Bmatrix}\sinh cx \\ \cosh cx\end{Bmatrix}\sin dx\, Re\,I_n\right]\begin{Bmatrix}n \text{ EVEN} \\ n \text{ ODD}\end{Bmatrix}
\end{aligned}
\tag{A-14}
$$

$$
\begin{aligned}
Cs^{1B}_{nk}(x) &= \pi e^{-cx}\left[\cos dx\,(Re\,I_0 - Re\,I_1) - \sin dx\,(Im\,I_0 - Im\,I_1)\right] \\
&+ 2(\sin\phi - \phi)\left[\cosh cx \cos dx\, Re\,I_0 + \sinh cx \sin dx\, Im\,I_0\right] \\
&+ 4\sum_{n=1}^{\infty}(-1)^{n}\left[\frac{\sin(n-1)\phi}{2(n-1)} - \frac{\sin n\phi}{n} + \frac{\sin(n+1)\phi}{2(n+1)}\right] \\
&\cdot\left[\begin{Bmatrix}\cosh cx \\ \sinh cx\end{Bmatrix}\cos dx\, Re\,I_n + \begin{Bmatrix}\sinh cx \\ \cosh cx\end{Bmatrix}\sin dx\, Im\,I_n\right]\begin{Bmatrix}n \text{ EVEN} \\ n \text{ ODD}\end{Bmatrix}
\end{aligned}
\tag{A-15}
$$

$$
\begin{aligned}
{}^{1B}S_{nk}(x) = {} & \pi e^{-cx}\left[\cos dx\,(\mathcal{I}m\, I_0 - \mathcal{I}m\, I_1) + \sin dx\,(\mathcal{R}e\, I_0 - \mathcal{R}e\, I_1)\right] \\
& - 2(\sin\phi - \phi)\left[\sinh cx \cos dx\, \mathcal{I}m\, I_0 - \cosh cx \sin dx\, \mathcal{R}e\, I_0\right] \\
& + 4\sum_{n=1}^{\infty}(-1)^{n+1}\left[\frac{\sin(n-1)\phi}{2(n-1)} - \frac{\sin n\phi}{n} + \frac{\sin(n+1)\phi}{2(n+1)}\right] \qquad \text{(A-16)} \\
& \cdot\left[\begin{Bmatrix}\sinh cx\\ \cosh cx\end{Bmatrix}\cos dx\, \mathcal{I}m\, I_n - \begin{Bmatrix}\cosh cx\\ \sinh cx\end{Bmatrix}\sin dx\, \mathcal{R}e\, I_n\right]\begin{Bmatrix}n \text{ EVEN}\\ n \text{ ODD}\end{Bmatrix}
\end{aligned}
$$

$$
\begin{aligned}
{}^{iB}C_{nk}(x) = {} & \frac{\pi}{2} e^{-cx}\left[\cos dx\,(\mathcal{R}e\, I_{i-2} - \mathcal{R}e\, I_i) - \sin dx\,(\mathcal{I}m\, I_{i-2} - \mathcal{I}m\, I_i)\right] \\
& - \left(\frac{\sin i\phi}{i} - \frac{\sin(i-2)\phi}{i-2}\right)\left[\sinh cx \cos dx\, \mathcal{R}e\, I_0 + \cosh cx \sin dx\, \mathcal{I}m\, I_0\right] \\
& + \sum_{n=1}^{\infty}(-1)^{n+1}\left[\frac{\sin(n-i)\phi}{(n-i)} + \frac{\sin(n+i)\phi}{(n+i)} - \frac{\sin(n-i+2)\phi}{(n-i+2)} - \frac{\sin(n+i-2)\phi}{(n+i-2)}\right] \\
& \cdot\left[\begin{Bmatrix}\sinh cx\\ \cosh cx\end{Bmatrix}\cos dx\, \mathcal{R}e\, I_n + \begin{Bmatrix}\cosh cx\\ \sinh cx\end{Bmatrix}\sin dx\, \mathcal{I}m\, I_n\right]\begin{Bmatrix}n \text{ EVEN}\\ n \text{ ODD}\end{Bmatrix} \\
& i \geq 2 \qquad \text{(A-17)}
\end{aligned}
$$

$$
\begin{aligned}
{}^{iB}S_{nk}(x) = {} & \frac{\pi}{2} e^{-cx}\left[\cos dx\,(\mathcal{I}m\, I_{i-2} - \mathcal{I}m\, I_i) + \sin dx\,(\mathcal{R}e\, I_{i-2} - \mathcal{R}e\, I_i)\right] \\
& + \left[\frac{\sin i\phi}{i} - \frac{\sin(i-2)\phi}{i-2}\right]\left[\cosh cx \cos dx\, \mathcal{I}m\, I_0 - \sinh cx \sin dx\, \mathcal{R}e\, I_0\right] \\
& + \sum_{n=1}^{\infty}(-1)^{n}\left[\frac{\sin(n-i)\phi}{(n-i)} + \frac{\sin(n+i)\phi}{(n+i)} - \frac{\sin(n-i+2)\phi}{(n-i+2)} - \frac{\sin(n+i-2)\phi}{(n+i-2)}\right] \\
& \cdot\left[\begin{Bmatrix}\cosh cx\\ \sinh cx\end{Bmatrix}\cos dx\, \mathcal{I}m\, I_n - \begin{Bmatrix}\sinh cx\\ \cosh cx\end{Bmatrix}\sin dx\, \mathcal{R}e\, I_n\right]\begin{Bmatrix}n \text{ EVEN}\\ n \text{ ODD}\end{Bmatrix} \\
& i \geq 2 \qquad \text{(A-18)}
\end{aligned}
$$

$$
\begin{aligned}
{}^{iB}Cs_{nk}(x) = {} & \frac{\pi}{2} e^{-cx}\left[\cos dx\,(Re\,I_{i-2} - Re\,I_i) - \sin dx\,(Im\,I_{i-2} - Im\,I_i)\right] \\
& + \left[\frac{\sin i\phi}{i} - \frac{\sin(i-2)\phi}{i-2}\right]\left[\cosh cx \cos dx\, Re\,I_0 + \sinh cx \sin dx\, Im\,I_0\right] \\
& + \sum_{n=1}^{\infty}(-1)^n\left[\frac{\sin(n-i)\phi}{(n-i)} + \frac{\sin(n+i)\phi}{(n+i)} - \frac{\sin(n-i+2)\phi}{(n-i+2)} - \frac{\sin(n+i-2)\phi}{(n+i-2)}\right] \\
& \cdot\left[\begin{Bmatrix}\cosh cx \\ \sinh cx\end{Bmatrix}\cos dx\, Re\,I_n + \begin{Bmatrix}\sinh cx \\ \cosh cx\end{Bmatrix}\sin dx\, Im\,I_n\right]\begin{Bmatrix} n \text{ EVEN} \\ n \text{ ODD}\end{Bmatrix}
\end{aligned}
$$

$$i \geq 2 \qquad \text{(A-19)}$$

$$
\begin{aligned}
{}^{iB}Ss_{nk}(x) = {} & \frac{\pi}{2} e^{-cx}\left[\cos dx\,(Im\,I_{i-2} - Im\,I_i) + \sin dx\,(Re\,I_{i-2} - Re\,I_i)\right] \\
& - \left[\frac{\sin i\phi}{i} - \frac{\sin(i-2)\phi}{i-2}\right]\left[\sinh cx \cos dx\, Im\,I_0 - \cosh cx \sin dx\, Re\,I_0\right] \\
& + \sum_{n=1}^{\infty}(-1)^{n+1}\left[\frac{\sin(n-i)\phi}{(n-i)} + \frac{\sin(n+i)\phi}{(n+i)} - \frac{\sin(n-i+2)\phi}{(n-i+2)} - \frac{\sin(n+i-2)\phi}{(n+i-2)}\right] \\
& \cdot\left[\begin{Bmatrix}\sinh cx \\ \cosh cx\end{Bmatrix}\cos dx\, Im\,I_n - \begin{Bmatrix}\cosh cx \\ \sinh cx\end{Bmatrix}\sin dx\, Re\,I_n\right]\begin{Bmatrix} n \text{ EVEN} \\ n \text{ ODD}\end{Bmatrix}
\end{aligned}
$$

$$i \geq 2 \qquad \text{(A-20)}$$

where the argument of I_n in the above expressions is $(c - id)$, where c and d are defined in Eq. (27c).

In the steady flow problem, for $i \geq 2$ it was found that the axial integrals evaluated at $-x$ differed from those at $+x$ by at most a change in sign, depending on i (see Appendix C of Ref. 2). Not surprisingly, these symmetry properties still hold true in the present case for the exponential integrals below cut-off. For those above cut-off and for the wake term integrals, the relationships are not so simple. In fact, they are no longer "symmetry" properties in the strict meaning of the word, but for want of a better terminology, they will be referred to here as such.

For the integrals in the wake terms, one finds that

$$C^{i}(-x) = (-1)^{i+1}\left[C^{i}(x) + \frac{\pi(i-1)}{\bar{\omega}}\begin{Bmatrix}\cos\bar{\omega} \times \mathcal{I}m\, I_{i-1} \\ \sin\bar{\omega} \times \mathcal{R}e\, I_{i-1}\end{Bmatrix}\right] \quad \begin{Bmatrix} i & EVEN \\ i & ODD \end{Bmatrix} \quad i \geq 2 \tag{A-21}$$

$$S^{i}(-x) = (-1)^{i} S^{i} x + \frac{\pi(i-1)}{\bar{\omega}}\begin{Bmatrix}\sin\bar{\omega} \times \mathcal{I}m\, I_{i-1} \\ \cos\bar{\omega} \times \mathcal{R}e\, I_{i-1}\end{Bmatrix} \quad \begin{Bmatrix} i & EVEN \\ i & ODD \end{Bmatrix} \quad i \geq 2 \tag{A-22}$$

where again the I_n have argument $(-i\bar{\omega})$.

For the axial integrals pertaining to modes above cut-off, one finds that

$$C^{iA}_{nk}(-x) = (-1)^{i+1} C^{iA}_{nk}(x)$$

$$+ (-1)^{i+1}\pi(i-1)\begin{Bmatrix}\dfrac{\cos(a-b)x}{(a-b)}\mathcal{I}m\, I^{-}_{i-1} + \dfrac{\cos(a+b)x}{(a+b)}\mathcal{I}m\, I^{+}_{i-1} \\ \dfrac{\sin(a-b)x}{(a-b)}\mathcal{R}e\, I^{-}_{i-1} + \dfrac{\sin(a+b)x}{(a+b)}\mathcal{R}e\, I^{+}_{i-1}\end{Bmatrix}\begin{Bmatrix} i & EVEN \\ i & ODD \end{Bmatrix} \quad i \geq 2 \tag{A-23}$$

$$S^{iA}_{nk}(-x) = (-1)^{i} S^{iA}_{nk}(x)$$

$$+ \pi(i-1)\begin{Bmatrix}\dfrac{\sin(a-b)x}{(a-b)}\mathcal{I}m\, I^{-}_{i-1} + \dfrac{\sin(a+b)x}{(a+b)}\mathcal{I}m\, I^{+}_{i-1} \\ \dfrac{\cos(a-b)x}{(a-b)}\mathcal{R}e\, I^{-}_{i-1} + \dfrac{\cos(a+b)x}{(a+b)}\mathcal{R}e\, I^{+}_{i-1}\end{Bmatrix}\begin{Bmatrix} i & EVEN \\ i & ODD \end{Bmatrix} \quad i \geq 2 \tag{A-24}$$

$$Cs_{nk}^{iA}(-x) = (-1)^{i+1}\, Cs_{nk}^{iA}(x)$$

$$+(-1)^{i+1}\,\pi(i-1)\left\{\begin{matrix}\dfrac{\cos(a-b)x}{(a-b)}\,\mathcal{I}m\, I_{i-1}^{-} - \dfrac{\cos(a+b)x}{(a+b)}\,\mathcal{I}m\, I_{i-1}^{+} \\ \dfrac{\sin(a-b)x}{(a-b)}\,\mathcal{R}e\, I_{i-1}^{-} - \dfrac{\sin(a+b)x}{(a+b)}\,\mathcal{R}e\, I_{i-1}^{+}\end{matrix}\right\}\left\{\begin{matrix} i \text{ EVEN} \\ i \text{ ODD}\end{matrix}\right\} \quad i \geq 2 \tag{A-25}$$

$$Ss_{nk}^{iA}(-x) = (-1)^{i}\, Ss_{nk}^{iA}(x)$$

$$+\pi(i-1)\left\{\begin{matrix}\dfrac{\sin(a-b)x}{(a-b)}\,\mathcal{I}m\, I_{i-1}^{-} - \dfrac{\sin(a+b)x}{(a+b)}\,\mathcal{I}m\, I_{i-1}^{+} \\ \dfrac{\cos(a-b)x}{(a-b)}\,\mathcal{R}e\, I_{i-1}^{-} - \dfrac{\cos(a+b)x}{(a+b)}\,\mathcal{R}e\, I_{i-1}^{+}\end{matrix}\right\}\left\{\begin{matrix} i \text{ EVEN} \\ i \text{ ODD}\end{matrix}\right\} \quad i \geq 2 \tag{A-26}$$

where again $I_n^{\pm}$ indicates $I_n\,[-i(a \pm b)]$.

Finally, for the axial integrals pertaining to modes below cut-off, we have for $i \geq 2$,

$$C_{nk}^{iB}(-x) = (-1)^{i}\, C_{nk}^{iB}(x) \tag{A-27}$$

$$S_{nk}^{iB}(-x) = (-1)^{i+1}\, S_{nk}^{iB}(x) \tag{A-28}$$

$$Cs_{nk}^{iB}(-x) = (-1)^{i+1}\, Cs_{nk}^{iB}(x) \tag{A-29}$$

$$Ss_{nk}^{iB}(-x) = (-1)^{i}\, Ss_{nk}^{iB}(x) \tag{A-30}$$

and

$$C^{iB}_{nk}(x=0) = 0 \qquad i \text{ odd} \tag{A-31}$$

$$Cs^{iB}_{nk}(x=0) = 0 \qquad i \text{ even} \tag{A-32}$$

$$S^{iB}_{nk}(x=0) = 0 \qquad i \text{ even} \tag{A-33}$$

$$Ss^{iB}_{nk}(x=0) = 0 \qquad i \text{ odd} \tag{A-34}$$

The symmetries described in Eqs. (A-21) through (A-34) can yield a big savings in computer time if the axial collocation points are symmetrically disposed about the mid-chord, $x = 0$. Everything on the right-hand side of these equations will be known from having evaluated the integrals at $+x$. The other half, at $-x$, can then be evaluated using these relations with very little effort.

The analytical expressions given in this appendix, though admittedly complicated, are nevertheless preferable to using numerical quadrature. This might not be true if one had only to perform on the order of ten, or perhaps even a hundred, such integrals. But when literally thousands are required, as is the case here, the systematic way in which these expressions separate the influence of the indices n , k , i and ℓ affords advantages in programming that outweigh their complexity. For example, once the collocation points x_ℓ are chosen, the corresponding values of ϕ and all the sines can be determined. Similarly, note that the arguments of the I_n in the integrals arising from the exponential terms depend only on the azimuthal and radial mode indices, n and k . Since the argument is independent of the order of the Bessel function, one can make use of a very efficient algorithm based on a recursion relation (Ref. 32) to calculate all orders of the function at once for a given mode. A subroutine to do this had already been written and debugged as part of our work on the steady flow problem. Furthermore, the evaluation of the analytical expressions renders the application of the symmetry properties in Eqs. (A-21) through (A-26) almost trivial, which would not be true if numerical quadrature were employed exclusively. For these reasons the use of the expressions given above yields a big savings in computer time over quadrature schemes, which require that each step of the evaluation be

repeated for all combinations of n, k, i, and ℓ. On the other hand, round-off error can ruin the accuracy of these expressions for some modes; this point is discussed in the main text.

Finally, we quote the results for the axial integrals which appear in the expressions for the acoustic farfield, Eqs. (38)-(39). These are:

<u>i = 1</u>

$$\left(C^{1}_{nk}\right)^{u,d} = \pi J_0\left(a^{u,d}_{nk}\right) \qquad \left(S^{1}_{nk}\right)^{u,d} = -\pi J_1\left(a^{u,d}_{nk}\right) \tag{A-35a}$$

<u>i ≥ 2 and even</u>

$$\left(C^{i}_{nk}\right)^{u,d} = \frac{\pi}{2}(-1)^{\frac{i-2}{2}}\left[J_{i-2}\left(a^{u,d}_{nk}\right) + J_i\left(a^{u,d}_{nk}\right)\right]$$
$$\left(S^{i}_{nk}\right)^{u,d} = 0 \tag{A-35b}$$

<u>i > 2 and odd</u>

$$\left(C^{i}_{nk}\right)^{u,d} = 0$$
$$\left(S^{i}_{nk}\right)^{u,d} = \frac{\pi}{2}(-1)^{\frac{i-3}{2}}\left[J_{i-2}\left(a^{u,d}_{nk}\right) + J_i\left(a^{u,d}_{nk}\right)\right] \tag{A-35c}$$

where J_i is the Bessel function of the first kind, of order i.

APPENDIX B

GOVERNING INTEGRAL EQUATION

For easy reference, we reproduce here the complete integral equation relating the velocity component normal to the blades, v_n, to the unknown loading, Δp :

$$
\begin{aligned}
v_n(r,\zeta,z) = {} & \frac{-B\delta_{p_0}}{2\pi\rho_0 U_R r}\int_0^z dz_0\, e^{i\frac{\omega}{U}(z_0-z)}\,\Delta p(\sigma,z_0) \\
& + \frac{B\left(\frac{\Omega r}{U}\right)^2\delta_{p_0}}{2\pi\rho_0 U_R r}\int_0^z dz_0\, e^{i\frac{\omega}{U}(z_0-z)}\sum_{k=1}^{\infty}\int_h^1 d\sigma_0\,\frac{\frac{\partial}{\partial\sigma_0}\left(\sigma_0\frac{\partial\Delta p}{\partial\sigma_0}\right)R_{0k}(\sigma_0)\,R_{0k}(\sigma)}{K_{0k}^2+\left(\frac{\omega r_T}{U}\right)^2} \\
& + \frac{B}{2\pi\rho_0 U_R r}\int_{r_H}^{r_T} dr_0\int_0^z dz_0\sum_{\substack{m=-\infty\\ n\neq 0}}^{\infty} e^{in\zeta+i\frac{\omega}{U}(z_0-z)}\sum_{k=1}^{\infty}\frac{R_{nk}(\sigma)\,R_{nk}(\sigma_0)}{\left[\left(\frac{K_{nk}}{n}\right)^2+\left(\frac{n\Omega+\omega}{nU}r_T\right)^2\right]} \\
& \cdot\left\{\left[1+\left(\frac{\Omega r}{U}\right)^2+\frac{1}{n}\left(\frac{\omega r}{U}\right)\left(\frac{\Omega r}{U}\right)\right]\frac{1}{n^2}\frac{\partial}{\partial r_0}\left(r_0\frac{\partial\Delta p}{\partial r_0}\right)\right. \\
& \left.-\frac{1}{n^2 r_0}\left[\left(\frac{\omega r_0}{U}\right)^2\left(1+\left(\frac{\Omega r}{U}\right)^2\right)+\left(\frac{\omega r}{U}\right)\left(\frac{\omega r_0}{U}\right)\left(\frac{\Omega r}{U}\right)\left(\frac{n\Omega+\omega}{nU}r_0\right)\right]\Delta p(r_0,z_0)\right\} \\
& - \frac{B\left[1+\left(\frac{\Omega r}{U}\right)^2\right]}{2\pi\rho_0 U_R r}\int_0^z dz_0\sum_{\substack{m=-\infty\\ n\neq 0}}^{\infty} e^{in\zeta+i\frac{\omega}{U}(z_0-z)}\sum_{k=1}^{\infty}\frac{R_{nk}(\sigma)}{\left[\left(\frac{K_{nk}}{n}\right)^2+\left(\frac{n\Omega+\omega}{nU}r_T\right)^2\right]} \\
& \cdot\left\{\frac{-2\left(\frac{\omega r_0}{U}\right)\left(\frac{\Omega r_0}{U}\right)}{n^3\left[1+\left(\frac{\Omega r_0}{U}\right)^2\right]^2}\,\Delta p(r_0,z_0)\,R_{nk}(\sigma_0)\Bigg|_{r_H}^{r_T}\right. \\
& + \int_{r_H}^{r_T} dr_0\,\frac{\left(\frac{\omega r_0}{U}\right)\left(\frac{\Omega r_0}{U}\right)R_{nk}(\sigma_0)}{n^3\left[1+\left(\frac{\Omega r_0}{U}\right)^2\right]}\left[\frac{\partial}{\partial r_0}\left(r_0\frac{\partial\Delta p}{\partial r_0}\right)+\frac{4}{1+\left(\frac{\Omega r_0}{U}\right)^2}\frac{\partial\Delta p}{\partial r_0}\right. \\
& \left. + \frac{4\left[1-\left(\frac{\Omega r_0}{U}\right)^2\right]}{\left[1+\left(\frac{\Omega r_0}{U}\right)^2\right]^2}\frac{\Delta p}{r_0}\right] \\
& \left. - \int_{r_H}^{r_T} dr_0\,\frac{\left(\frac{\omega r_0}{U}\right)\left(\frac{\Omega r_0}{U}\right)R_{nk}(\sigma_0)}{1+\left(\frac{\Omega r_0}{U}\right)^2}\left[\frac{2}{n^2}\left(\frac{\omega r_0}{U}\right)\left(\frac{\Omega r_0}{U}\right)+\frac{1}{n^3}\left(\frac{\omega r_0}{U}\right)^2\right]\frac{\Delta p}{r_0}\right\}
\end{aligned}
$$

$$
- \frac{B}{4\pi \rho_o U_R} \int_{r_H}^{r_T} dr_o \int_0^{c_a} dz_o \sum_{m=-\infty}^{\infty} \sum_{k=0}^{\infty} \frac{R_{nk}(\sigma) R_{nk}(\sigma_o) e^{in\zeta}}{\lambda_{nk}\left[(K_{nk})^2 + \left(\frac{n\Omega+\omega}{U} r_T\right)^2\right]}
$$

$$
\cdot \left\{ \lambda_{nk} \left[g(r) g(r_o) - \frac{\left(\frac{\Omega r}{U}\right)\left(\frac{\Omega r_o}{U}\right)}{\beta^2} \left[\left(\frac{K_{nk}}{r_T}\right)^2 + \left(\frac{n\Omega+\omega}{U}\right)^2 \right] \right] sgn(z-z_o) \right.
$$

$$
+ i \left[\left(\frac{n\Omega+\omega}{\beta^2 U}\right) \left[f(r) f(r_o) - \left(\frac{\Omega r}{U}\right)\left(\frac{\Omega r_o}{U}\right) \lambda_{nk}^2 \right] - \lambda_{nk}^2 \left[\left(\frac{\Omega r_o}{U}\right) f(r) \right. \right.
$$

$$
\left. \left. \left. + \left(\frac{\Omega r}{U}\right) f(r_o) \right] \right] \right\} e^{i\left(\frac{n\Omega + M^2\omega}{\beta^2 U}\right)(z-z_o) - \lambda_{nk}|z-z_o|} \Delta p(r_o, z_o) \tag{B-1}
$$

The remaining symbols are defined in the main text. For a derivation of this equation, the reader is referred to Ref. 2.

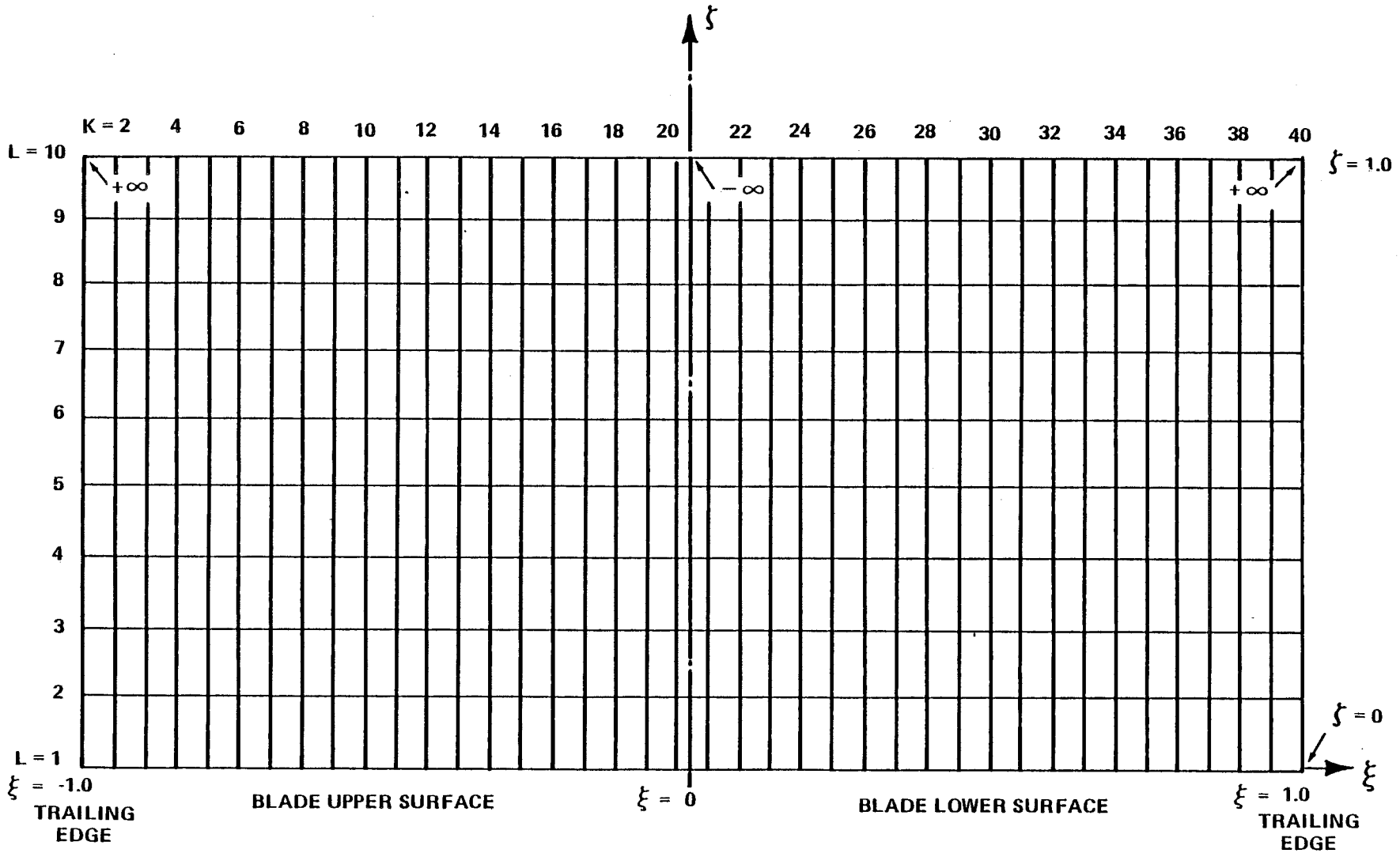

Figure 1 COMPUTATIONAL DOMAIN

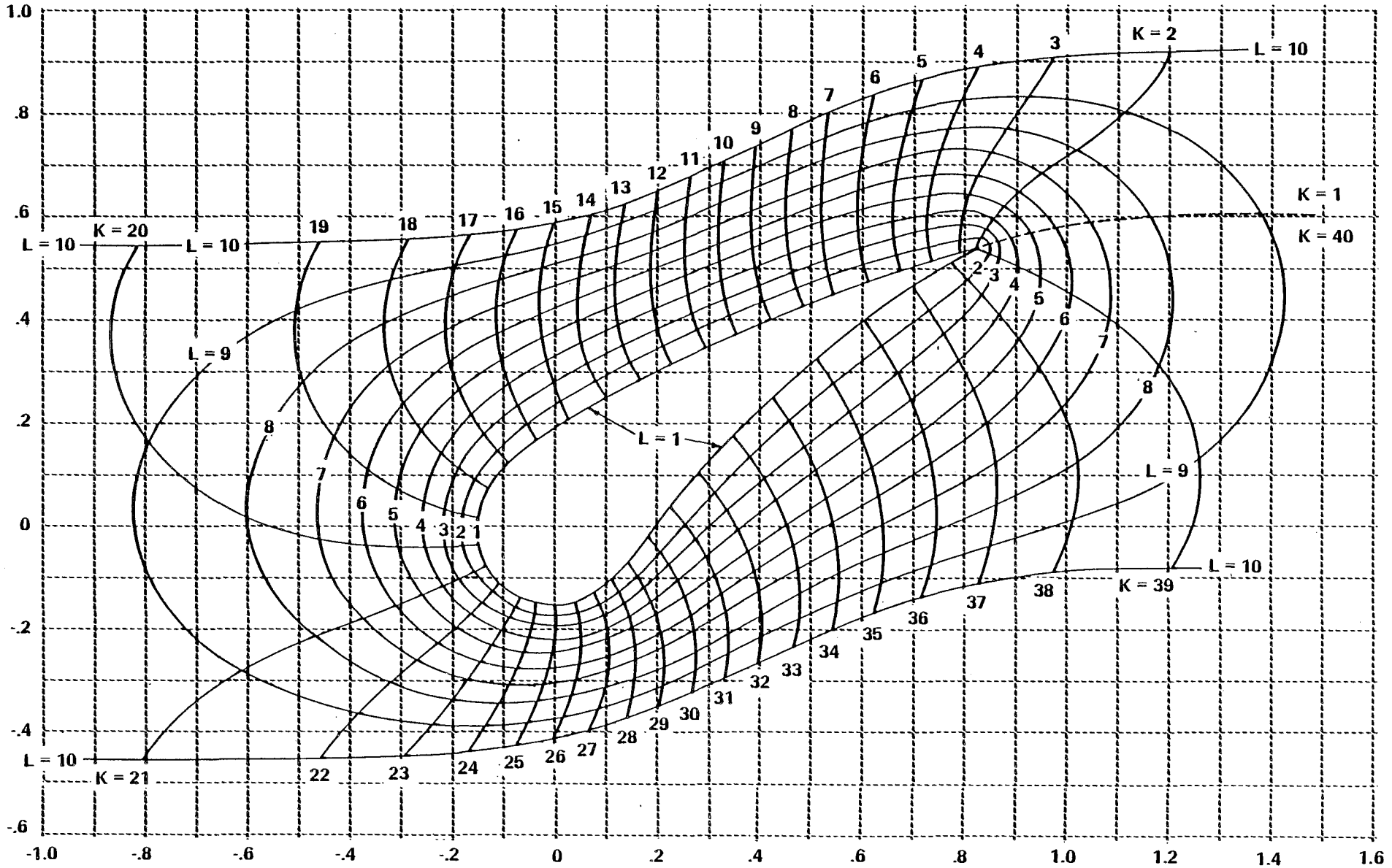

Figure 2 COMPUTATIONAL GRID IN PHYSICAL PLANE FOR TW-1 CASCADE SOLIDITY, $\sigma = 1.16$

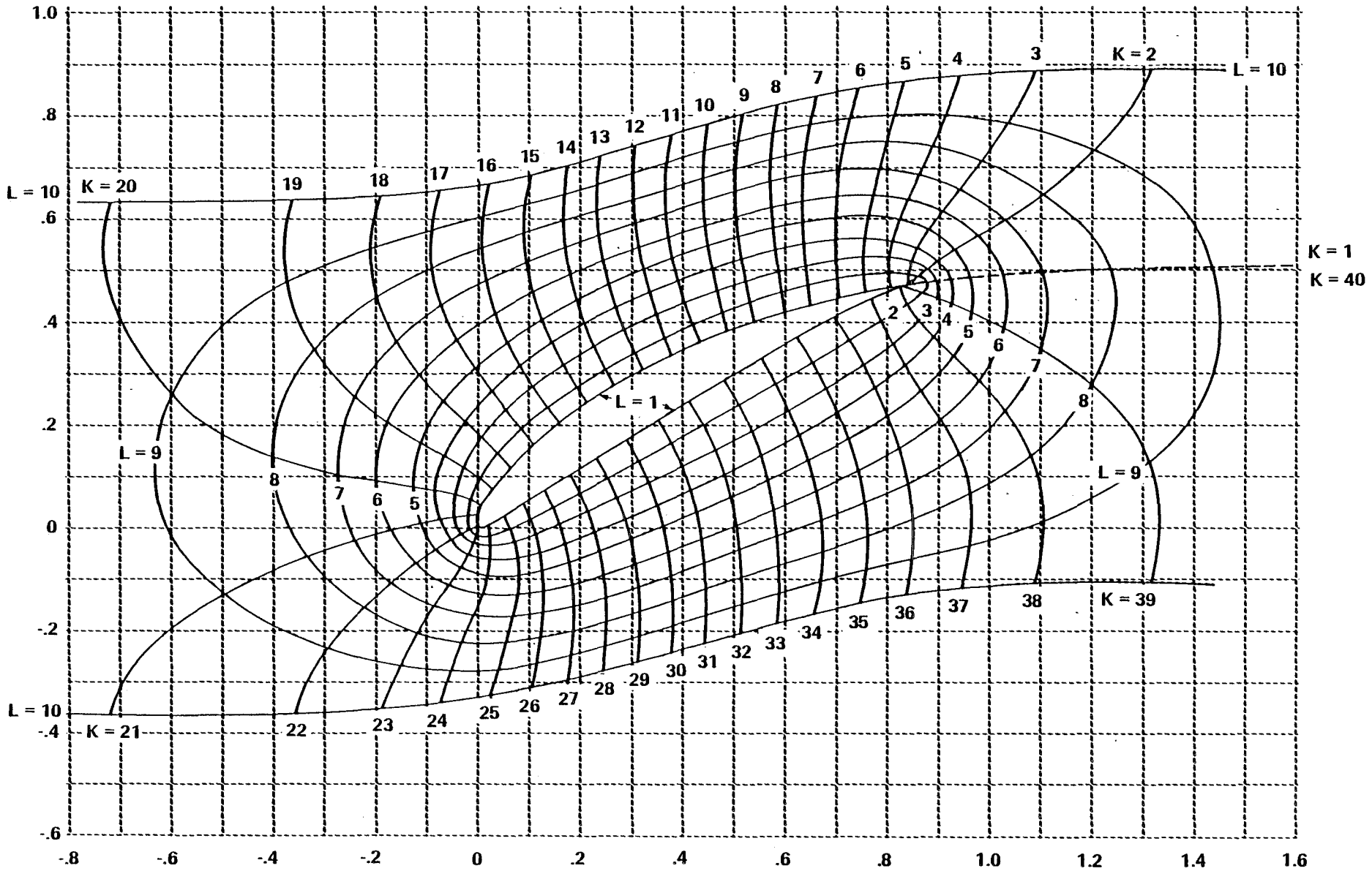

Figure 3 COMPUTATIONAL GRID IN PHYSICAL PLANE

NACA 65 (12) 10 CASCADE

SOLIDITY, $\sigma = 1.0$

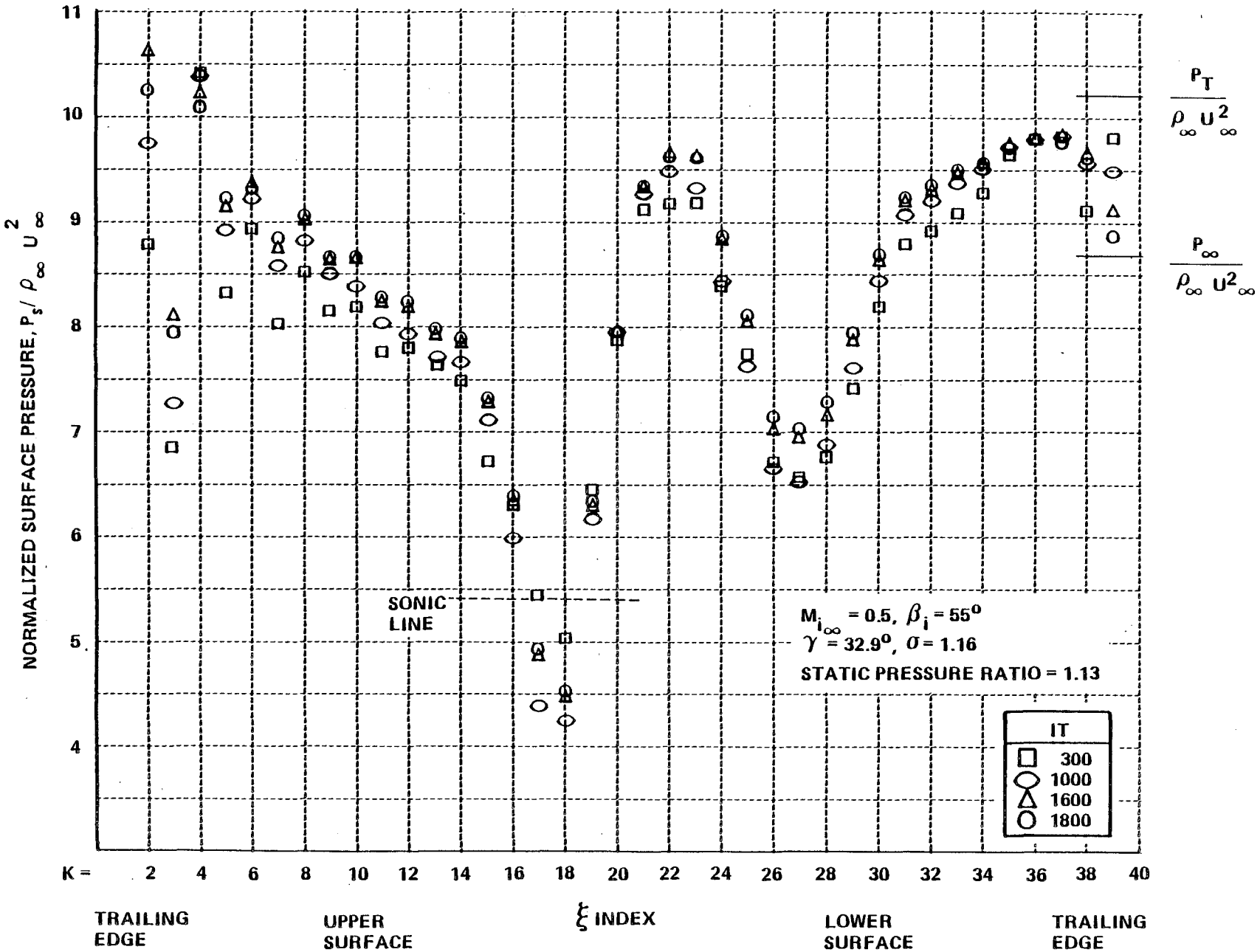

Figure 4 SURFACE PRESSURE DISTRIBUTION FOR TW-1 CASCADE

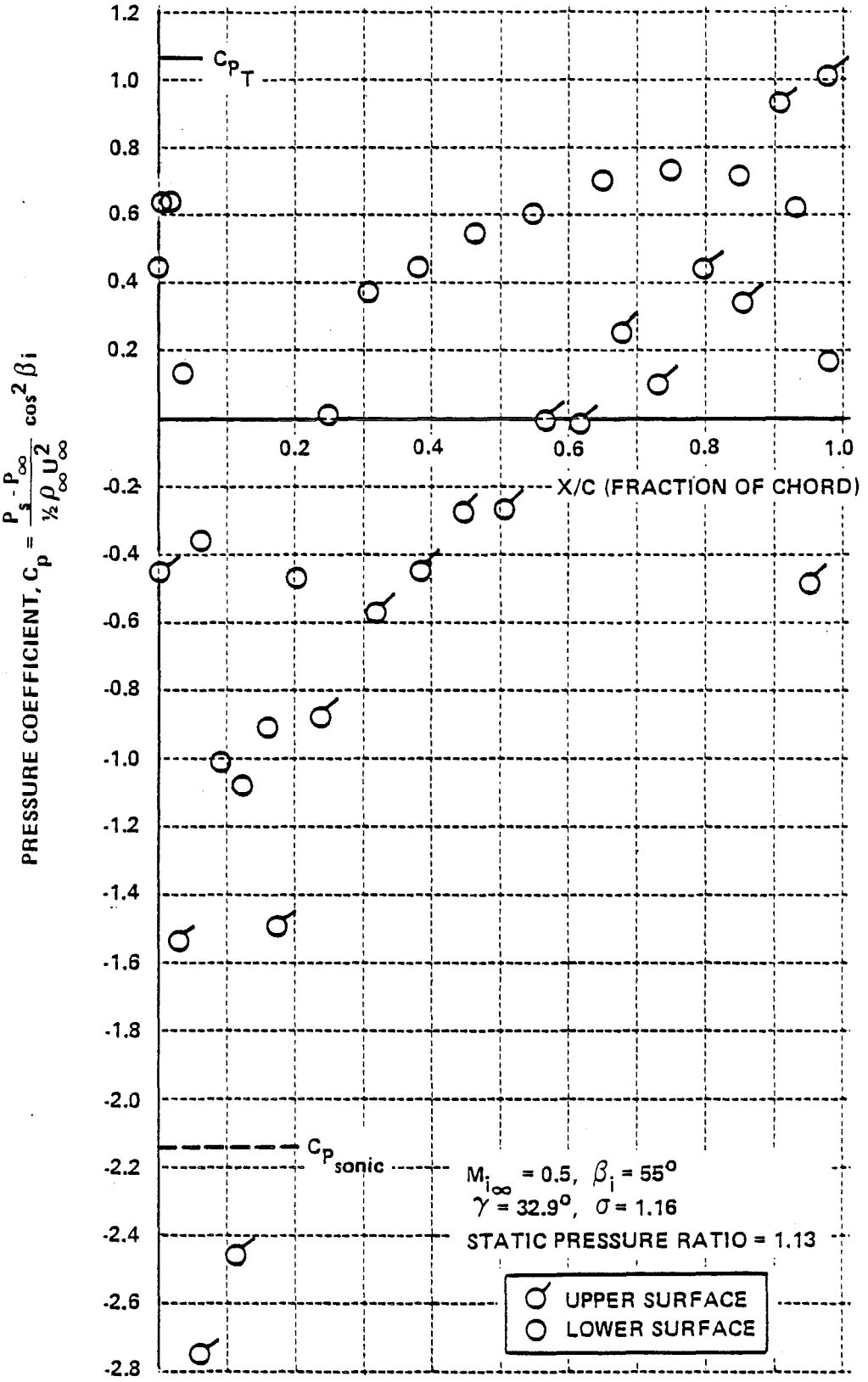

Figure 5 SURFACE PRESSURE COEFFICIENT FOR TW-1 CASCADE

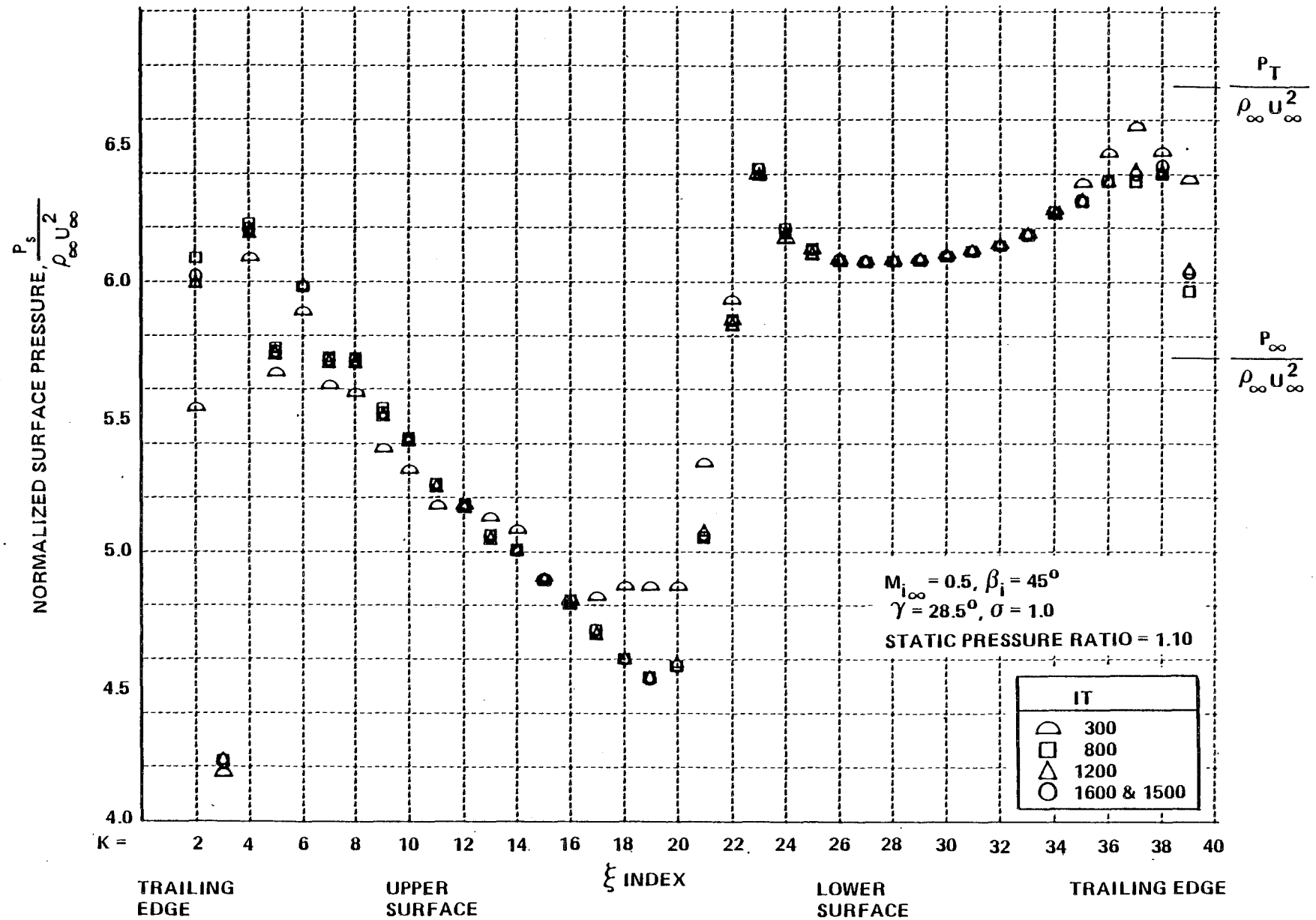

Figure 6 SURFACE PRESSURE DISTRIBUTION FOR NACA 65 (12) 10 CASCADE

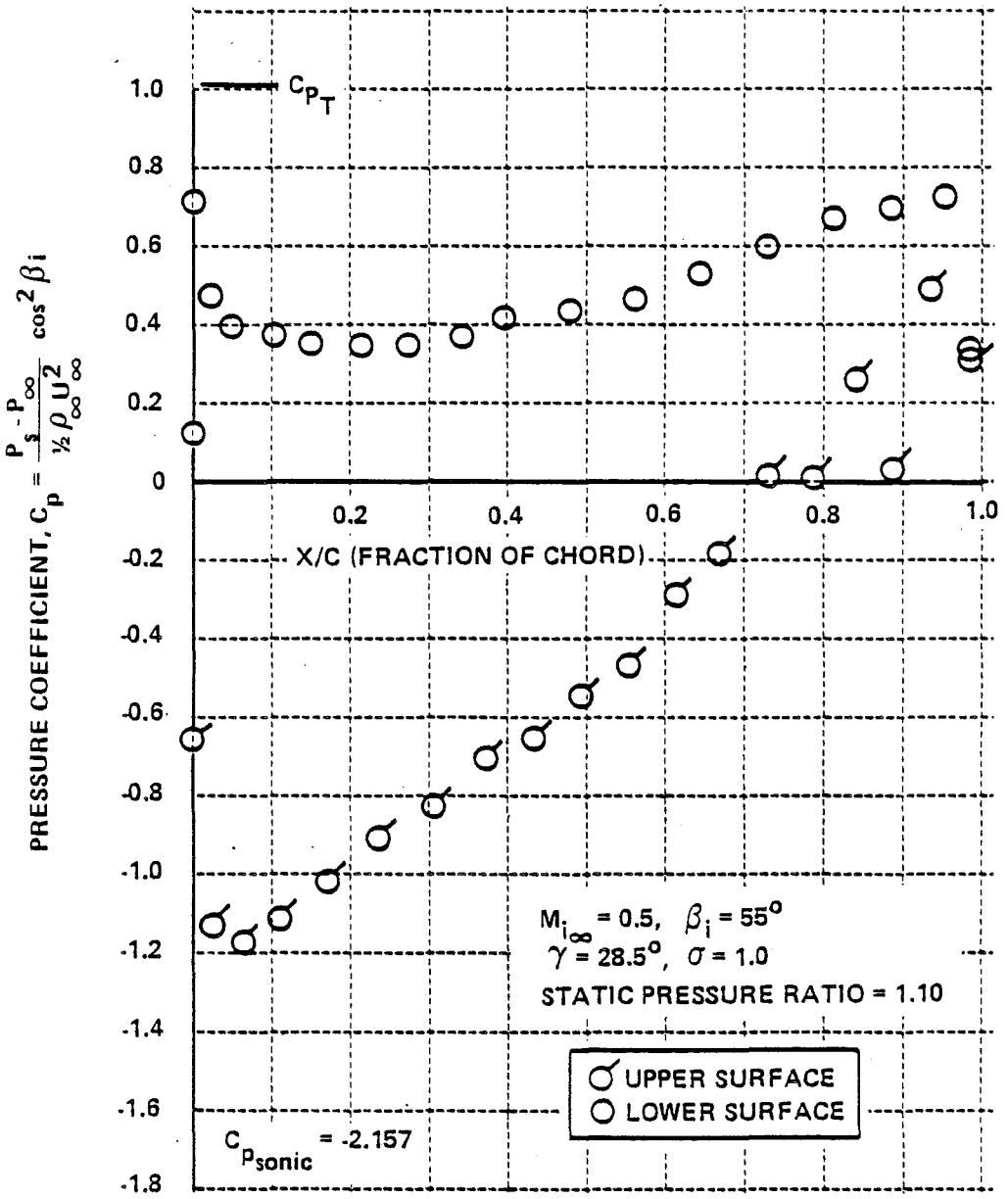

Figure 7 SURFACE PRESSURE COEFFICIENT FOR NACA 65 (12) 10 CASCADE

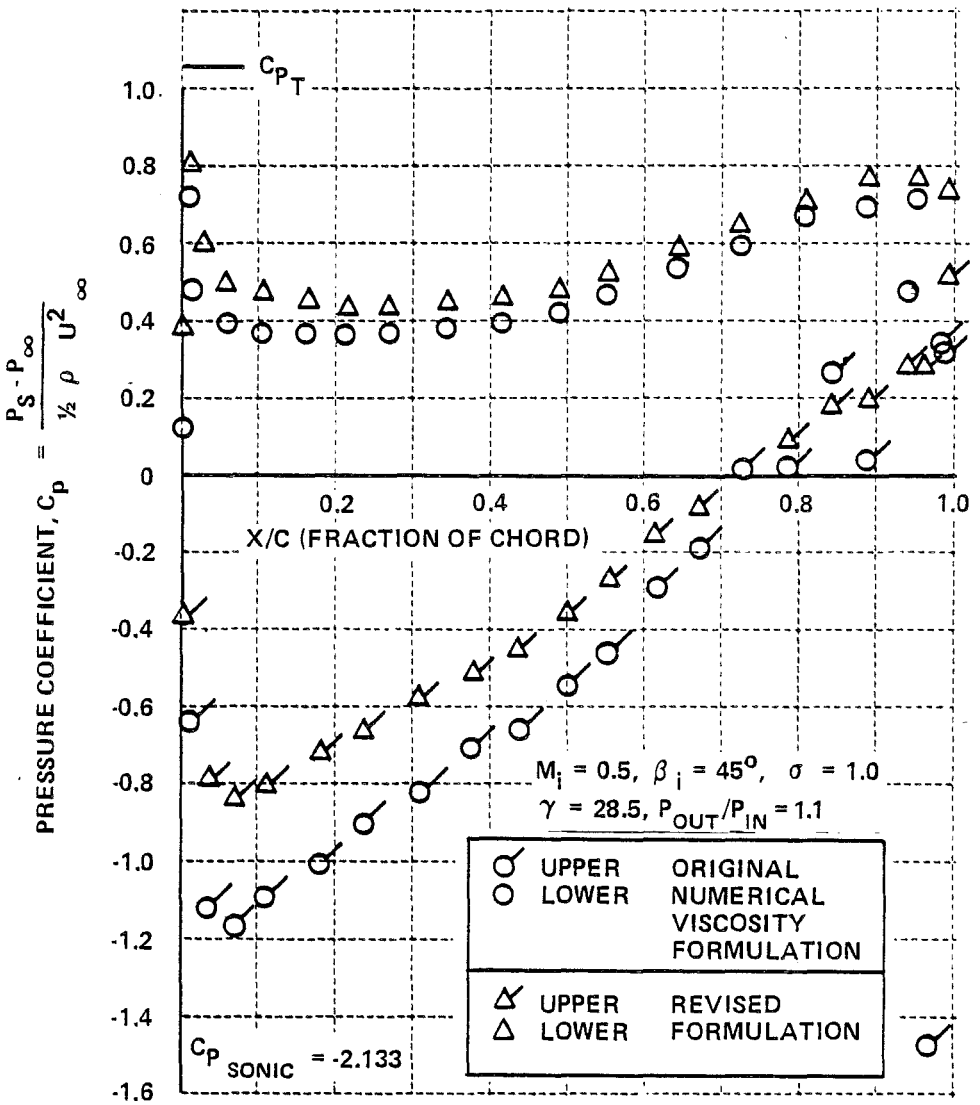

Figure 8 SURFACE PRESSURE DISTRIBUTION NACA 65 (12) 10 CASCADE

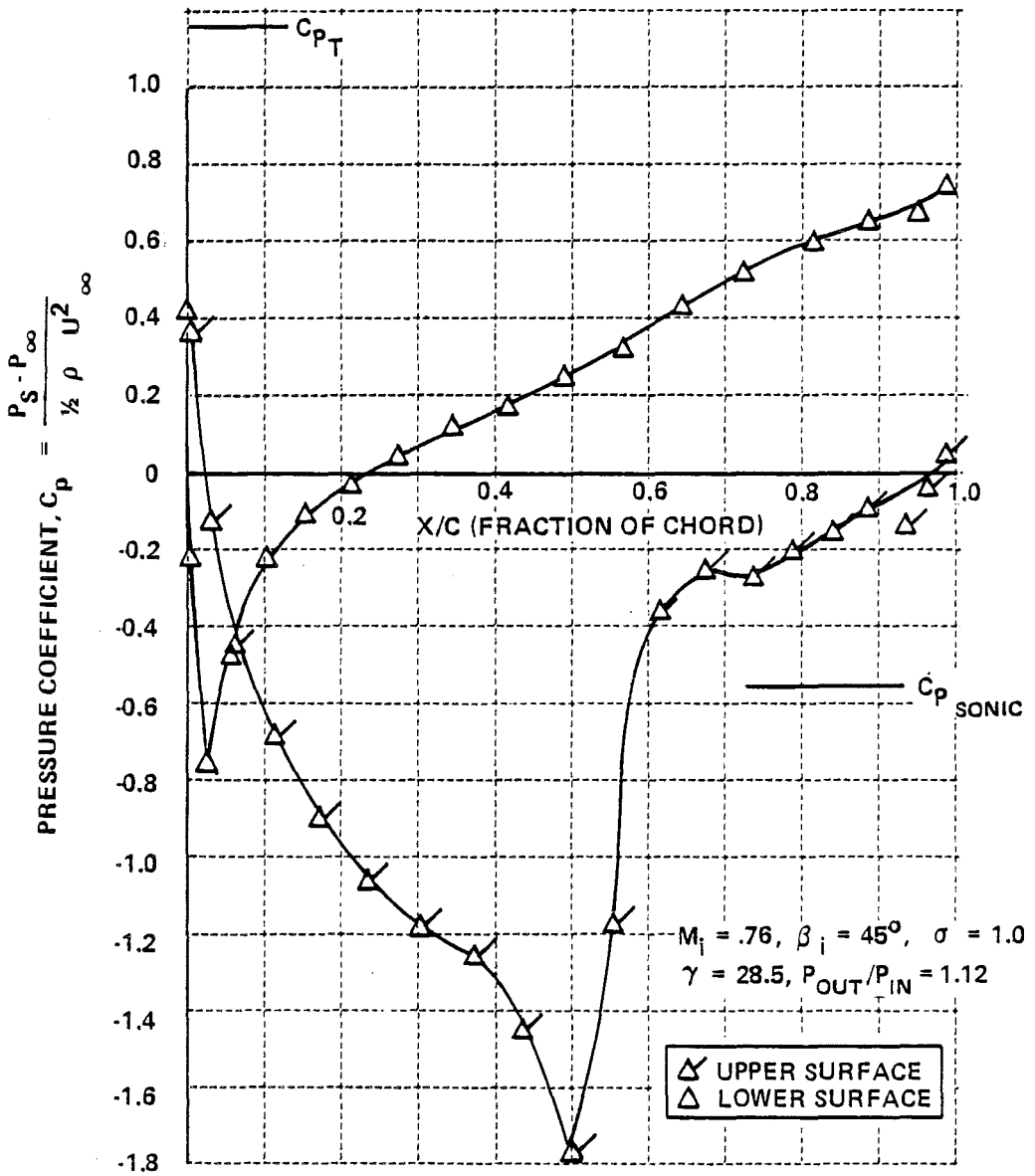

Figure 9 SURFACE PRESSURE DISTRIBUTION NACA 65 (12) 10 CASCADE WITH EXIT CONDITIONS SPECIFIED

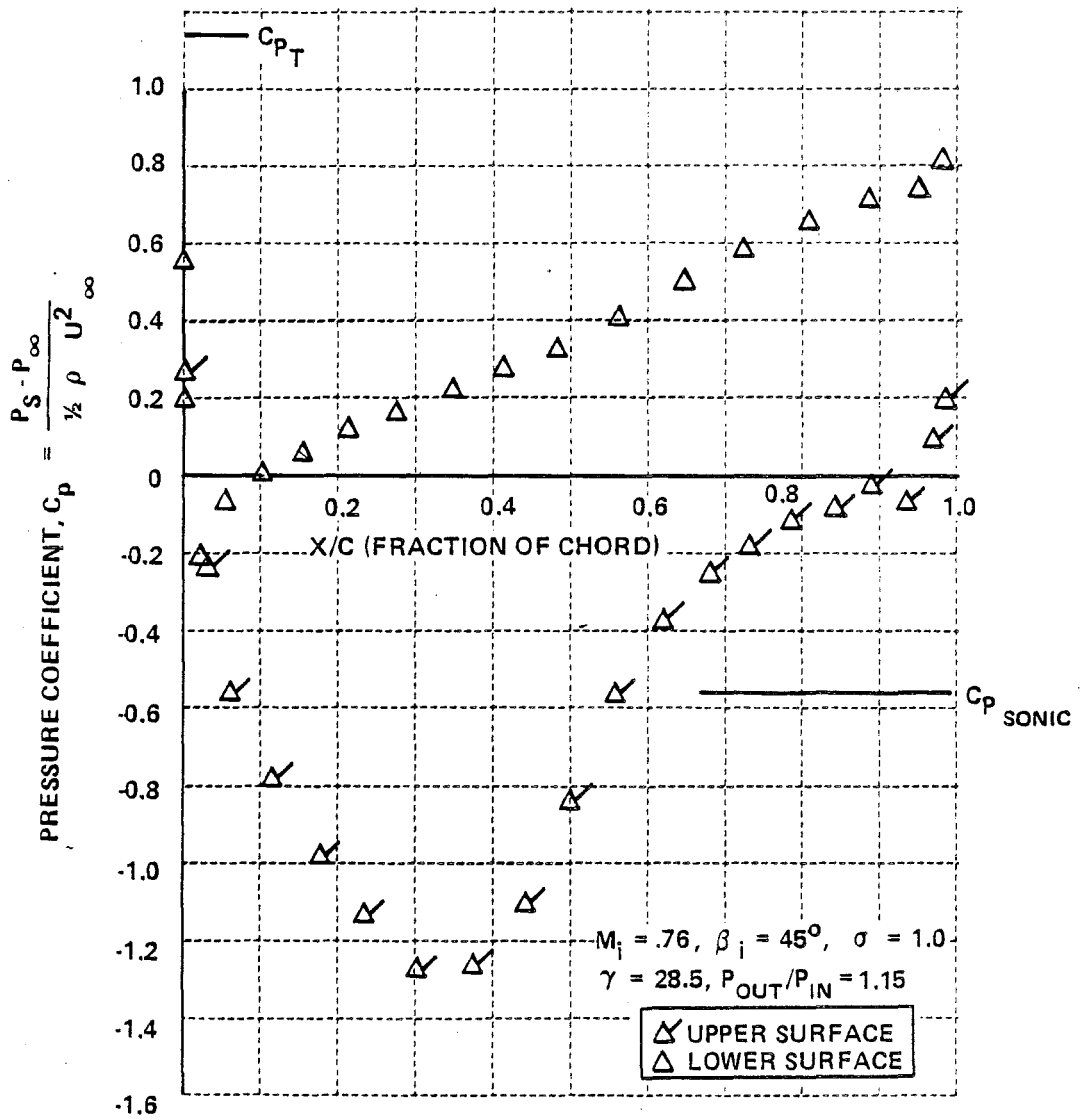

Figure 10 SURFACE PRESSURE DISTRIBUTION NACA 65 (12) 10 CASCADE

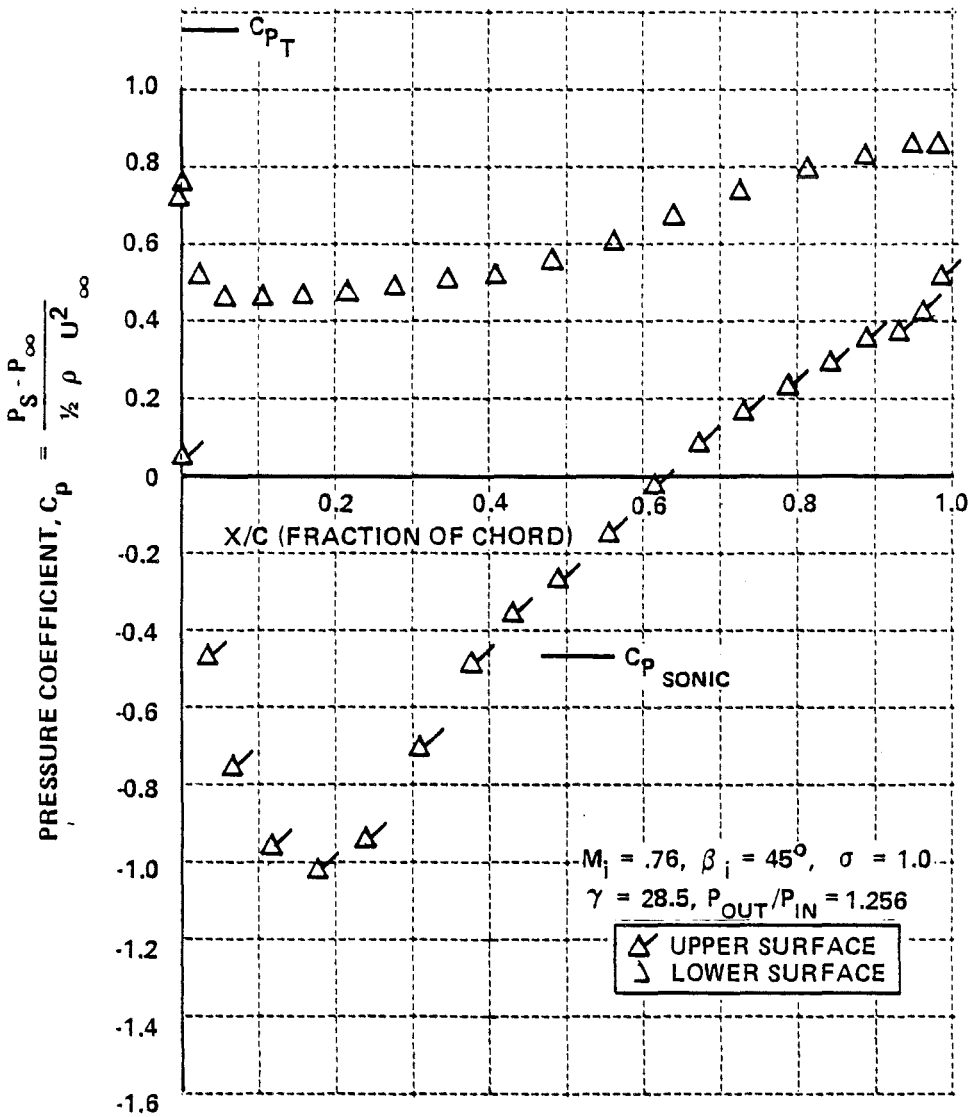

Figure 11 SURFACE PRESSURE DISTRIBUTION NACA 65 (12) 10 CASCADE

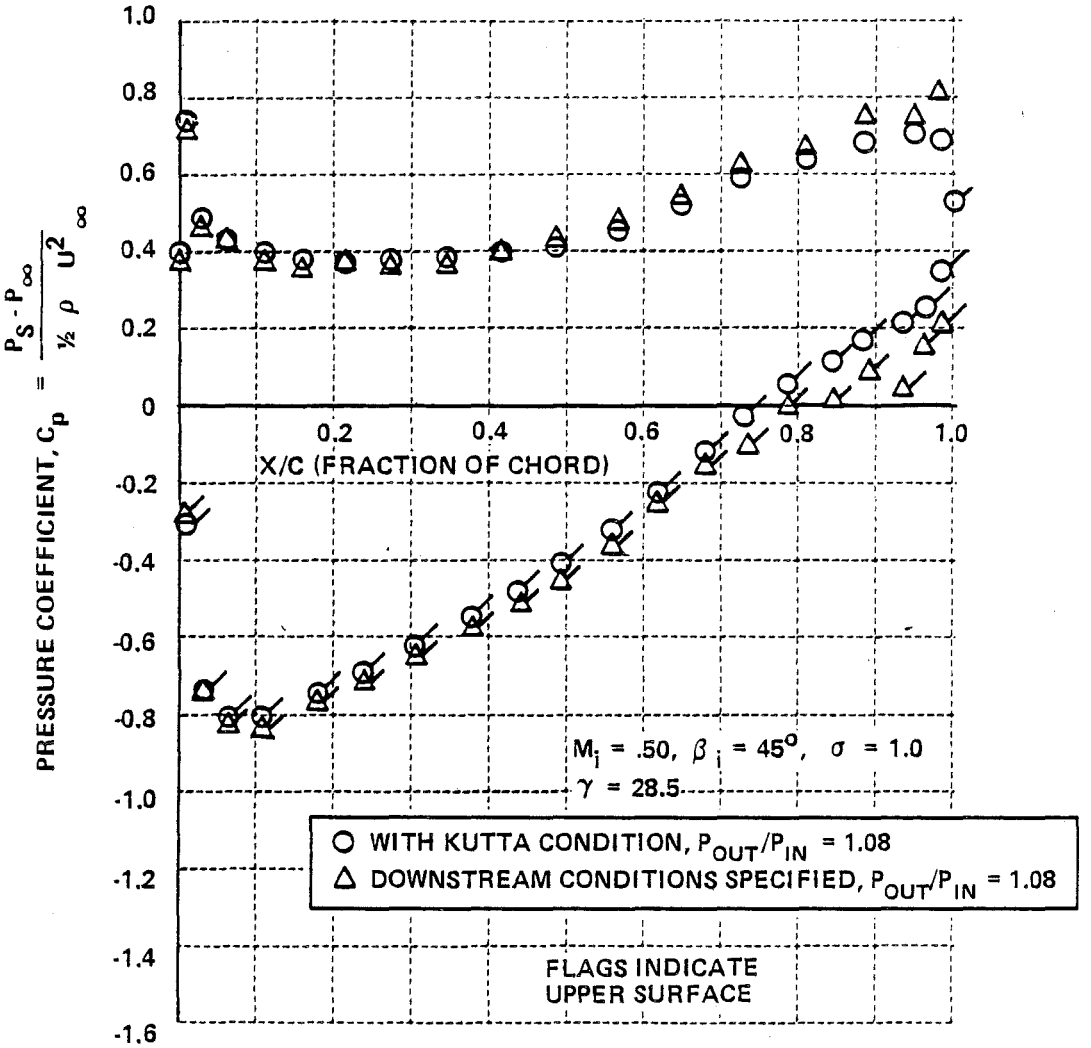

Figure 12 SURFACE PRESSURE DISTRIBUTION NACA 65 (12) 10 CASCADE WITH AND WITHOUT KUTTA CONDITION

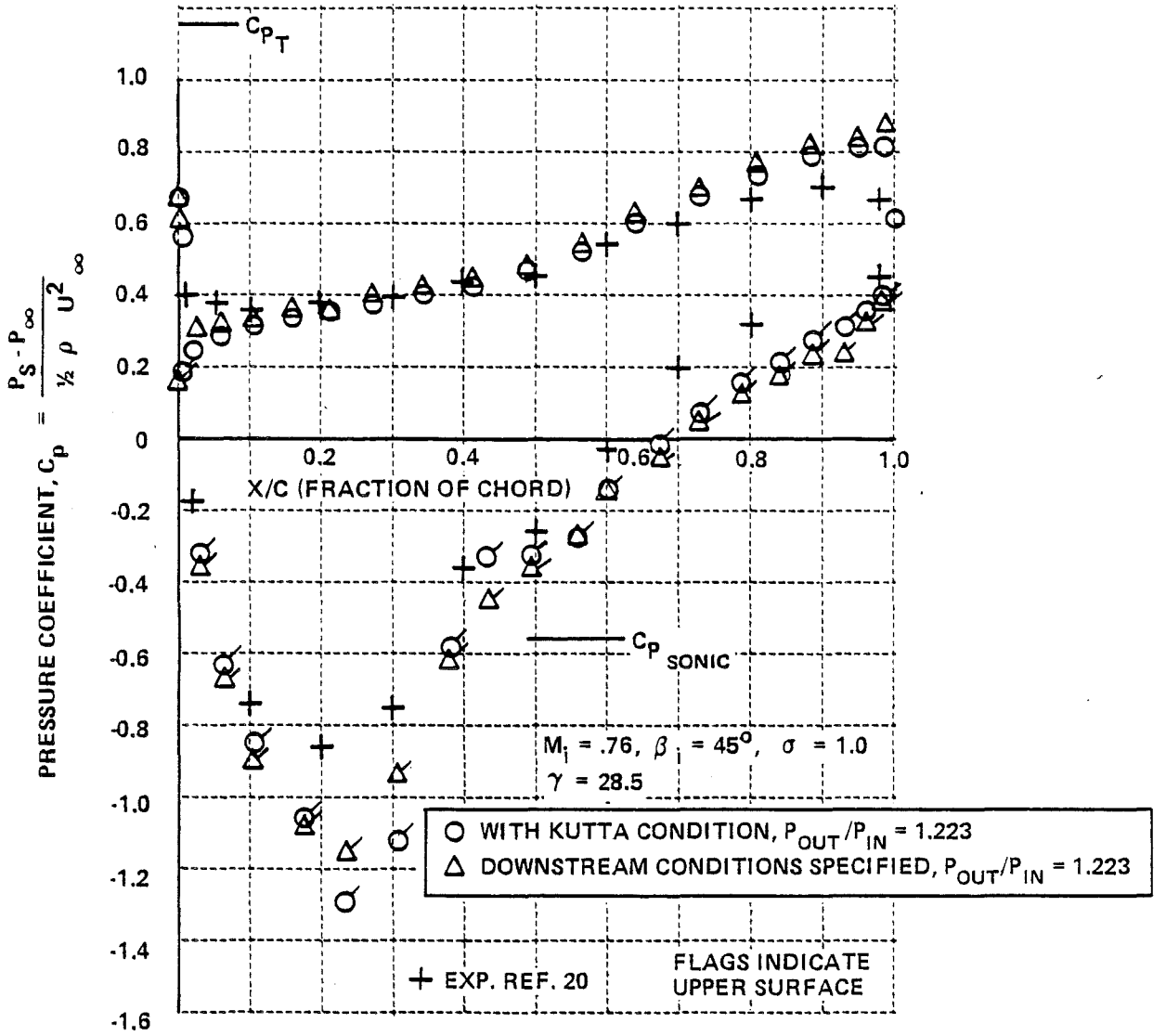

Figure 13 SURFACE PRESSURE DISTRIBUTION NACA 65 (12) 10 CASCADE WITH AND WITHOUT KUTTA CONDITION

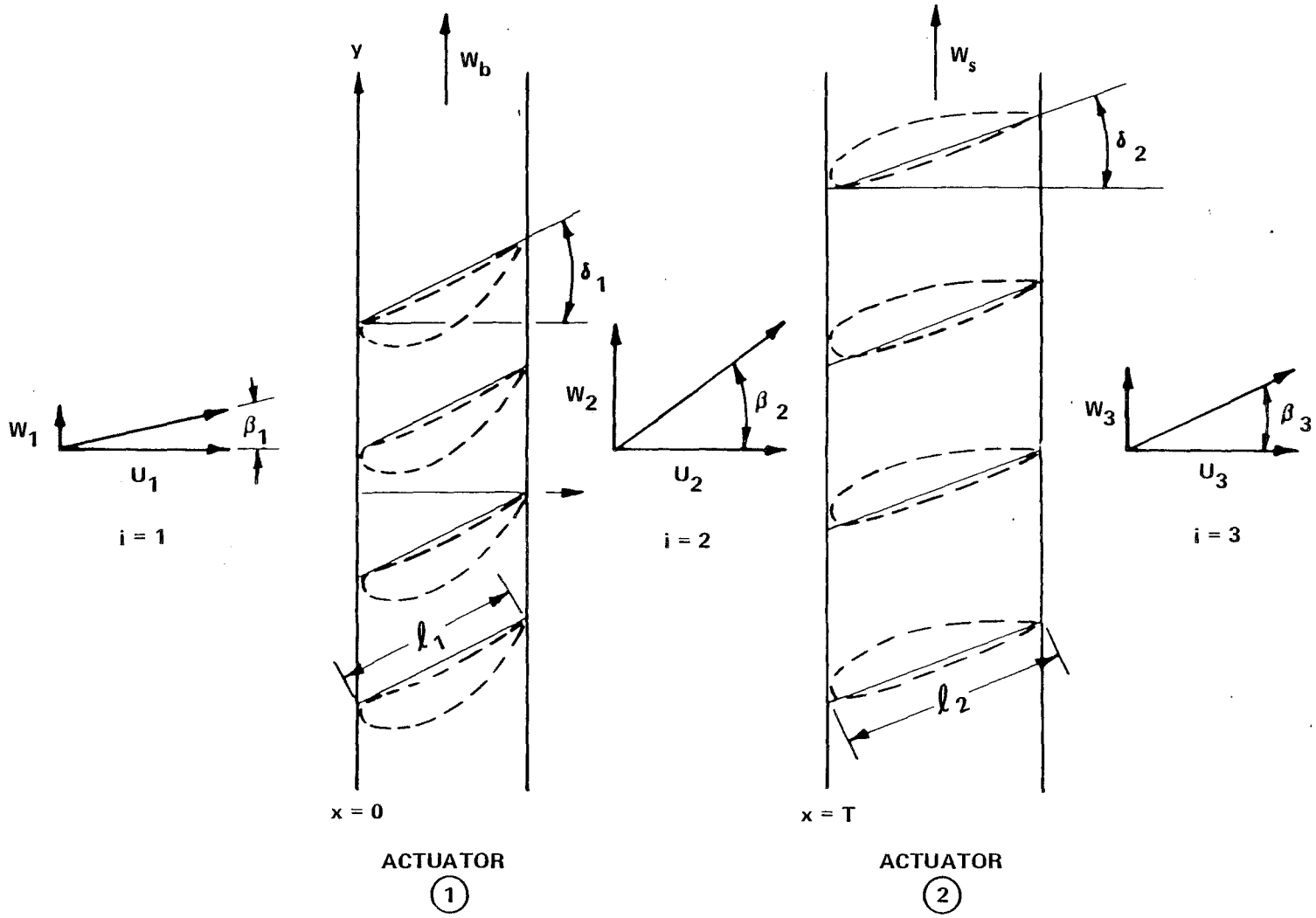

Figure 14 FINITE THICKNESS MODEL FOR TWO BLADE ROW THEORY

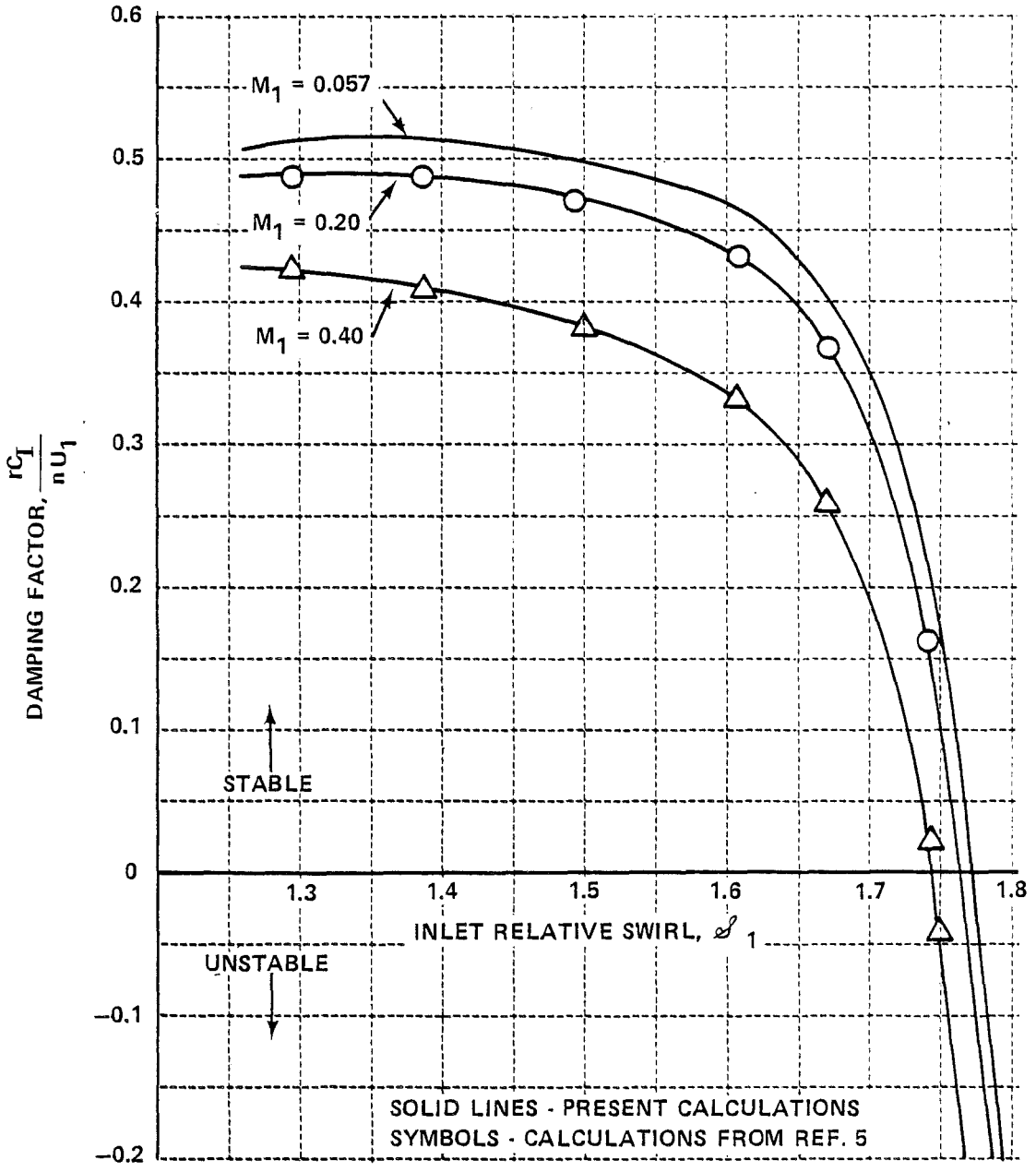

Figure 15 THEORETICAL STABILITY CHARACTERISTICS OF STATOR SET NO. 4, SINGLE BLADE ROW THEORY

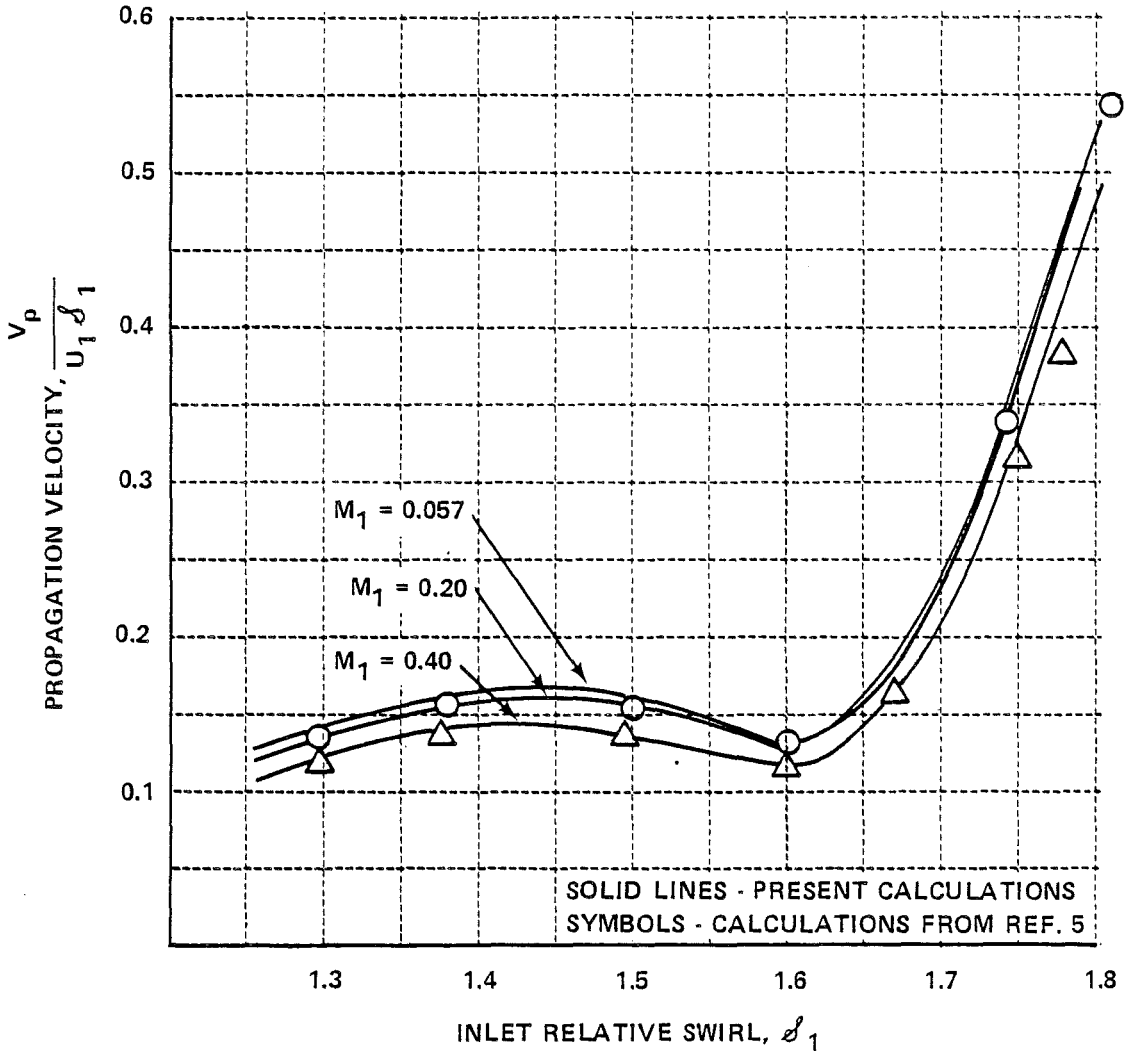

Figure 16 THEORETICAL PROPAGATION VELOCITIES FOR STATOR SET NO. 4, SINGLE BLADE ROW THEORY

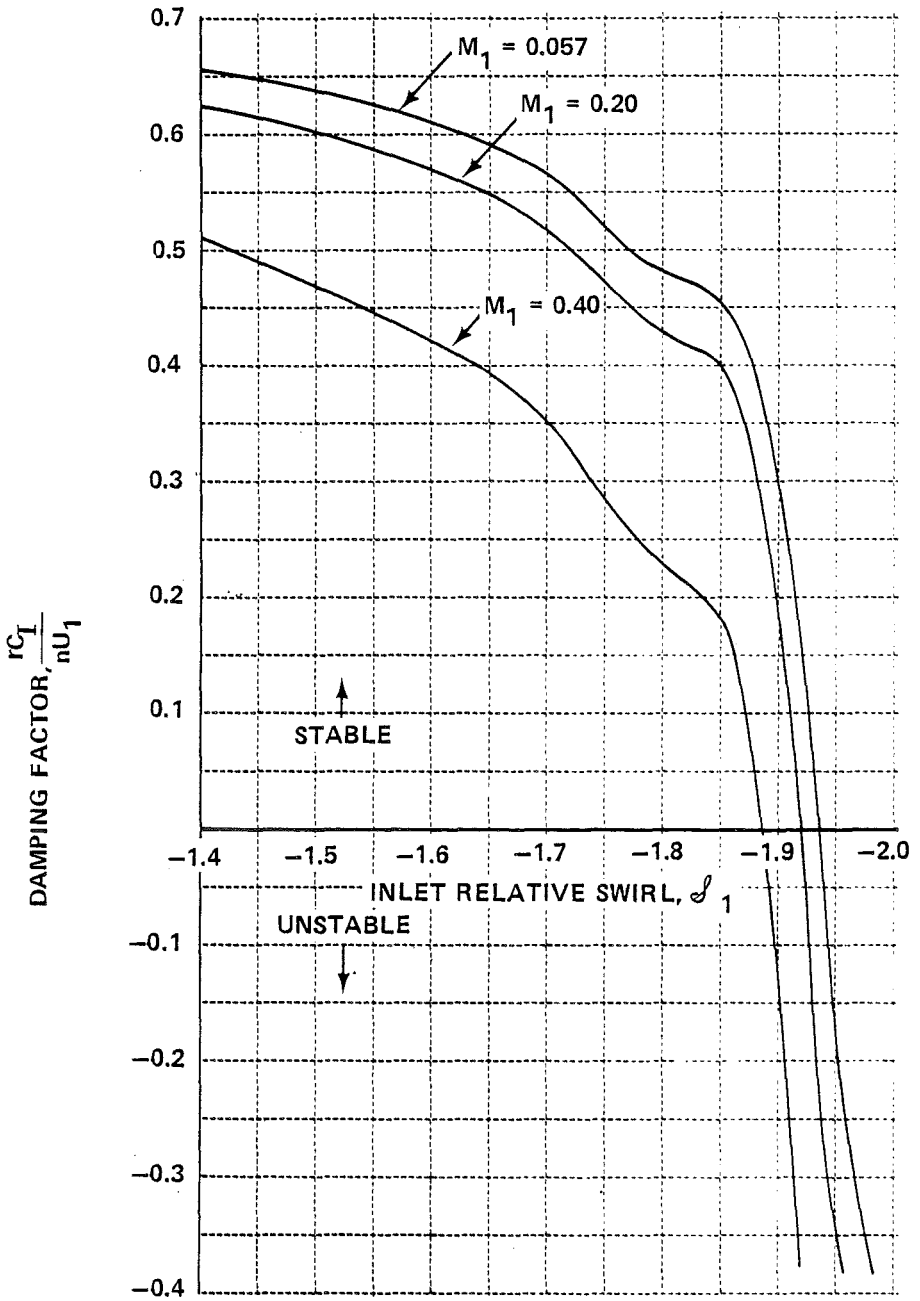

Figure 17 THEORETICAL STABILITY CHARACTERISTICS OF ROTOR NO. 1, SINGLE BLADE ROW THEORY

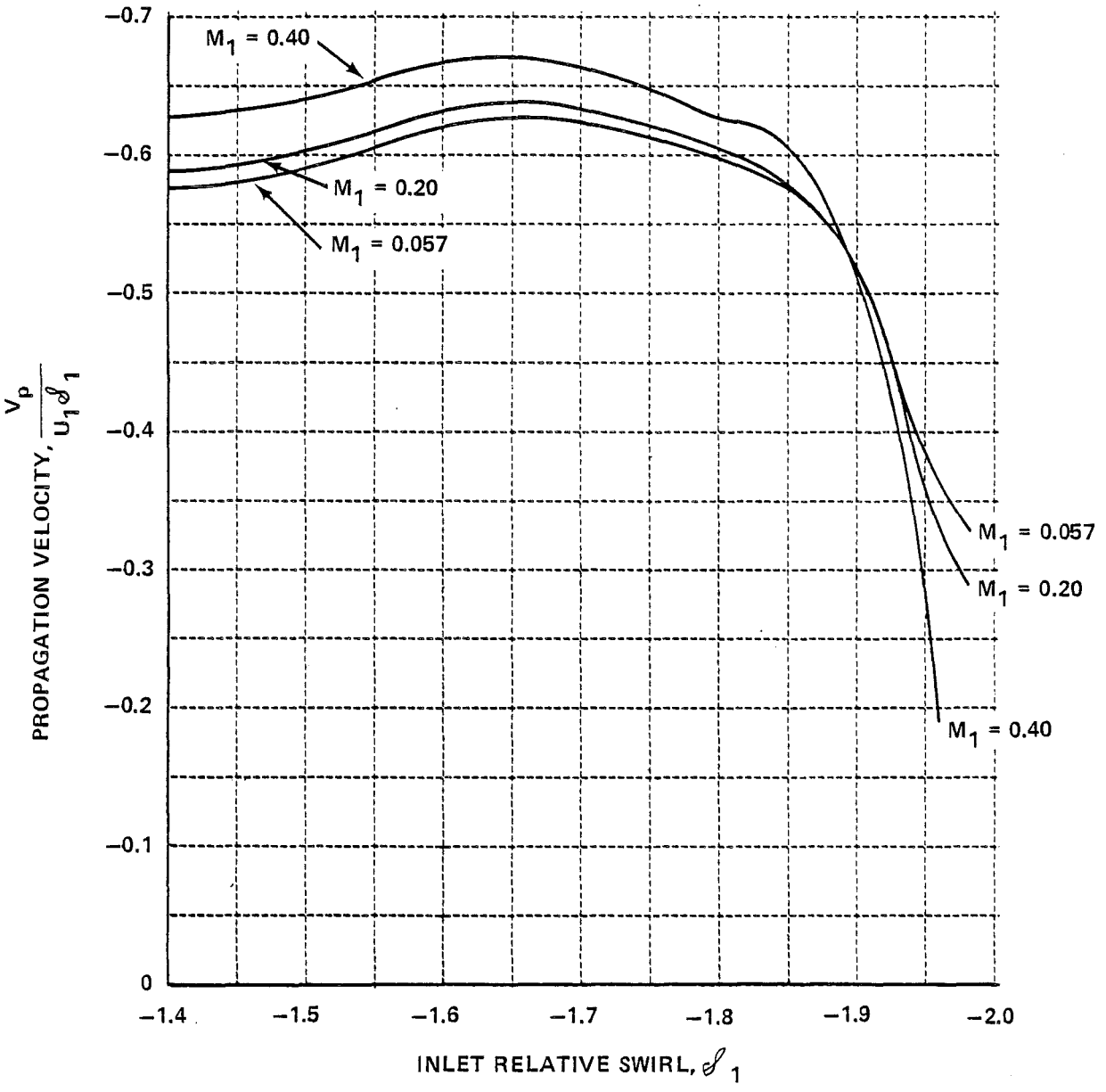

Figure 18 THEORETICAL PROPAGATION VELOCITIES OF ROTOR NO. 1, SINGLE BLADE ROW THEORY

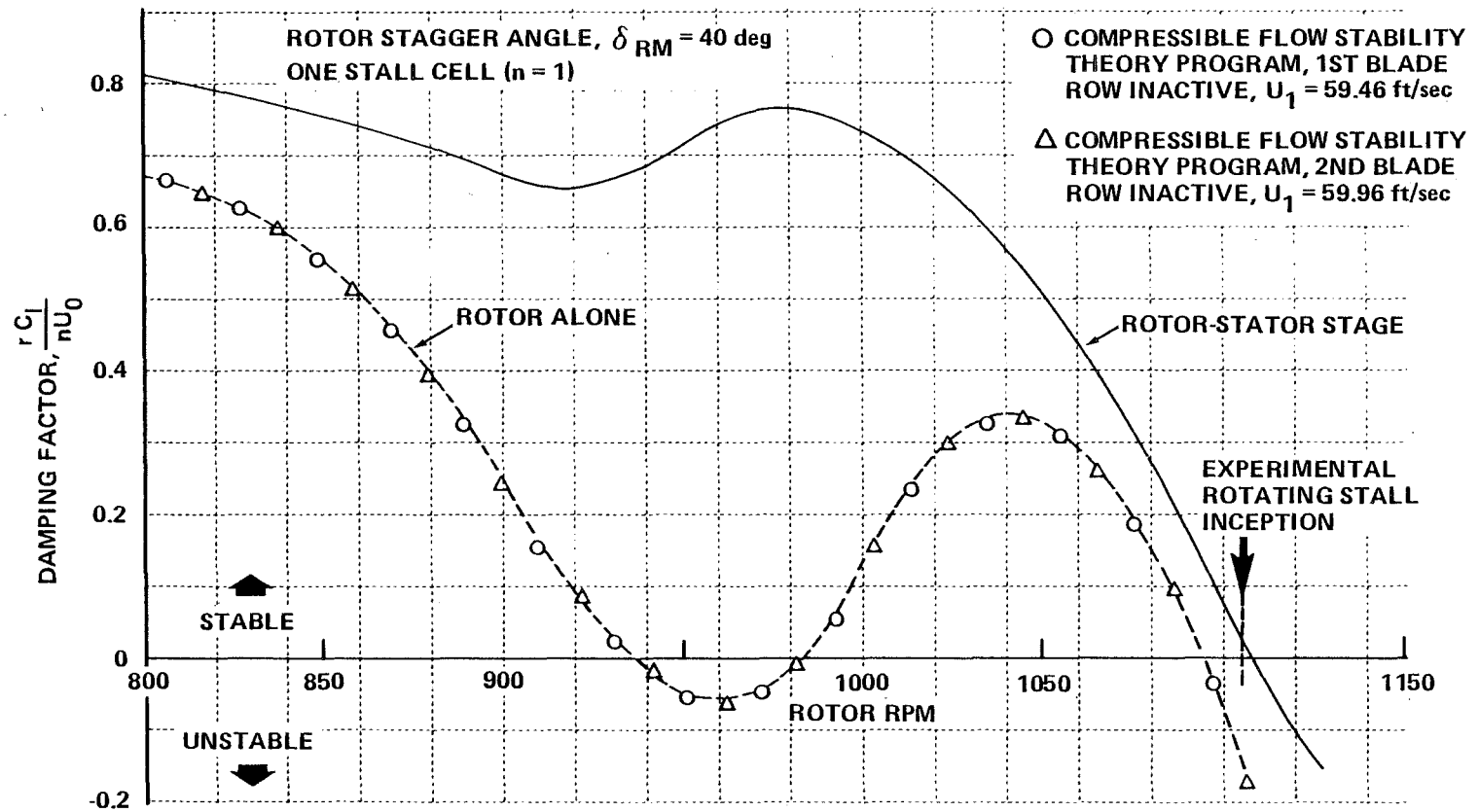

Figure 19 THEORETICAL STABILITY CHARACTERISTICS OF ROTOR-STATOR STAGE, STATOR STAGGER ANGLE, δ_{SM} = 37.2 deg

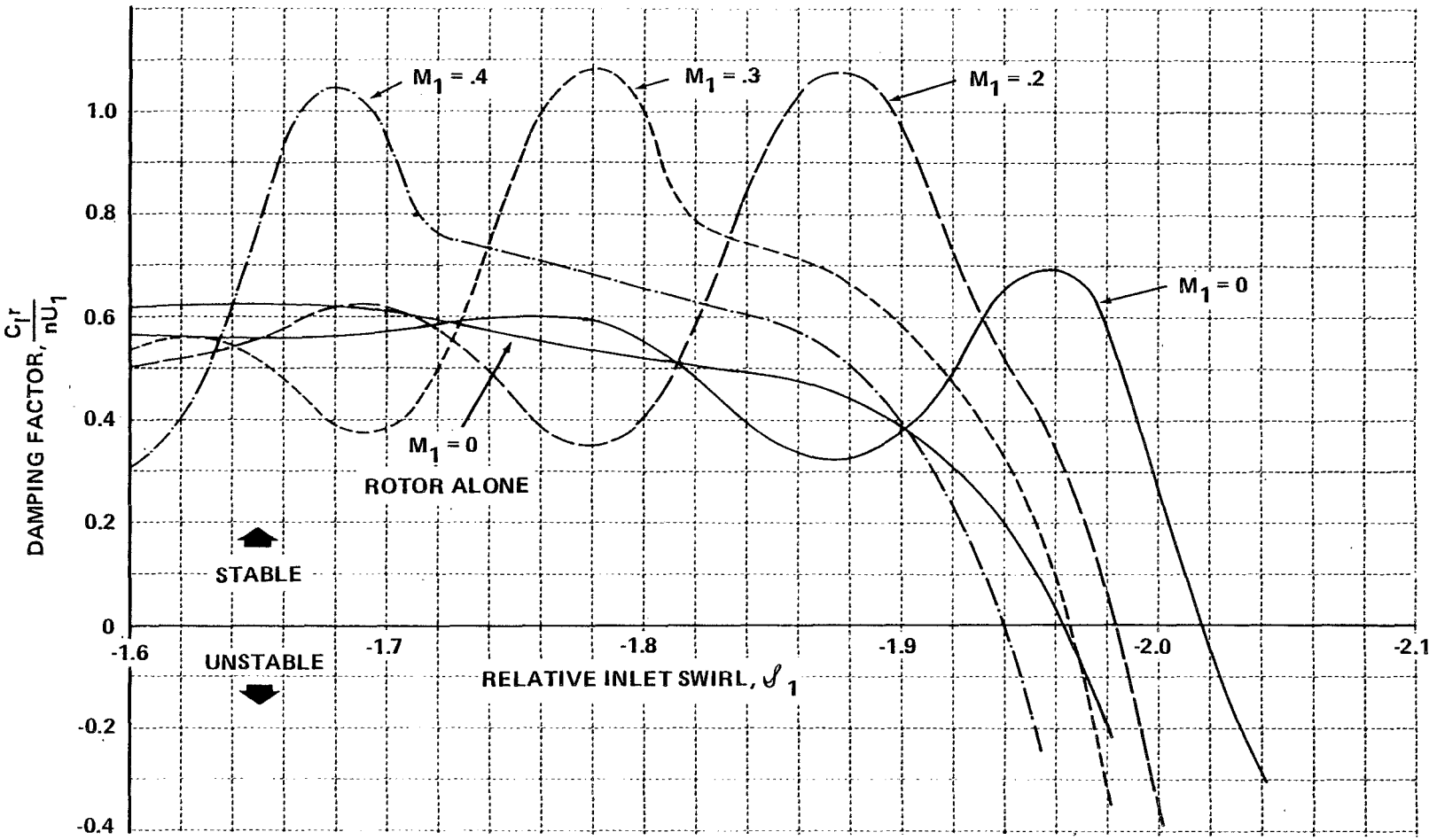

Figure 20 INFLUENCE OF AXIAL MACH NO. ON STAGE STABILITY CHARACTERISTICS, OF ROTOR-STATOR STAGE; $\delta_{SM} = 28.2^{o}$, n = 1

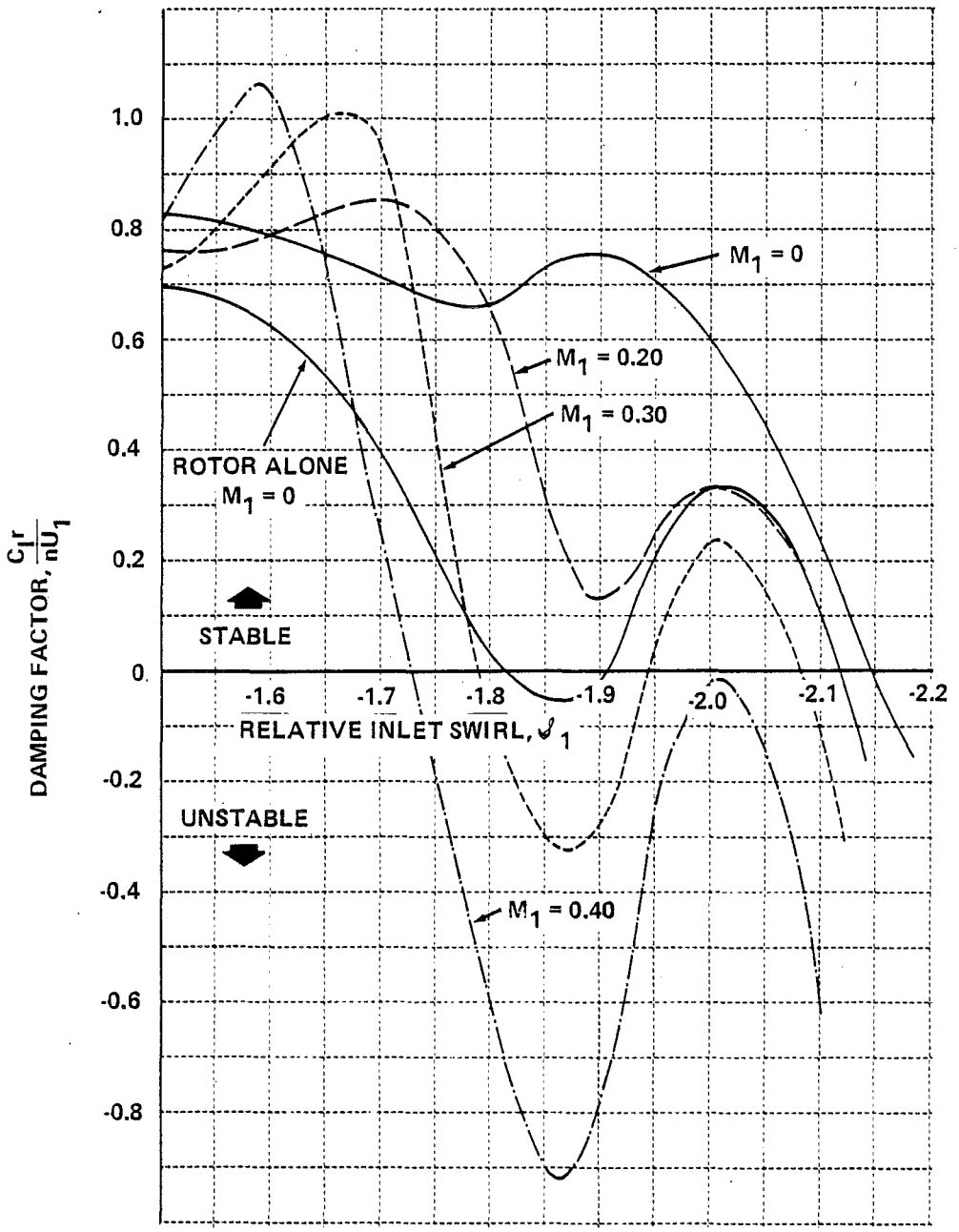

Figure 21 INFLUENCE OF AXIAL MACH NO. ON STAGE STABILITY CHARACTERISTICS OF ROTOR-STATOR STAGE; $\delta_{SM} = 37.2^{o}$, n = 1

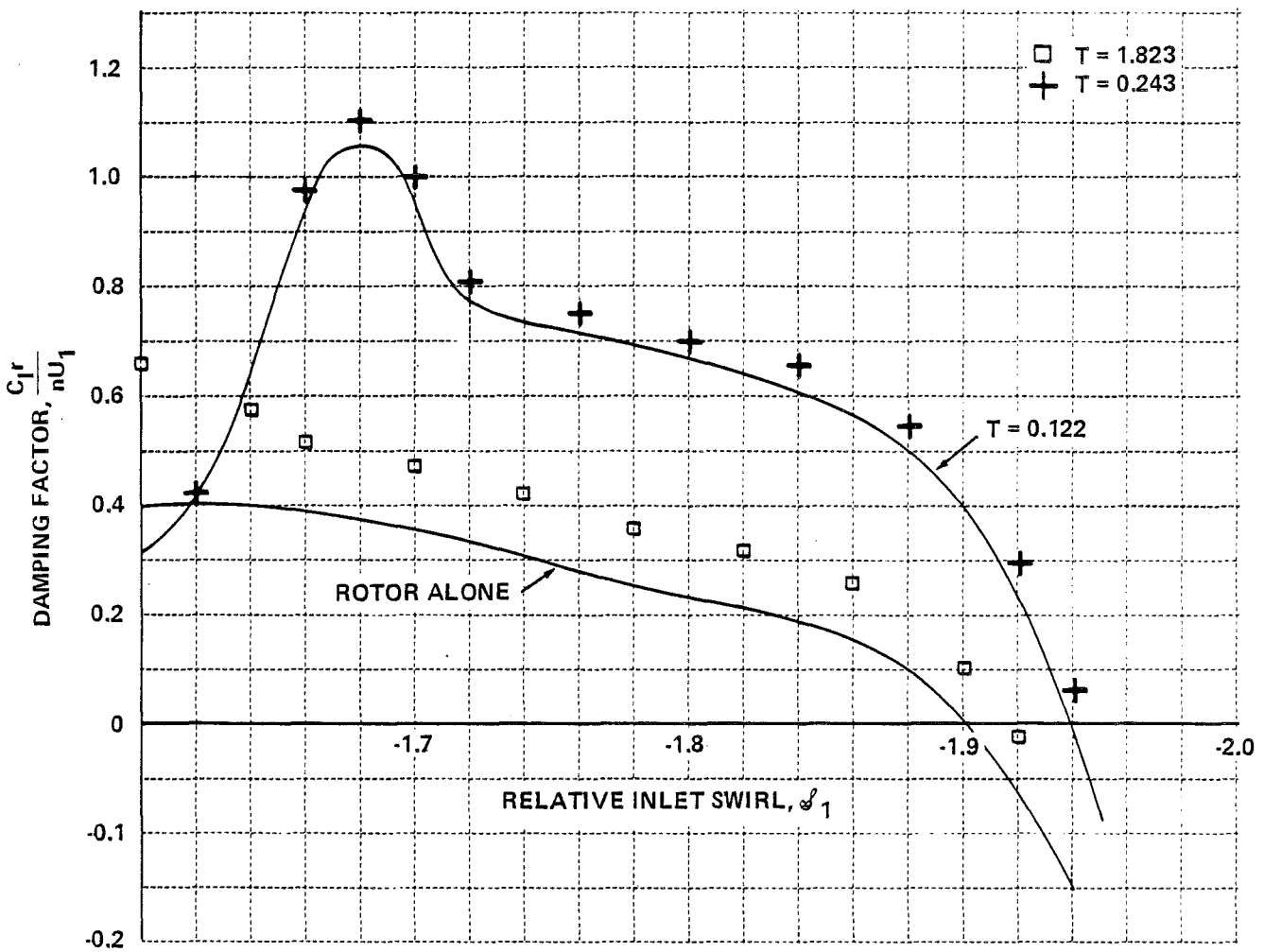

Figure 22 EFFECTS OF BLADE ROW SPACING AT $M_1 = 0.4$, $\delta_{SM} = 28.2^{o}$, n = 1

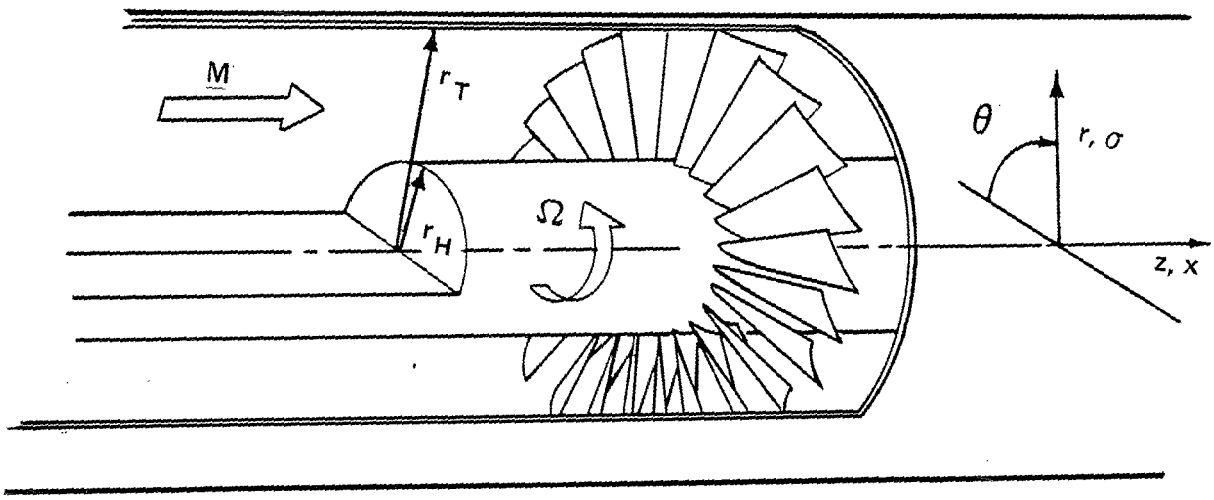

Figure 23 ROTOR GEOMETRY AND COORDINATE SYSTEM

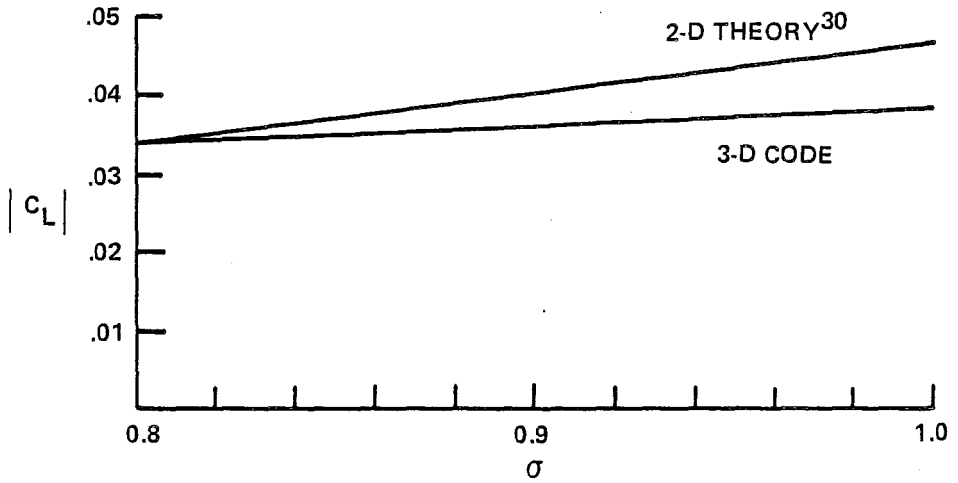

(a) SPANWISE VARIATION IN MAGNITUDE OF LIFT COEFFICIENT

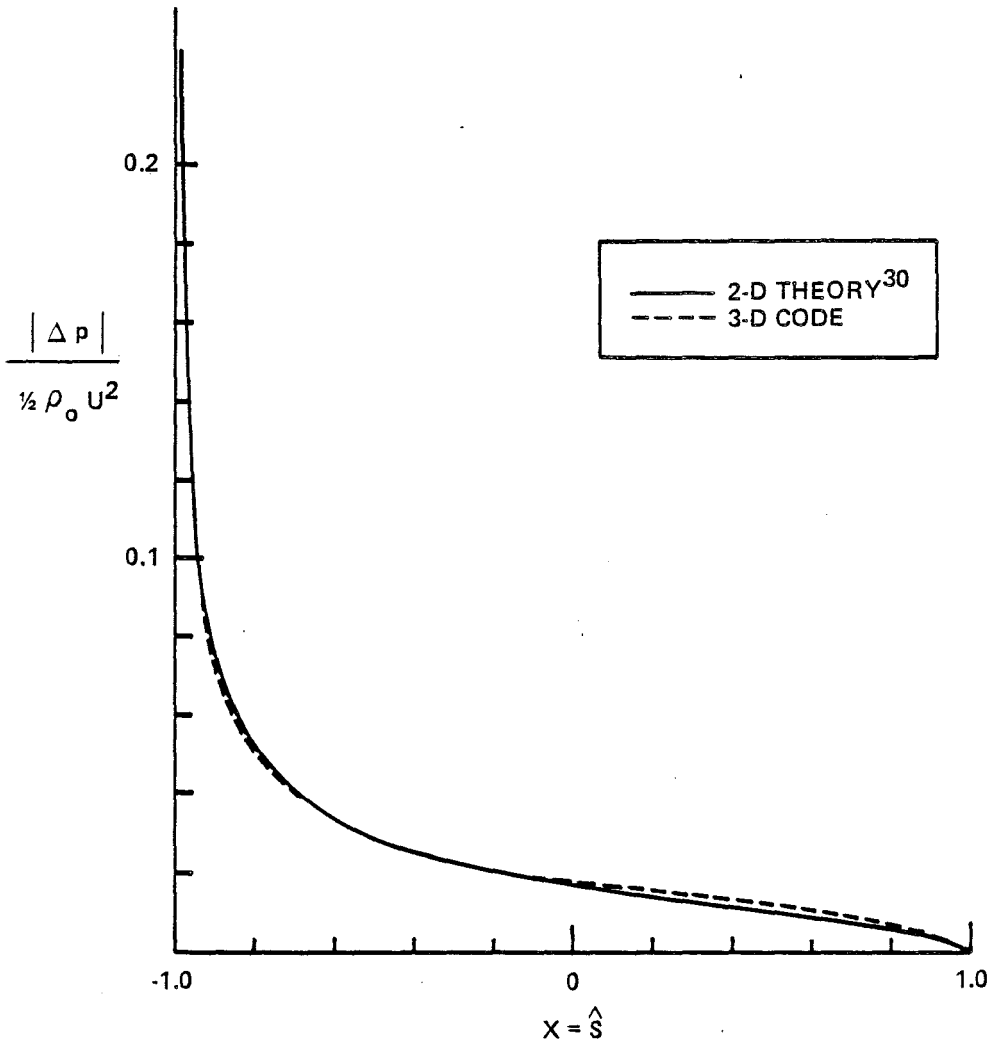

(b) CHORDWISE VARIATION IN LOADING AT THE HUB

Figure 24 COMPARISON OF PRESENT THEORY VERSUS 2-D STRIP THEORY FOR A HIGH HUB/TIP RATIO, LOW SOLIDITY, LOW SPEED BLADE ROW

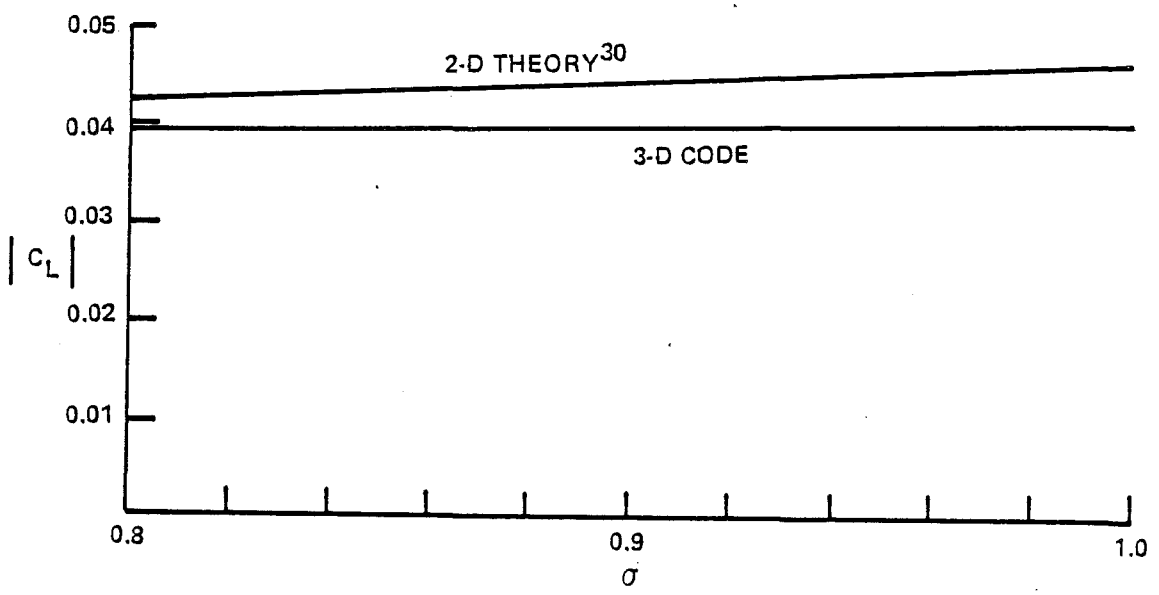

Figure 25 COMPARISON OF PRESENT THEORY VERSUS 2-D STRIP THEORY FOR CASE WITH NEARLY CONSTANT CIRCULATION

*USGPO: 1983-659-062-893